DATA ASSOCIATION ALGORITHMS FOR MULTISENSOR-MULTITARGET TRACKING

DATA ASSOCIATION ALGORITHMS FOR MULTISENSOR-MULTITARGET TRACKING

BY

TONGYU GE, B.Eng., M.Sc.,

A THESIS

SUBMITTED TO THE DEPARTMENT OF ELECTRICAL & COMPUTER ENGINEERING

AND THE SCHOOL OF GRADUATE STUDIES

OF MCMASTER UNIVERSITY

IN PARTIAL FULFILMENT OF THE REQUIREMENTS

FOR THE DEGREE OF

DOCTOR OF PHILOSOPHY

Doctor of Philosophy (2020) McMaster University

(Electrical & Computer Engineering) Hamilton, Ontario, Canada

TITLE:	Data Association Algorithms for Multisensor-Multitarget Tracking
AUTHOR:	Tongyu Ge M.Sc. (Information and Communication Engineering), China Academy of Engineering Physics, Beijing, China B.Eng. (Electronic Information Engineering), University of Electronic Science and Technology of China, Chengdu, China
SUPERVISOR:	Prof. T. Kirubarajan
NUMBER OF PAGES:	xvii, 159

To my family

Abstract

In this thesis, the data association problem in multisensor-multitarget tracking is explored. Algorithms that improve data association performance by eliminating sensor biases or utilizing available domain knowledge are proposed.

Sensor calibration and data association are two essential steps in multisensor-multitarget tracking systems to correct local measurements using estimated sensor biases and to associate measurements from different sensors. The problem of multitarget localization using time difference of arrival (TDOA) measurements at multiple unsynchronized sensors under measurement origin uncertainty is considered. A novel joint multidimensional association algorithm for multisensor synchronization is proposed. This algorithm is extended to a multiframe case to ensure the observability of unknown parameters consisting of target positions and sensor clock offsets. To improve the proposed algorithm's efficiency, a gating method and a multidimensional plus sequential two-dimensional association approach are developed. The Cramér-Rao lower bound for this problem is derived as a performance benchmark. Numerical results show that the proposed algorithm outperforms the algorithms that address sensor calibration and data association separately in terms of correct association rate and target position and sensor clock bias estimation accuracies.

Exploring and exploiting domain knowledge can improve tracking performance,

especially in the context of on-road target tracking. Due to traffic rules and limited lane capacity, on-road targets tend to move in an orderly manner along the centerline of each lane of the roads except for occasional lane changes. A novel sequence-aided 2D assignment (SA-2DA) algorithm, which integrates the target position sequence information into data association by utilizing this information in evaluating the probability of association hypothesis, is proposed. The sequence information is further exploited within the joint probabilistic data association (JPDA) framework, making it suitable for high false alarm rate or high association ambiguity scenarios, and within the tracking framework consisting of the interacting multiple model (IMM) estimator and the JPDA algorithm, making it suitable for tracking maneuvering targets. The uncertainty in target position sequence due to target lane-changing behavior is addressed by two strategies: a) The multiple-hypothesis method combined with the modeling of target lane-changing behavior as a homogeneous Markov chain; b) The track segment association algorithm. The posterior Cramér-Rao lower bound is derived for tracking multitarget along a multi-lane road. Numerical results show that the proposed algorithms (i.e., SA-2DA, SA-JPDA and SA-IMMJPDA) achieve better track accuracy and consistency than the existing multitarget tracking algorithms (i.e., standard 2DA, JPDA and IMMJPDA)) that do not make use of target position sequence information.

Acknowledgements

I would like to take this opportunity to express my sincere gratitude to a number of people very special to me. First and foremost, I would like to acknowledge my deepest gratitude to my supervisor, Prof. T. Kirubarajan, for accepting me as a Ph.D. student, for supporting me spiritually and financially, for providing me expert advice, insightful guidance and continuous encouragement throughout my Ph.D. career.

I would like to express my gratitude to Prof. R. Tharmarasa for giving me generous advice and help every time I encounter difficulties in my research work. I would like to thank my supervisory committee members, Prof. I. Bruce and Prof. T. R. Field, who assisted me with valuable comment and feedback on my research works.

I would like to thank all colleagues in the Estimation, Tracking and Fusion research laboratory for their help throughout my Ph.D. studies. They are the greatest team members I have ever been with. I would like to thank our sponsors and collaborators from Thales and L3Harris for providing real-world problems which motivate the research covered in this thesis. I am also thankful to the administrative staff of the ECE department, specially Ms. C. Gies and Ms. T. Coop, for the administrative support.

Last, but by no means least, I would like to express my special gratitude to my parents for their unconditional love and consistent support through all these years.

Abbreviations

AEW	Airborne Early Warning
AOA	Angle Of Arrival
ASKF	Augmented State Kalman Filter
CCAR	Completely Correct Association Rate
CFM	Car-following Model
CRLB	Cramér-Rao Lower Bound
EKF	Extended Kalman Filter
EM	Expectation Maximization
FIM	Fisher Information Matrix
GBM	Group Behavior Model
GMTI	Ground Moving Target Indicator
ILS	Iterated Least Squares
IMM	Interacting Multiple Model

JDE	Joint Decision and Estimation
JPDA	Joint Probabilistic Data Association
KF	Kalman Filter
LS	Least Squares
MDA	Multidimensional Assignment
MDL	Minimum Description Length
MHE	Moving Horizon Estimator
MHT	Multiple Hypothesis Tracking
ML	Maximum Likelihood
MOBIL	Minimizing Overall Braking Induced by Lane-change
MTT	Multitarget Tracking
NCA	Nearly Constant Acceleration
NCV	Nearly Constant Velocity
NLLR	Negative Log-likelihood Ratio
NLS	Nonlinear Least Squares
NN	Nearest Neighbor
PCRLB	Posterior Cramér-Rao Lower Bound
PDAF	Probabilistic Data Association Filter

PDF	Probability Density Function
PF	Particle Filter
RFS	Random Finite Set
RMSE	Root Mean Square Error
RSS	Received Signal Strength
RTS	Rauch-Tung-Striebel
SFM	Social Force Model
TDOA	Time Difference Of Arrival
TOA	Time Of Arrival
TOF	Time Of Flight
TPM	Transition Probability Matrix
TSA	Track Segment Association
UKF	Unscented Kalman Filter
1D	One-dimensional
2D	Two-dimensional

Declaration of Academic Achievement

This research presents analytical and computational work carried out solely by Tongyu Ge, herein referred to as "the author", with advice and guidance provided by the academic supervisor Prof. T. Kirubarajan. Information that is presented from outside sources, which has been used towards analysis or discussion, has been cited when appropriate, all other materials are the sole work of the author.

Contents

List of Figures

List of Tables

Chapter 1

Introduction

1.1 Data Association in Multisensor-Multitarget Tracking: A Brief Review

Multisensor-multitarget tracking has a broad area of applications ranging from ground and maritime surveillance, situation awareness and navigation in defense to air and urban traffic control, autonomous driving systems and intelligence transportation.

In general, there are four possible configurations for information processing in multisensor-multitarget tracking systems [1]. As shown in Fig. 1.1, these configurations differ in the information available to each processor and the sequence in which the data association and track filtering are carried out. A standard single-sensor multitarget tracking system usually uses the Type I configuration (Fig. 1.1a), where the data association (i.e., the measurement-to-track association) step is carried out to determine from which target a certain measurement originated in the presence of

missed detections and false alarms. The type II configuration has multiple single-sensor trackers followed by a track fusion center which associates and fuses the local tracks into system tracks. This configuration is important in distributed tracking systems and has different information flowcharts depending on whether the fusion algorithm uses the track estimates from the previous fusion and whether the information feedback is available [2]. Fig. 1.1b shows the flowchart of a track-to-track fusion without memory and feedback. In the Type III configuration, as shown in Fig. 1.1c, the static inter-sensor association and fusion, where the measurements from various sensors are associated and fused yielding composite measurements, is followed by a central tracking processor. In the Type IV configuration, also called centralized tracker [1], all measurements are sent to the center for association and updating the tracks. It can provide the best results (subject to the used data association algorithm's limitations) by exploiting the maximum available information but requires high computational capacity [1]. No matter which configuration is used, the data association, ranging from the basic measurement-to-track association to the measurement-to-measurement association and the track-to-track association, is an indispensable component in multisensor-multitarget tracking systems.

In multisensor tracking systems, sensors usually observe the targets in their local coordinates. Then, the measurements or local track estimates at each sensor are transformed to a global reference coordinate for association and fusion. Any biases that may present in the sensor's local coordinate need to be estimated to calibrate local measurements or track estimates. Otherwise, association and fusion can not be performed successfully, leading to large tracking errors and potentially to the formation of multiple tracks (ghosts) for the same target [3]. The augmented state Kalman

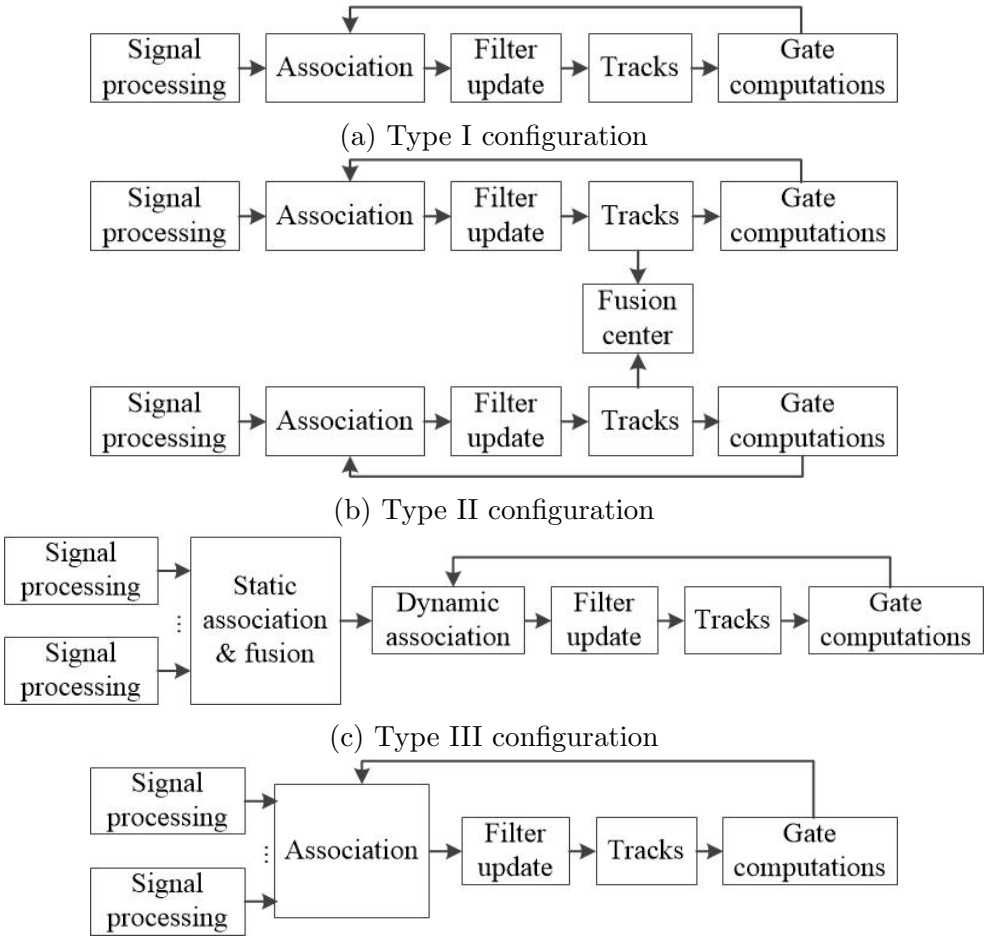

(a) Type I configuration

(b) Type II configuration

(c) Type III configuration

(d) Type IV configuration

Figure 1.1: Configurations for multisensor-multitarget tracking systems.

filter (ASKF) [3] is one classical but computationally expensive approach for sensor bias estimation, where all target states and sensor biases are stacked into one vector for filtering. The algorithms that are proposed to improve the efficiency of ASKF approach can be found in [4, 5, 6]. The least square method and the maximum likelihood method are also widely used for bias estimation [7, 8, 9]. These sensor calibration algorithms assume that there is no measurement origin uncertainty. That is, the sensor

biases are estimated using correctly associated data. However, the measurement-origin information is not known a priori in multisensor tracking systems. To address this problem, the approaches that perform sensor calibration and data association simultaneously are proposed in [10, 11, 12]. The joint sensor calibration and data association problem is especially challenging in the scenario where multiple unsynchronized sensors are used to track multiple targets by receiving the signals emitted by the targets and measuring the time of arrivals of these signals. Since the time of arrival is incomplete position measurement, the inter-sensor measurement-to-measurement association needs to be performed to obtain composite position measurements. At the same time, the sensor biases that exist in time measurements also need to be well-addressed to avoid wrong association. A novel joint multidimensional association algorithm, which performs data association, multisensor synchronization and multitarget localization simultaneously, is proposed in this thesis.

The classic approaches used for data association in the multitarget tracking systems are the nearest neighbor (NN) [13], joint probabilistic data association (JPDA) [14], multiple hypothesis tracking (MHT) [15] and the multidimensional assignment (MDA) algorithm [16]. The NN algorithm is commonly used in the simplest case of single target tracking or the case where the targets to be tracked are well-separated. The other three algorithms are usually more effective in the complex multitarget tracking scenarios. Typically, only kinematic measurements are used to solve the data association problem [16]. Many strategies exploring other available information are developed to improve the performance of data association algorithms. Target feature, attribute or classification information are commonly used in data association algorithms, especially for resolving the kinematic ambiguity among neighboring

targets [16, 17, 18].

Domain knowledge in specific scenarios is another important prior information sources to enhance tracking performance. On-road target tracking is an essential component in various civil and military applications. The motion characteristics of on-road targets make on-road target tracking problem distinct from the standard multitarget tracking problem. First, target motions are subjected to various constraints imposed by the roads that they move on. Many different approaches for using road map information in on-road target tracking haven been studied in the literature, such as directional process noise [19, 20] and constrained state estimation [21, 22, 23, 24]. Second, due to the limits imposed by traffic rules and lane capacity, targets usually interact with their neighbors and tend to move in an orderly manner along the centerline of each lane of the road. The interactions among targets are usually modeled as empirical motion behavior models, such as the social force model [25] and the microscopic traffic flow model [26, 27, 28], which may not accurately describe the real target motion. To the best of our knowledge, the target position sequence information has not yet been well studied in target tracking literature. In this thesis, three novel data association algorithms, which exploit target position sequence information to obtain improved association and tracking performances, are proposed. To address the uncertainty in target position sequence due to target lane-changing behavior, a multi-hypothesis approach and a track segment association algorithm are proposed.

1.2 Theme and Objectives of Dissertation

In compliance with the terms and regulations of McMaster University, this dissertation has been assembled by three articles in a *sandwich thesis* format. These articles

represent the independent research work of the author of this dissertation, Tongyu Ge.

The articles in the dissertation focuses on the data association algorithms for multisensor-multitarget tracking. The general research topics are the following:

1. To propose a multidimensional TDOA association algorithm for joint multitarget localization and multisensor synchronization (Paper I).

2. To mathematically formulate target position sequence information and propose sequence-aided data association algorithms for on-road target tracking (Paper II and III).

3. To address the uncertainty in target position sequence due to target lane-changing behavior (Paper II and III).

4. To derive the (posterior) Cramér-Rao lower bound as the theoretical performance benchmark (Paper I, II and III).

1.3 Related Publications

1.3.1 Journal Articles

- T.Ge, R. Tharmarasa, B. Lebel, M. Florea, T. Kirubarajan, "A Multidimensional TDOA Association Algorithm for Joint Multitarget Localization and Multisensor Synchronization", Accepted in final form for *IEEE Transactions on Aerospace and Electronic Systems*, vol. 56, no. 3, pp. 2083-2100, 2019. (doi: 10.1109/TAES.2019.2943786)

- T.Ge, R. Tharmarasa, M. Bradford, T. Kirubarajan, "Sequence-Aided Data Association for Tracking Multiple On-road Targets With Unknown Interactions", Submitted to *IEEE Transactions on Aerospace and Electronic Systems*, May 2020.

- T.Ge, R. Tharmarasa, M. Bradford, T. Kirubarajan, "Sequence-Aided Joint Probabilistic Data Association for Multiple On-road Target Tracking", Submitted to *IEEE Transactions on Intelligent Transportation Systems*, May 2020.

1.3.2 Conference Publications

- T.Ge, R. Tharmarasa, B. Lebel, M. Florea, T. Kirubarajan, "Target Localization and Sensor Synchronization in the Presence of Data Association Uncertainty", In *22nd International Conference on Information Fusion*, Ottawa, Canada, July 2019.

The following chapter is a reproduction of an Institute of Electrical and Electronics Engineers (IEEE) copyrighted, published paper:

T.Ge, R. Tharmarasa, B. Lebel, M. Florea, T. Kirubarajan, "A Multidimensional TDOA Association Algorithm for Joint Multitarget Localization and Multisensor Synchronization", Accepted in final form for *IEEE Transactions on Aerospace and Electronic Systems*, Sep. 2019. (doi: 10.1109/TAES.2019.2943786)

Chapter 2

A Multidimensional TDOA Association Algorithm for Joint Multitarget Localization and Multisensor Synchronization

2.1 Abstract

This paper considers the problem of multitarget localization using time difference of arrival (TDOA) measurements at multiple sensors with misaligned clocks in the presence of data association uncertainty. Sensor synchronization and data association are two essential steps in target localization and tracking to align sensor clocks and to associate measurements from different sensors. In practice, sensor synchronization errors can adversely affect data association performance and vice versa. Although

these two processes affect each other, they are usually addressed separately. We propose a novel joint multidimensional association algorithm for multisensor synchronization (JMDA4MS), which performs data association and yields sensor clock offset and target position estimates simultaneously using TDOA measurements. Considering the observability of the unknown parameters, the joint multiframe multidimensional association (JMF-MDA) algorithm is developed as a multiframe extension of the JMDA4MS algorithm. A gating method and a multidimensional plus sequential two-dimensional association approach are utilized to improve the efficiency of the proposed algorithms. The Cramér-Rao lower bound (CRLB) for the proposed maximum likelihood (ML) estimator is derived as a performance benchmark. Computer simulations are carried out to evaluate the performance of the proposed algorithms on different scenarios.

2.2 Introduction

Estimating the states of moving objects with high accuracy is of interest in many applications, ranging from airborne and underwater surveillance to indoor guided navigation and intelligent transportation [29, 30, 31, 32]. A variety of target localization techniques that utilize different measurements of signals transmitted or reflected by target of interest, such as received signal strength (RSS), angle of arrival (AOA), time of arrival (TOA) and time difference of arrival (TDOA), have been proposed in the literature [33]. RSS-based techniques estimate the distance from a target to the receiving sensor based on an assumed signal propagation model and then calculate the target's position. In practice, the positioning accuracy of RSS-based methods is limited because it is hard to build an accurate signal propagation model in the

presence of multipath, interference and noise in the environment [34]. AOA-based techniques require precise calibration and maintenance of a directional antenna or an antenna array on each sensor, which is difficult to implement in practical systems [35]. TOA-based techniques calculate the range between a target and the sensor based on the time of flight (TOF) of signals, which requires the precise knowledge of signals' absolute transmission times at the target and absolute reception times at the receiver [34]. Unlike TOA-based methods, TDOA-based techniques require only relative synchronization among receivers and are suitable for passive localization. TDOA-based systems also achieve better localization accuracy than RSS-based and AOA-based systems in general [36]. As such, TDOA-based systems provide the motivation for our work.

Clock synchronization is an important prerequisite to ensure optimal data fusion in sensor networks. An offset between the local clocks of sensors can introduce biases into TDOA measurements — even a microsecond offset can significantly degrade the overall localization performance due to the high signal propagation speed [36]. The synchronization problem can be formulated as a parameter estimation problem and studied from a statistical signal processing perspective [37]. Assuming exponential random delays, the maximum likelihood (ML) estimate of clock skew is obtained in [38]. By modeling the time-varying behavior of local clocks, joint clock offset and skew estimation algorithms for sensor networks have been developed in [39].

Considering the close connection between sensor synchronization and target localization, some works have focused on solving these two problems within a unified framework [40]. An ML estimator and a least squares (LS) estimator are proposed in

[41] to estimate target positions and clock offsets simultaneously. For the joint target localization and time-varying clock synchronization problem, one ML estimator and two suboptimal estimators are utilized in [42] and the expectation-maximization (EM) based algorithm is studied in [43]. In [36], TDOA-based localization is investigated using a set of imperfect sensors, where clock offsets and random position errors exist among different sensor groups. The problem of localizing a single mobile target with unsynchronized sensors is studied in [44, 45, 46]. However, these works only consider the localization of a single target with unity detection probability and zero false alarm probability, which means that there is no measurement-origin uncertainty [47].

In a multitarget localization scenario, one fundamental issue is to determine from which target a certain measurement originated in the presence of missed detections and false alarms, which is referred to as the data association problem [47]. A number of algorithms have been developed to solve this problem, ranging from the simple nearest neighbor (NN) algorithm to the highly effective but computationally expensive techniques such as the joint probabilistic data association (JPDA) algorithm and the multiple hypothesis tracking (MHT) algorithm [1, 48].

Data association becomes especially challenging if the sensors are passive and only incomplete position measurements, e.g., TOAs or AOAs, are available. Measurements from multiple sensors have to be associated to generate full position measurements and then to determine the positions of targets [49]. A class of solutions for this association problem is based on the multidimensional assignment (MDA) technique, which uses a discrete optimization formulation [50, 51, 52, 53, 54, 55]. In [56], an efficient $(S+1)$-D assignment algorithm, which performs the measurement-to-measurement

association and the measurement-to-track association in one step, is developed for the localization and tracking of an unknown number of targets using TDOA measurements from S receivers. The gated $(S+1)$-D assignment algorithm utilizing prior tracking information is proposed in [57] as an improvement over [56]. Computational cost is an important issue that needs to be considered when the MDA algorithm is implemented to solve a practical data association problem with more than two sensors. A generalized S-dimensional algorithm employing successive Lagrangian relaxations is proposed and applied to azimuth-angle-based multisensor-multitarget localization in [58]. Fast data association using clustering techniques is investigated in [59]. Motivated by large-scale data association problems, the S_0-D+seq(2-D) algorithm is proposed in [60]. However, one crucial assumption in these works is that sensor registration has been done perfectly. That is, it is assumed that multisensor measurements have been transformed into a common reference coordinate and aligned properly.

While many algorithms have been developed for target localization, sensor synchronization and data association, these three issues have rarely been studied together. More precisely, it is routinely assumed in data association algorithms that sensors have been aligned perfectly, and most localization and synchronization algorithms are developed based on correctly-associated measurements. However, sensor clock alignment errors may result in wrong associations, and erroneous data association may degrade the localization and synchronization accuracies [12]. Therefore, it is necessary to treat these three problems simultaneously. Joint data association, sensor synchronization and target localization is an application of the joint decision and estimation (JDE) problem, where data association decision and parameter estimation have to be carried out under measurement origin uncertainty [61]. The JDE problem is

challenging because it involves inter-dependent discrete-valued and continuous-valued uncertainties and thus data association decision and parameter estimation affect each other [62]. In [61], a gating-based detection method and a modified ML-PDA framework are presented for the joint track initialization and parameter estimation problem. In [12], a joint data association and bias estimation method is proposed for linear measurement models based on the expectation-maximization (EM) algorithm, where active sensors are utilized to measure target positions. In [63], sensor bias estimation is performed in the presence of data association uncertainty, where each sensor measures the azimuth and elevation angles of targets. However, target localization (or track initialization) using TDOA measurements in the presence of data association uncertainty has its own challenges since only incomplete position measurements are available at unsynchronized passive sensors, which motivates the work in this paper.

There are three main contributions in this paper. First, we present a unified framework to realize multitarget localization, multisensor synchronization and data association simultaneously. The joint multidimensional association algorithm for multisensor synchronization (JMDA4MS) is proposed to resolve measurement-origin uncertainty in unsynchronized sensor networks using TDOA data. The joint multiframe multidimensional association (JMF-MDA) algorithm is developed as an extension of the JMDA4MS algorithm to ensure the observability of the unknown parameters. Second, a gating method and a multidimensional plus sequential two-dimensional association approach are utilized to improve the efficiency of the proposed algorithms by reducing the number of possible hypotheses. Third, an ML estimator for joint target localization and sensor synchronization is proposed and the corresponding Cramér-Rao Lower Bound (CRLB) is derived.

The rest of the paper is organized as follows. Section II introduces the time-based measurement model and the measurement-to-measurement association problem in passive sensor networks. In Section III, the standard MDA algorithm to solve the data association problem is introduced. Then, the MDA algorithm for correlated TDOA measurements is formulated and the limitations in applying it to unsynchronized sensor networks are analyzed. In Section IV, two novel MDA algorithms are proposed to realize simultaneous data association, sensor synchronization and target localization and an ML estimator is developed to obtain the estimates of the unknown parameters. The proposed algorithms can also be used for system calibration and track initialization in target tracking applications. Moreover, the corresponding computational cost is analyzed and several options are considered to improve algorithm efficiency. The CRLB for joint target position and sensor clock offset estimation is derived in Section V. Simulation results are presented in Section VI along with discussions on the performance of different algorithms. Finally, conclusions are discussed in Section VII.

2.3 Problem Formulation

This section introduces the time-based measurements consisting of TOA and TDOA data that are commonly used in range-based localization algorithms. Then, the measurement-to-measurement association problem with application to multitarget tracking is discussed.

2.3.1 Time-Based Measurements

Consider a scenario where multiple targets emit signals and move in a two-dimensional surveillance region. Targets independently emit signals at unknown discrete-time instants. The unknown position from which target t transmits its kth signal is denoted by $X_{t,k} = [x_{t,k}, y_{t,k}]^T$. The signals are passively received by N_s omnidirectional sensors located at known positions $X_s = [x_s, y_s]^T$, $s = 1, ..., N_s$. In general, the number and positions of sensors may vary over time and are assumed to be known. The sensors measure the arrival times of the received signals according to their local clocks. For sensor s, the TOA measurement of the kth signal from target t is denoted by

$$y_{s,t,k} = tr_{t,k} + \frac{\|X_{t,k} - X_s\|}{c} + \beta_s + w_s \tag{2.3.1}$$

where $tr_{t,k}$ is the unknown transmission time based on the global clock, c is the propagation speed of the signal, $\|X_{t,k} - X_s\|$ is the range from sensor s to the position from which target transmits the signal, β_s is the clock offset of sensor s with respect to the global clock, and w_s is the arrival time measurement noise of sensor s, which is assumed to be a zero-mean white Gaussian noise with variance σ_s^2 and uncorrelated with other sensors. Since the signal propagation speed is much larger than target speeds, it is assumed that target positions remain fixed during signal propagation interval.

In general, the transmission time $tr_{t,k}$ is unknown and need not be estimated, and it can be eliminated by calculating the time differences of TOA measurements between pairs of sensors. For convenience and without loss of generality, all measurements are considered with reference to a particular sensor (denoted by sensor 1). The TDOA

measurement of the kth signal from target t between sensor s and sensor 1 is given by

$$\begin{aligned}\Delta y_{s,t,k} &= y_{s,t,k} - y_{1,t,k} \\ &= \frac{\|X_{t,k} - X_s\|}{c} + \beta_s + w_s \\ &\quad - \frac{\|X_{t,k} - X_1\|}{c} - \beta_1 - w_1.\end{aligned} \tag{2.3.2}$$

Letting

$$\begin{aligned}h_s(X_{t,k}) &= \frac{\|X_{t,k} - X_s\|}{c} - \frac{\|X_{t,k} - X_1\|}{c}, \\ b_s &= \beta_s - \beta_1, \\ w_{s1} &= w_s - w_1,\end{aligned} \tag{2.3.3}$$

we have

$$\Delta y_{s,t,k} = h_s(X_{t,k}) + b_s + w_{s1} \tag{2.3.4}$$

where b_s is the clock offset of sensor s with respect to sensor 1 and w_{s1} is a zero-mean white Gaussian noise with variance $\sigma^2 = \sigma_1^2 + \sigma_s^2$. With the assumption that the sensor clock offset β_s is time-invariant during the positioning interval, the relative clock offset b_s is a constant parameter.

Stacking all the TDOA measurement equations of the kth signal from target t results in a vector equation of the form

$$\Delta Y_{t,k} = H(X_{t,k}) + B + W_{t,k}, \tag{2.3.5}$$

$$\begin{bmatrix} \Delta y_{2,t,k} \\ \Delta y_{3,t,k} \\ \vdots \\ \Delta y_{N_s,t,k} \end{bmatrix} = \begin{bmatrix} h_2(X_{t,k}) \\ h_3(X_{t,k}) \\ \vdots \\ h_{N_s}(X_{t,k}) \end{bmatrix} + \begin{bmatrix} b_2 \\ b_3 \\ \vdots \\ b_{N_s} \end{bmatrix} + \begin{bmatrix} w_{21} \\ w_{31} \\ \vdots \\ w_{N_s1} \end{bmatrix} \tag{2.3.6}$$

where $W_{t,k}$ is a zero-mean Gaussian noise vector with covariance matrix $R_{t,k}$ given by

$$\begin{aligned} R_{t,k} &= E\left[W_{t,k}{W_{t,k}}^T\right] \\ &= \begin{bmatrix} \sigma_2^2+\sigma_1^2 & \sigma_1^2 & \cdots & \sigma_1^2 \\ \sigma_1^2 & \sigma_3^2+\sigma_1^2 & \cdots & \sigma_1^2 \\ \vdots & \vdots & \ddots & \vdots \\ \sigma_1^2 & \sigma_1^2 & \cdots & \sigma_{N_s}^2+\sigma_1^2 \end{bmatrix}. \end{aligned} \tag{2.3.7}$$

In practice, signals may not be received by some sensors due to signal attenuation or limited coverage of sensors. Therefore, the number of TDOA measurements in $\Delta Y_{t,k}$ might be less than $N_s - 1$. It is assumed that the reference sensor has sufficient coverage to receive all signals from the target.

2.3.2 Measurement-to-Measurement Association

Target tracking and data association algorithms usually rely on frames of measurements to resolve the measurement origin uncertainty [55, 56, 57]. A frame means a batch of TDOA measurements that resulted from different emissions and received at different sensors over an interval T. The duration of a measurement frame, T, which is the receiver sampling interval in practice, is a design parameter that needs to be selected such that the TDOA measurements (across different sensors) resulting from a

common emission are included in the same frame. Note that multipath propagation is not addressed in this paper. Assuming that there are $m_{s,k}$ measurements received by the sth sensor at frame k, the measurement set is denoted by $\left\{y_{s,i_{s,k}}, i_{s,k} = 1, ..., m_{s,k}\right\}$, where $y_{s,i_{s,k}}$ refers to the $i_{s,k}$th measurement in the set. Each measurement either originated from a target of interest or from clutter. For a target-originated measurement, the measurement model is given in (2.3.1). Otherwise, the measurement is assumed to be uniformly distributed in the volume of the measurement space. Note that the volume in our case is the length of frame interval T. That is,

$$p(y_{s,i_{s,k}}) = \frac{1}{T}, \quad y_{s,i_{s,k}} \in [0, T). \tag{2.3.8}$$

The number of false alarms from clutter at each frame is assumed to have a Poisson distribution, i.e.,

$$p_\lambda(n_{fa}) = e^{-\lambda}\frac{\lambda^{n_{fa}}}{n_{fa}!}, \quad n_{fa} = 0, 1, ... \tag{2.3.9}$$

where λ is the average number of false alarms in each frame. To address the case of missed detections, one dummy measurement is added to the measurement set of each sensor. Therefore, the measurement set of sensor s is denoted by $\left\{y_{s,i_{s,k}}, i_{s,k} = 0, 1, ..., m_{s,k}\right\}$, where $y_{s,0}$ refers to the dummy measurement.

The time measurement is an incomplete position measurement, which means that one time measurement is insufficient to estimate the target position. Specifically, at least three TOA sensors are needed to localize a target in two-dimensional space. Therefore, it is necessary to group the measurements across sensors that could have originated from the common signal. Then, the grouped measurements are used to generate the composite measurement, which is a full-position measurement. This

process, called measurement-to-measurement association, is performed during each frame.

In practice, the received signals may not contain transmitter identification information, or the sensors may not transmit the measurement-origin information to the fusion center due to limited communication bandwidth. In the presence of measurement-origin uncertainty, the measurement-to-measurement association becomes especially challenging. In a synchronized sensor network, when the interval between signal transmission times of different targets is much larger than signal propagation time, the time-difference value of a pair of TOA measurements having a common origin is much smaller than that of the measurements having different origins. Thus, the measurement-to-measurement association can be performed using a gating technique [1]. However, when sensor clocks are unsynchronized and the arrival times of signals are measured by the local clock of each sensor, the time-difference value of a pair measurements contains sensor clock offset and cannot be used directly to associate measurements.

2.4 Multidimensional Assignment Algorithm

The multidimensional assignment algorithm using various constrained discrete optimization formulations is an efficient solution for the measurement-to-measurement association problem [50]. In this section, we review the standard MDA algorithm based on the TOA measurements and its extension to the correlated TDOA measurements [56]. Then, the limitations in applying the algorithms to unsynchronized sensor networks are discussed.

2.4.1 Standard Multidimensional Assignment Algorithm

In the MDA algorithm, an N_s-tuple of TOA measurements consisting of one measurement from each sensor at frame k is denoted by

$$Y_{i_{1,k}i_{2,k}...i_{N_s,k}} = \left\{ y_{s,i_{s,k}}, s = 1, ..., N_s \right\} \tag{2.4.1}$$

which represents a possible association, that is, all measurements in the tuple are deemed to have originated from the same target. Each N_s-tuple of measurements is assigned a cost $c_{i_{1,k}i_{2,k}...i_{N_s,k}}$, which is defined as the negative log-likelihood ratio [58]:

$$c_{i_{1,k}i_{2,k}...i_{N_s,k}} = -\log \frac{\Lambda\left(Y_{i_{1,k}i_{2,k}...i_{N_s,k}}|X_{t,k}\right)}{\Lambda\left(Y_{i_{1,k}i_{2,k}...i_{N_s,k}}|\emptyset\right)} \tag{2.4.2}$$

where $\Lambda\left(Y_{i_{1,k}i_{2,k}...i_{N_s,k}}|X_{t,k}\right)$ represents the likelihood that the N_s-tuple of measurements $Y_{i_{1,k}i_{2,k}...i_{N_s,k}}$ has originated from the same signal transmitted by the target located at $X_{t,k}$, while $\Lambda\left(Y_{i_{1,k}i_{2,k}...i_{N_s,k}}|\emptyset\right)$ represents the likelihood that the N_s-tuple is from a spurious source. The goal is to find the set of N_s-tuples that minimizes the global assignment cost.

Then, the data association can be formulated as an optimization problem with the constraints that each non-dummy measurement is assigned to only one target or declared a false alarm and that each target is associated with at most one measurement from each sensor. For brevity, the frame index k is ignored here. Then, the optimization problem is [58]

$$\min_{\rho_{i_1 i_2 ... i_{N_s}}} \sum_{i_1=0}^{m_1} \sum_{i_2=0}^{m_2} ... \sum_{i_{N_s}=0}^{m_{N_s}} c_{i_1 i_2 ... i_{N_s}} \rho_{i_1 i_2 ... i_{N_s}} \tag{2.4.3}$$

subject to

$$\begin{aligned}
\sum_{i_2=0}^{m_2}\sum_{i_3=0}^{m_3}\cdots\sum_{i_{N_s}=0}^{m_{N_s}}\rho_{i_1 i_2 \ldots i_{N_s}} &= 1 \qquad i_1 = 1,2,\ldots,m_1 \\
\sum_{i_1=0}^{m_1}\sum_{i_3=0}^{m_3}\cdots\sum_{i_{N_s}=0}^{m_{N_s}}\rho_{i_1 i_2 \ldots i_{N_s}} &= 1 \qquad i_2 = 1,2,\ldots,m_2 \\
&\vdots \qquad\qquad\qquad\quad \vdots \\
\sum_{i_1=0}^{m_1}\sum_{i_2=0}^{m_2}\cdots\sum_{i_{N_s-1}=0}^{m_{N_s-1}}\rho_{i_1 i_2 \ldots i_{N_s}} &= 1 \quad i_{N_s} = 1,2,\ldots,m_{N_s}
\end{aligned} \tag{2.4.4}$$

where $\rho_{i_1 i_2 \ldots i_{N_s}}$ is a binary indicator function defined as

$$\rho_{i_1 i_2 \ldots i_{N_s}} = \begin{cases} 1 & \text{if } \rho_{i_1 i_2 \ldots i_{N_s}} \text{ is included in the solution set} \\ 0 & \text{otherwise} \end{cases}. \tag{2.4.5}$$

The number of targets is equal to the number of N_s-tuples in the solution set. When $N_s = 2$, the MDA problem can be solved in polynomial time using the Auction algorithm [64, 65]. The MDA problem is NP-hard when $N_s \geq 3$, but it can be solved suboptimally based on Lagrangian relaxations [58].

Prior to the optimization step in the MDA algorithm, the first step is to calculate the cost of each candidate association. In general, it is assumed that the measurement noises of different sensors are uncorrelated. Thus, the likelihood $\Lambda\left(Y_{i_{1,k} i_{2,k} \ldots i_{N_s,k}} | X_{t,k}\right)$ is given by [58]

$$\Lambda\left(Y_{i_{1,k} i_{2,k} \ldots i_{N_s,k}} | X_{t,k}\right) = \prod_{s=1}^{N_s}\left(\left(1 - P_{D_s}\right)^{1-u(i_{s,k})}\left(P_{D_s} p(y_{s,i_{s,k}} | X_{t,k})\right)^{u(i_{s,k})}\right) \tag{2.4.6}$$

where P_{D_s} is the detection probability of sensor s and $u(i_{s,k})$ is a binary indicator function defined as

$$u(i_{s,k}) = \begin{cases} 0 & \text{if } i_{s,k} = 0 \\ 1 & \text{otherwise} \end{cases}. \tag{2.4.7}$$

With the assumption that the TOA measurement noise is a zero-mean white Gaussian random variable, $p(y_{s,i_{s,k}}|X_{t,k})$, the conditional probability density function (pdf) of a single TOA measurement $y_{s,i_{s,k}}$, is given by

$$p(y_{s,i_{s,k}}|X_{t,k}) = N\left(y_{s,i_{s,k}}; tr_{t,k} + \frac{\|X_{t,k} - X_s\|}{c} + \beta_{s,t}, \sigma_s^2\right) \tag{2.4.8}$$

where $X_{t,k}$ is unknown and replaced by its ML estimate, i.e.,

$$\hat{X}_{t,k} = \arg\max_{X_{t,k}} \Lambda\left(Y_{i_{1,k}i_{2,k}\ldots i_{N_s,k}}|X_{t,k}\right). \tag{2.4.9}$$

Note that it is assumed that $tr_{t,k}$ and $\beta_{s,t}$ in (2.4.8) are known in this case. Here, $N(y;\mu,\Sigma)$ refers to the normal distribution of a random variable y having mean μ and variance Σ. Since the false alarms are assumed to be uniformly distributed over the frame interval, the likelihood that the N_s-tuple is from a spurious source is defined as

$$\Lambda\left(Y_{i_{1,k}i_{2,k}\ldots i_{N_s,k}}|\emptyset\right) = \prod_{s=1}^{N_s}\left(\frac{1}{T}\right)^{u(i_{s,k})}. \tag{2.4.10}$$

2.4.2 MDA Algorithm Formulation for Correlated TDOA Measurements

As shown in (2.4.8), the transmission time of each signal is needed to estimate target positions and to evaluate the generalized log-likelihood ratios when TOA measurements are used in the MDA algorithm. However, this information is not available for passive localization of non-cooperative targets. To overcome this limitation, the MDA algorithm formulation for TDOA measurements, which are independent of the unknown transmission times, is developed in [56].

Given the N_s-tuple of TOA measurements $Y_{i_{1,k}i_{2,k}\ldots i_{N_s,k}}$, at most (N_s-1) non-dummy TDOA measurements can be obtained. By stacking them, we have an augmented vector $\Delta Y_{i_{1,k}i_{2,k}\ldots i_{N_s,k}}$ denoted by

$$\Delta Y_{i_{1,k}i_{2,k}\ldots i_{N_s,k}} = \begin{bmatrix} y_{2,i_{2,k}} - y_{1,i_{1,k}} \\ y_{3,i_{3,k}} - y_{1,i_{1,k}} \\ \vdots \\ y_{N_s,i_{N_s,k}} - y_{1,i_{1,k}} \end{bmatrix}. \tag{2.4.11}$$

Noted that these TDOA measurements are correlated due to the presence of the common measurement noise of the reference sensor, which constitutes a correlated joint Gaussian process. The conditional pdf of this joint Gaussian process is given by

$$p(\Delta Y_{i_{1,k}i_{2,k}\ldots i_{N_s,k}}|X_{t,k}) = N\left(\Delta Y_{i_{1,k}i_{2,k}\ldots i_{N_s,k}}; H(X_{t,k}) + B, R_{t,k}\right) \tag{2.4.12}$$

where $R_{t,k}$ is defined in (2.3.7). If the dummy measurement from sensor s is included in $Y_{i_{1,k}i_{2,k}\ldots i_{N_s,k}}$, the corresponding row and column are removed from $R_{t,k}$. Then, the likelihood $\Lambda(Y_{i_{1,k}i_{2,k}\ldots i_{N_s,k}}|X_{t,k})$, which is based on the correlated TDOA measurements $\Delta Y_{i_{1,k}i_{2,k}\ldots i_{N_s,k}}$ and independent of the transmission time, is given by

$$\Lambda\left(Y_{i_{1,k}i_{2,k}\ldots i_{N_s,k}}|X_{t,k}\right) = p(\Delta Y_{i_{1,k}i_{2,k}\ldots i_{N_s,k}}|X_{t,k}) \prod_{s=1}^{N_s} \left((1-P_{D_s})^{1-u(i_{s,k})} P_{D_s}^{u(i_{s,k})}\right). \tag{2.4.13}$$

However, it is still impossible to evaluate the pdf in (2.4.12) because the sensor clock offsets B and target position $X_{t,k}$ are unknown. It is assumed in most works using the MDA algorithm for measurement-to-measurement association that the sensors are aligned perfectly in advance [56, 60]. That is, sensor clock offset estimate $\hat{B}$

is known a priori. Then, the ML estimate of target position from $\Delta Y_{i_{1,k}i_{2,k}\ldots i_{N_s,k}}$ is given by

$$\hat{X}_{t,k} = \arg\max_{X_{t,k}} p(X_{t,k}|\Delta Y_{i_{1,k}i_{2,k}\ldots i_{N_s,k}}). \tag{2.4.14}$$

Since the noise $W_{t,k}$ is assumed to be Gaussian, the ML estimate $\hat{X}_{t,k}$ is given by

$$\hat{X}_{t,k} = \arg\min_{X_{t,k}} \left(\Delta Y_{i_{1,k}i_{2,k}\ldots i_{N_s,k}} - H(X_{t,k}) - \hat{B}\right)^T R_{t,k}^{-1} \left(\Delta Y_{i_{1,k}i_{2,k}\ldots i_{N_s,k}} - H(X_{t,k}) - \hat{B}\right). \tag{2.4.15}$$

Then the unknown target position is substituted by its ML estimate $\hat{X}_{t,k}$ in calculating the likelihood in (2.4.12).

If the sensor clock offsets are not known a priori, the target position cannot be estimated as in (2.4.14)–(2.4.15). Given an N_s-tuple of TOA measurements, there are at most $N_s - 1$ linearly independent equations but $N_s + 1$ unknown parameters including two target position parameters and $N_s - 1$ sensor clock offset parameters. As a result, the MDA algorithm [56] presented above cannot be used directly to solve the measurement-to-measurement association problem when sensors are not aligned perfectly in advance.

2.5 Joint Data Association, Sensor Synchronization and Target Localization

Considering the limitations in the application of the standard MDA algorithm to unsynchronized sensor networks, two novel MDA algorithms are proposed in this Section to realize data association, sensor synchronization and target localization simultaneously.

2.5.1 Joint Multidimensional Assignment Algorithm for Multisensor Synchronization

The goal of data association is to resolve the measurement origin uncertainties by finding the most likely set of N_s-tuples of TOA measurements. Each hypothesis gives one possible association result. To be specific, given the association hypothesis Φ_{l_k}, the measurements that originated from certain target t are deemed to be the N_s-tuple:

$$\left\{ y_{s,i_{s,k}^t}, s = 1, ..., N_s \right\}, t = 1, ..., N_t, \tag{2.5.1}$$

where $y_{s,i_{s,k}^t}$ is the $i_{s,k}^t$th measurement received by sensor s at frame k and is assumed to have originated from target t given Φ_{l_k}. The number of targets N_t is assumed to be known first and the extension to the case with an unknown number of targets is discussed later. For each association hypothesis, each non-dummy measurement is assigned to only one target or declared a false alarm, and each target has at most one non-dummy measurement from each sensor. Thus, the constraints on the association hypotheses Φ_{l_k} are

$$\begin{aligned} &\sum_{t=1}^{N_t} \rho_t^{l_k}\left(i_{s,k}^t\right) \leq 1, \quad i_{s,k}^t = 1, ..., m_{s,k}, \;\; s = 1, ..., N_s \\ &\sum_{i_{s,k}^t=1}^{n_{s,k}} \rho_t^{l_k}\left(i_{s,k}^t\right) \leq 1, \quad t = 1, ..., N_t, \;\; s = 1, ..., N_s \end{aligned} \tag{2.5.2}$$

where $\rho_t^{l_k}(i_{s,k}^t)$ is a binary variable defined as

$$\rho_t^{l_k}(i_{s,k}^t) = \begin{cases} 1 & \text{if the } i_{s,k}^t\text{th measurement at sensor } s \\ & \text{is included in the } t\text{th tuple of hypothesis } \Phi_{l_k} \\ 0 & \text{otherwise} \end{cases}. \tag{2.5.3}$$

The likelihood of measurements under hypothesis Φ_{l_k} is given by

$$\Lambda\left(Y_k|\theta_k, \Phi_{l_k}\right) = p\left(M_k|\Phi_{l_k}\right) p\left(Y_k|\theta_k, M_k, \Phi_{l_k}\right) \tag{2.5.4}$$

where Y_k denotes the set of all measurements received at frame k, M_k denotes the set of the number of measurements at each sensor, i.e., $M_k = \{m_{s,k}, s = 1, ..., N_s\}$, and parameter vector θ_k consisting of unknown target positions at frame k and sensor clock offsets is denoted by

$$\theta_k = \left[{X_{1,k}}^T, \cdots, {X_{N_t,k}}^T, B^T\right]^T. \tag{2.5.5}$$

With the assumption that sensors receive signals independently, $p\left(M_k|\Phi_{l_k}\right)$ can be evaluated as

$$\begin{aligned} & p\left(M_k|\Phi_{l_k}\right) \\ &= \prod_{s=1}^{N_s} p\left(m_{s,k}|\Phi_{l_k}\right) \\ &= \prod_{s=1}^{N_s} \left(\left(\prod_{t=1}^{N_t} \left(1 - P_{D_s}\right)^{1-u(i_{s,k}^t)} P_{D_s}^{u(i_{s,k}^t)} \right) p_\lambda\left(m_{fa}^s\right) \right) \end{aligned} \tag{2.5.6}$$

where $p_\lambda(\cdot)$ is the Poisson distribution given in (2.3.9), and m_{fa}^s denotes the number

of measurements that are declared as false alarms at sensor s and is given by

$$m_{fa}^{s} = \sum_{i_{s,k}=1}^{m_{s,k}} \zeta\left(i_{s,k}\right) \tag{2.5.7}$$

where

$$\zeta\left(i_{s,k}\right) = \begin{cases} 1 & \text{if } y_{s,i_{s,k}} \text{ is declared as a false alarm} \\ 0 & \text{otherwise} \end{cases}. \tag{2.5.8}$$

Since the targets transmit signals independently of one another, $p\left(Y_k|\theta_k, M_k, \Phi_{l_k}\right)$ is given by

$$p\left(Y_k|\theta_k, M_k, \Phi_{l_k}\right) = \prod_{t=1}^{N_t} p(\Delta Y^{l_k}_{i^t_{1,k} i^t_{2,k} \cdots i^t_{N_s,k}} | X_{t,k}, B) \prod_{s=1}^{N_s} \prod_{i_{s,k}=1}^{m_{s,k}} \left(\frac{1}{T}\right)^{\zeta(i_{s,k})} \tag{2.5.9}$$

where $\Delta Y^{l_k}_{i^t_{1,k} i^t_{2,k} \cdots i^t_{N_s,k}}$ is a correlated joint Gaussian process denoted by

$$\Delta Y^{l_k}_{i^t_{1,k} i^t_{2,k} \cdots i^t_{N_s,k}} = \begin{bmatrix} y_{2,i^t_{2,k}} - y_{1,i^t_{1,k}} \\ y_{3,i^t_{3,k}} - y_{1,i^t_{1,k}} \\ \vdots \\ y_{N_s,i^t_{N_s,k}} - y_{1,i^t_{1,k}} \end{bmatrix} \tag{2.5.10}$$

and $p(\Delta Y^{l_k}_{i^t_{1,k} i^t_{2,k} \cdots i^t_{N_s,k}} | X_{t,k}, B)$ is the conditional pdf given by

$$p(\Delta Y^{l_k}_{i^t_{1,k} i^t_{2,k} \cdots i^t_{N_s,k}} | X_{t,k}, B) = N\left(\Delta Y^{l_k}_{i^t_{1,k} i^t_{2,k} \cdots i^t_{N_s,k}}; H(X_{t,k}) + B, R_{t,k}\right) \tag{2.5.11}$$

where $R_{t,k}$ is defined in (2.3.7). If the dummy measurement from sensor s is included in $Y^{l_k}_{i^t_{1,k} i^t_{2,k} \cdots i^t_{N_s,k}}$, the corresponding row and column are removed from $R_{t,k}$.

Note that target positions and sensor clock offsets in (2.5.11) are unknown and they are thus substituted by their ML estimates. Since sensor clock offsets are the same for all targets, the parameter estimation problem must be solved as coupled across targets. That is,

$$\hat{\theta}_k^{l_k} = \arg\max_{\theta_k} \Lambda\left(Y_k|\theta_k, \Phi_{l_k}\right). \tag{2.5.12}$$

The likelihood function of unknown parameter θ_k can be expressed as

$$\Lambda\left(Y_k|\theta_k, \Phi_{l_k}\right) \propto N(\Delta Y^{l_k}; G_k(\theta_k), R_k) \tag{2.5.13}$$

where

$$\Delta Y^{l_k} = \begin{bmatrix} \Delta Y^{l_k}_{i^1_{1,k} i^1_{2,k} \cdots i^1_{N_s,k}} \\ \Delta Y^{l_k}_{i^2_{1,k} i^2_{2,k} \cdots i^2_{N_s,k}} \\ \vdots \\ \Delta Y^{l_k}_{i^{N_t}_{1,k} i^{N_t}_{2,k} \cdots i^{N_t}_{N_s,k}} \end{bmatrix}, \tag{2.5.14}$$

$$G_k(\theta_k) = \begin{bmatrix} H(X_{1,k}) + B \\ H(X_{2,k}) + B \\ \vdots \\ H(X_{N_t,k}) + B \end{bmatrix}, \tag{2.5.15}$$

and

$$R_k = \begin{bmatrix} R_{1,k} & 0 & \cdots & 0 \\ 0 & R_{2,k} & \cdots & 0 \\ \vdots & \vdots & \ddots & \vdots \\ 0 & 0 & \cdots & R_{N_t,k} \end{bmatrix}. \tag{2.5.16}$$

In order to find the ML estimate, one has to solve a nonlinear least squares (NLS) problem. This will be done using a numerical search via the iterated least squares (ILS) technique which will be discussed in Section IV-C.

The association result is the hypothesis with the maximum value of the generalized likelihood, i.e.,

$$\hat{\Phi}_k = \arg\max_{l_k} \Lambda\left(Y_k|\theta_k, \Phi_{l_k}\right). \tag{2.5.17}$$

The final estimates of target positions and sensor clock offsets are the ML estimates corresponding to association result $\hat{\Phi}_k$, i.e.,

$$\hat{\theta}_k = \arg\max_{\theta_k} \Lambda\left(Y_k|\theta_k, \hat{\Phi}_k\right). \tag{2.5.18}$$

When the number of targets is unknown, resolving the additional uncertainty in target cardinality is computationally expensive. This is a joint identification (determining the number of targets) and estimation (estimating target related parameters) problem [61]. Assuming that the maximum number of targets is Γ, the total number of hypotheses of target cardinality is $\Gamma + 1$. For a particular hypothesis H_k^γ assuming that target cardinality equals to γ, the unknown parameter vector is

$$\theta_k^\gamma = \left[{X_{1,k}}^T, \cdots, {X_{\gamma,k}}^T, B^T\right]^T \tag{2.5.19}$$

The JMDA4MS algorithm developed above is applied to each hypothesis H_k^γ to obtain the association result $\hat{\Phi}_k^\gamma$, the parameter estimates $\hat{\theta}_k^\gamma$ and the corresponding value of the generalized likelihood $\Lambda\left(Y_k|\theta_k^\gamma, \hat{\Phi}_k^\gamma\right)$. Then, the best hypothesis of target

cardinality can be identified as

$$\hat{H}_k^{\gamma} = \arg\max_{\gamma} \Lambda \left(Y_k | \theta_k^{\gamma}, \hat{\Phi}_k^{\gamma} \right). \tag{2.5.20}$$

An alternative approach is the minimum description length (MDL) criterion, which penalizes complicated models with a carefully designed complexity term [66, 67].

2.5.2 Joint Multiframe Multidimensional Assignment Algorithm

The observability of the parameters requires that the number of target-originated measurements be at least equal to the number of the parameters to be estimated. In the ideal case without missed detections or false alarms, we must have

$$(N_s - 1) \cdot N_t \geq 2N_t + N_s - 1 \tag{2.5.21}$$

where $(N_s - 1) \cdot N_t$ is the number of target-originated TDOA measurements in one frame, and $2N_t + N_s - 1$ is the number of the unknown parameters including target positions and sensor clock offsets. The above equation can be rewritten as

$$N_t \geq \frac{N_s - 1}{N_s - 3} \tag{2.5.22}$$

which specifies the requirement on the relationship between the number of targets and the number of sensors in two-dimensional space in the ideal case. For example, in a scenario where 4 sensors are used to localize 2 targets, there are at most 6 target-originated TDOA measurements and a number of false alarms but 7 unknown

parameters in one frame. Since false alarms should not be used for parameter estimation, target-related measurements are insufficient to obtain unique solutions for the unknown parameters. To overcome this problem, a joint multiframe multidimensional assignment (JMF-MDA) algorithm is developed here.

The JMF-MDA algorithm estimates target positions and sensor clock offsets using measurements in multiple frames. Since the measurement-to-measurement association is performed within each frame, the association hypothesis in the JMF-MDA algorithm is constituted by one hypothesis in each frame, i.e.,

$$\bar{\Phi}_l = \{\Phi_{l_k}\}_{k=1}^{K} \tag{2.5.23}$$

where Φ_{l_k} is the l_kth hypothesis at frame k as defined in (2.5.1) and has constraints given in (2.5.2), and K is the number of frames used in the JMF-MDA algorithm to guarantee observability. Since the exact number of target-originated measurements is unknown, one possible method to determine the value of K is to use

$$\sum_{k=1}^{K}\sum_{s=2}^{N_s} m_{s,k} \geq N_p + n_0 \tag{2.5.24}$$

where the left side of the equation is the number of TDOA measurements, the number of unknown parameters is $N_p = 2N_tK + N_s - 1$, and the positive integer n_0 is set as the average of the number of total false alarms in K frames, i.e., $n_0 = KN_s\lambda$.

Since each target emits signals independently from frame to frame, the likelihood of all measurements under hypothesis $\bar{\Phi}_l$ is given by

$$\Lambda\left(Y^{1:K}|\theta, \bar{\Phi}_l\right) = \prod_{k=1}^{K} \Lambda\left(Y_k|\theta_{X,k}, B, \Phi_{l_k}\right) \tag{2.5.25}$$

where $Y^{1:K}$ is the cumulative set of measurements available up to frame K, the likelihood of measurements in each frame is given in (2.5.4) and $\theta_{X,k}$ is unknown target positions at frame k

$$\theta_{X,k} = \left[{X_{1,k}}^T, \cdots, {X_{N_t,k}}^T\right]^T. \tag{2.5.26}$$

Thus, the augmented parameter vector θ is denoted by

$$\theta = \left[{\theta_{X,1}}^T, \cdots, {\theta_{X,K}}^T, B^T\right]^T. \tag{2.5.27}$$

Since the target positions and sensor clock offsets in (2.5.25) are unknown, they are substituted by their ML estimates. The likelihood function of θ can be expressed as

$$\Lambda\left(Y^{1:K}|\theta, \bar{\Phi}_l\right) \propto N(\Delta\bar{Y}^l; \bar{G}(\theta), \bar{R}) \tag{2.5.28}$$

where

$$\Delta\bar{Y}^l = \begin{bmatrix} \Delta Y^{l_1} \\ \vdots \\ \Delta Y^{l_K} \end{bmatrix}, \tag{2.5.29}$$

$$\bar{G}(\theta) = \begin{bmatrix} G_1(\theta_{X,1}, B) \\ \vdots \\ G_K(\theta_{X,K}, B) \end{bmatrix}, \tag{2.5.30}$$

and

$$\bar{R} = \begin{bmatrix} R_1 & \cdots & 0 \\ \vdots & \ddots & \vdots \\ 0 & \cdots & R_K \end{bmatrix}. \tag{2.5.31}$$

The ML estimate of θ is obtained by maximizing the likelihood funtion, i.e.,

$$\hat{\theta}^l = \arg\max_{\theta} \Lambda\left(Y^{1:K}|\theta, \bar{\Phi}_l\right). \tag{2.5.32}$$

This NLS problem can be solved using the ILS technique as illustrated in the next Section.

The association result and the parameter estimates are determined according to the hypothesis with the maximum generalized likelihood. When the number of targets is unknown, the additional uncertainty in target cardinality can be resolved as in (2.5.20). Note that the number of frames required in the JMF-MDA algorithm may be different across different hypotheses since the number of unknown parameters is hypothesis-dependent.

2.5.3 ML Estimator and ILS Technique

The maximization in (2.5.32) is a nonlinear, nonconvex optimization problem and a closed-form solution is not available [56]. We use the ILS technique here to obtain the ML estimate since no Hessian is needed for its implementation and it also provides an approximate covariance matrix for its estimate [48].

Given the ILS estimate after j iterations given by

$$\hat{\theta}^j = \left[\left(\hat{X}^j_{1,1}\right)^T, \cdots, \left(\hat{X}^j_{N_t,K}\right)^T, \left(\hat{B}^j\right)^T\right]^T, \tag{2.5.33}$$

the ILS estimate after the $(j+1)$th iteration will be

$$\hat{\theta}^{j+1} = \hat{\theta}^{j} + \left[(G_{\theta}^{j})^{T} \bar{R}^{-1} G_{\theta}^{j} \right]^{-1} (G_{\theta}^{j})^{T} \bar{R}^{-1} \left[\Delta \bar{Y}^{l} - \bar{G}(\hat{\theta}^{j}) \right] \tag{2.5.34}$$

where G_{θ}^{j} is the Jacobian matrix of the vector consisting of the stacked measurement functions with respect to augmented parameter evaluated at $\hat{\theta}^{j}$, denoted by

$$G_{\theta}^{j} = \left. \frac{\partial \bar{G}(\theta)}{\partial \theta} \right|_{\theta=\hat{\theta}^{j}} \tag{2.5.35}$$

Here, the Jacobian matrix is

$$G_{\theta} = \left[{G_{\theta,1,1}}^{T}, \cdots, {G_{\theta,t,k}}^{T}, \cdots, {G_{\theta,N_t,K}}^{T} \right]^{T} \tag{2.5.36}$$

where

$$G_{\theta,t,k} = \begin{bmatrix} \frac{\partial g_{t,2,k}}{\partial x_{1,1}} & \cdots & \frac{\partial g_{t,N_s,k}}{\partial x_{1,1}} \\ \frac{\partial g_{t,2,k}}{\partial y_{1,1}} & \cdots & \frac{\partial g_{t,N_s,k}}{\partial y_{1,1}} \\ \vdots & \ddots & \vdots \\ \frac{\partial g_{t,2,k}}{\partial x_{N_t,K}} & \cdots & \frac{\partial g_{t,N_s,k}}{\partial x_{N_t,K}} \\ \frac{\partial g_{t,2,k}}{\partial y_{N_t,K}} & \cdots & \frac{\partial g_{t,N_s,k}}{\partial y_{N_t,K}} \\ \frac{\partial g_{t,2,k}}{\partial b_{1}} & \cdots & \frac{\partial g_{t,N_s,k}}{\partial b_{1}} \\ \vdots & \ddots & \vdots \\ \frac{\partial g_{t,2,k}}{\partial b_{N_s}} & \cdots & \frac{\partial g_{t,N_s,k}}{\partial b_{N_s}} \end{bmatrix}^{T} \tag{2.5.37}$$

and

$$
\begin{aligned}
g_{t,s,k} &= h_s(X_{t,k}) + b_s \qquad s = 2, .., N_s \\
\frac{\partial g_{t,s,k}}{\partial x_{t,k}} &= \frac{1}{c} \cdot \left(\frac{x_{t,k} - x_s}{\|X_{t,k} - X_s\|} - \frac{x_{t,k} - x_1}{\|X_{t,k} - X_1\|} \right) \\
\frac{\partial g_{t,s,k}}{\partial y_{t,k}} &= \frac{1}{c} \cdot \left(\frac{y_{t,k} - y_s}{\|X_{t,k} - X_s\|} - \frac{y_{t,k} - y_1}{\|X_{t,k} - X_1\|} \right) \\
\frac{\partial g_{t,s,k}}{\partial x_{p,q}} &= 0 \qquad t \neq p \quad \text{or} \quad k \neq q \\
\frac{\partial g_{t,s,k}}{\partial y_{p,q}} &= 0 \qquad t \neq p \quad \text{or} \quad k \neq q \\
\frac{\partial g_{t,s,k}}{\partial b_s} &= 1 \\
\frac{\partial g_{t,s,k}}{\partial b_v} &= 0 \qquad v \neq s
\end{aligned}
\tag{2.5.38}
$$

An initial estimate $\hat{\theta}^0$ is necessary to perform the numerical search using the ILS technique [48]. Assuming that the initial estimates of the clock offsets are zero, the initial estimate of each target position can be obtained with each tuple of measurements using the trilateration method [68].

2.5.4 Improving Algorithm Efficiency

Computational cost is an important issue that needs to be considered when an algorithm is implemented to solve a practical data association problem. As indicated in [56, 57, 59], 95%–99% of the execution time is spent on the calculation of association cost, which involves the process of obtaining the ML estimates of the unknown parameters for each possible hypothesis. In order to improve the efficiency of the proposed algorithms, the number of hypotheses is analyzed and then several strategies are proposed here.

Number of Hypotheses

Given N_s sets of measurements at frame k, the total number of N_s-tuples of measurements is

$$N_{tuple,k} = n_{1,k} \prod_{s=2}^{N_s} (n_{s,k} + 1). \tag{2.5.39}$$

Note that there is no dummy measurement at reference sensor 1. Then, the number of hypotheses at frame k is

$$N_{h,k} = \frac{N_{tuple,k}!}{(N_{tuple,k} - N_t)!}. \tag{2.5.40}$$

In the JMF-MDA algorithm, the total number of hypotheses is

$$N_h = \prod_{k=1}^{K} N_{h,k} \tag{2.5.41}$$

In the case of localizing 3 targets using 4 sensors without missed detections or false alarms, the number of N_s-tuples is 192 and the number of hypotheses is 6.96768×10^6, which is a large number limiting application to real-time systems.

Gating Method

A gating process is set up to select the N_s-tuples that have high probability. When calculating the time-difference value between two TOA measurements that originate from a common signal, the same transmission time of signal can be subtracted out. Thus, the time difference of two measurements having the same origin will not exceed

a certain threshold with 95% confidence level, that is,

$$\Delta y_{th} = b_{\max} + \frac{d_{\max}}{c} + 4\sigma \tag{2.5.42}$$

where $b_{\max}$ is the maximum clock offset of sensors, $d_{\max}$ is the maximum distance between sensors, and σ is the standard deviation of TDOA measurement noise. When $b_{\max}$ is not available a priori, it can be estimated using a testing signal in the preprocessing period. That is,

$$\hat{b}_{\max} = \max_{s} |y_s - y_1 - h_s(X_t)| + 4\sigma \tag{2.5.43}$$

where y_s and y_1 are the arrival times of the testing signal at sensor s and sensor 1, respectively, X_t is the position from which the testing signal is transmitted, and 4σ is used to account for the measurement noise. After enumerating all possible N_s-tuples, the time-difference threshold Δy_{th} is used to prune unlikely tuples. Specifically, given an N_s-tuple, the TOA measurement with maximum value should fall inside the gate bounded by Δy_{th} around the measurement with the minimum value, which ensures that any two measurements in the tuple can pass the gating test. If an N_s-tuple fails the gating test, there is no need to use it in the hypothesis cost calculation. The decreased number of tuples will reduce the number of possible hypotheses.

N_{s_0}-D+Seq(2-D) Method

The total number of hypotheses increases exponentially with the number of sensors. To overcome this problem, the N_{s_0}-D+Seq(2-D) method, which is an efficient data association technique for large-scale sensor networks first proposed in [60], is considered

here. There are two steps in this method, namely, the N_{s_0}-D step and the Seq(2-D) step, which are modified here based on the needs of the algorithms proposed in this paper.

In the N_{s_0}-D step, the measurement-to-measurement association is performed among N_{s_0} sensors ($N_{s_0} < N_s$) using the proposed JMDA4MS (or JMF-MDA) algorithm. To be specific, the association hypotheses are built using the N_{s_0}-tuples that pass the gating test. Then, the generalized likelihood of the measurements at N_{s_0} sensors is evaluated for each association hypothesis as in (2.5.4). The association result, which is determined by the hypothesis with the highest generalized likelihood, consisting of N_t N_{s_0}-tuples is obtained. To meet the observability requirements, the value of N_{s_0} should be at least 4 as shown in (2.5.22), and the JMF-MDA algorithm is used if necessary as shown in (2.5.24).

The Seq(2-D) step involves a series of 2-D assignments and the number of 2-D assignments is $N_s - N_{s_0}$. After the N_{s_0}-D step, partial association result is available. In each 2-D step, a new sensor is selected from the remaining sensors and a 2-D assignment is formulated and solved using the proposed JMDA4MS (or JMF-MDA) algorithm. Specifically, the $N_{s'}$-tuples are built using the $(N_{s'} - 1)$-tuples in the previous association result and the measurements at sensor s' and validated using the gating method. Next, the generalized likelihood of the measurements at $N_{s'}$ sensors is evaluated for each association hypothesis as in (2.5.4). Then, the updated association results consisting of N_t $N_{s'}$-tuples are obtained with the corresponding parameter estimates. After one 2-D step, the length of each tuple in the association result is incremented by one. This process is performed repetitively until full tuples are obtained in the final association result.

To illustrate the effectiveness of the N_{s_0}-D+Seq(2-D) method, we compare the numbers of hypotheses before and after using this method. For simplicity, assume that the number of measurements is n_0 for each sensor. Then, the number of hypotheses in one frame without applying the N_{s_0}-D+Seq(2-D) method is

$$N_{h_1} = \frac{({n_0}^{N_s})!}{({n_0}^{N_s} - N_t)!} \tag{2.5.44}$$

where the number of hypotheses increases exponentially as the number of sensors increases. In the N_{s_0}-D+Seq(2-D) method, the number of hypotheses in the N_{s_0}-D step is

$$N_{h_{2,1}} = \frac{({n_0}^{N_{s_0}})!}{({n_0}^{N_{s_0}} - N_t)!} \tag{2.5.45}$$

and the number of hypotheses in each 2-D assignment is

$$N_{h_{2,2}} = \frac{(n_0)!}{(n_0 - N_t)!}. \tag{2.5.46}$$

Therefore, the total number of hypotheses after using the S_0-D+Seq(2-D) technique is

$$N_{h_2} = \frac{({n_0}^{N_{s_0}})!}{({n_0}^{N_{s_0}} - N_t)!} + (N_s - N_{s_0}) \times \frac{(n_0)!}{(n_0 - N_t)!} \tag{2.5.47}$$

where the number of hypotheses increases linearly as the number of sensors increases. As shown in Section VI, the gating method and the N_{s_0}-D+Seq(2-D) approach decrease the number of hypotheses and improve the efficiency of the proposed algorithms.

2.5.5 Extension to Target Tracking

In target tracking applications, the proposed algorithms can be used for system calibration so that the sensor clocks are synchronized by the estimated clock offsets and for track initialization so that tracks are initialized using the one-point initialization method [48] combined with the estimated target positions provided by the JMDA4MS algorithm or using the two-points initialization method [48] with the estimated target positions in first two frames provided by the JMF-MDA algorithm. Assume that target dynamic motion model is given by

$$X_{t,k+1} = f(X_{t,k}) + v_k \tag{2.5.48}$$

where $f(\cdot)$ is state transition function and v_k is a zero-mean white Gaussian process noise with standard deviation σ_v. With synchronized sensors, the MDA algorithm reviewed in Section III.B can be used to solve the measurement-to-measurement association problem at each frame, which provides a set of N_s-tuples of measurements. With initialized tracks, the measurement-to-track association problem to determine from which track an N_s-tuple of measurements originated is formulated as a 2-D assignment problem, where the target motion model is used for track state prediction. The details on 2-D assignment algorithm for measurement-to-track association can be found in [47]. With the associated N_s-tuple of measurements, the state of each track is updated with, for example, the Kalman filter or the extended Kalman filter [48].

2.6 Cramér-Rao Lower Bound

To evaluate the efficiency of the ML estimator, we calculate the CRLB for joint target position and sensor clock offset estimation. The CRLB provides a lower bound on the covariance matrix of an unbiased estimator as [48]

$$E\left[\left(\theta-\hat{\theta}\right)\left(\theta-\hat{\theta}\right)^{T}\right] \geq J(\theta)^{-1} \tag{2.6.1}$$

where $J(\theta)$ is the Fisher information matrix (FIM), θ is the parameter vector to be estimated and $\hat{\theta}$ is the estimate. The FIM is

$$J(\theta) = E\left[\left(\nabla_{\theta} \ln \Lambda\left(\theta\right)\right)\left(\nabla_{\theta} \ln \Lambda\left(\theta\right)\right)^{T}\right]\Big|_{\theta=\theta_{\text{true}}} \tag{2.6.2}$$

in which θ_{true} is the true value of the parameter and ∇ is gradient operator. With the likelihood function of parameter given in (2.5.27), the gradient of the log-likelihood function is defined as

$$\nabla_{\theta} \ln\left(\Lambda\left(\theta\right)\right) = {G_{\theta}}^{T} \bar{R}^{-1}\left(\bar{Y}-\bar{G}(\theta)\right) \tag{2.6.3}$$

which, when plugged into (2.6.2), gives

$$J(\theta) = {G_{\theta}}^{T} \bar{R}^{-1} G_{\theta}\big|_{\theta=\theta_{\text{true}}} \tag{2.6.4}$$

where $\bar{R}$ and G_{θ} are given in (2.5.31) and (2.5.36), respectively.

2.7 Simulations

A series of simulations is presented in this Section to evaluate the performances of the proposed algorithms. Two different scenarios are designed each for the JMDA4MS algorithm and the JMF-MDA algorithm. In the first scenario, the positions of the first three targets are uniformly distributed in the region surrounded by the sensors where the ranges of the X and Y coordinates are both 0–1000m, while target 4 is randomly located in the region where the ranges of the X and Y coordinates are 0–1000m and 1000–1200m, respectively. In the second scenario, the positions of targets 1 and 2 in the first two frames are considered. It is assumed that targets move with a nearly constant velocity motion model such that their speeds and directions are uniformly distributed in 10–20 m/s and 0–2π, respectively, with process noise standard deviation 0.01 m/s^2. The duration of a measurement frame is 5s. It is assumed that the targets periodically emit signals with the frame interval but the transmission times of their initial signals are uniformly distributed over the first frame time. Note that the JMDA4MS algorithm and JMF-MDA algorithm are not limited to any particular target motion model and emission pattern. The propagation speed of signals is set as $c = 3 \times 10^8$ m/s.

The sensors are located at (0m, 0m), (0m, 500m), (500m, 1000m), (1000m, 600m) and (1000m, 0m). For each sensor, the measurement noise standard deviation is equal to 10^{-9}s and the probability of detection is 0.9. As shown in Table 2.1, six sets of sensor clock offset parameters are considered in the simulations to demonstrate the performances of the proposed algorithms in different situations. The number of false alarms is assumed to be Poisson distributed with an average of 2 false alarms per

sensor per frame. The arrival times of false alarms are assumed to be uniformly distributed over the frame period. Fig. 2.1 presents TOA measurements from five sensors in one frame and their origins. As shown in Fig. 2.1(a), resolving measurement-origin uncertainty is not a trivial task, especially in the presence of sensor clock offsets, missed detections and false alarms.

The algorithms compared on the first scenario include the proposed JMDA4MS algorithm with gating technique (named JMDA4MS in the tables and figures), the efficient JMDA4MS algorithm using both the gating technique and the N_{s_0}-D+Seq(2-D) method (named E-JMDA4MS), the standard MDA algorithm [56], and the MDA-ML algorithm that applies the MDA algorithm to obtain association results and then uses the ML estimator to estimate clock offsets. Similarly, the proposed JMF-MDA algorithm with gating technique (named JMF-MDA), the proposed JMF-MDA algorithm algorithm using both the gating technique and the N_{s_0}-D+Seq(2-D) method (named E-JMF-MDA), the standard MDA algorithm [56], and the MDA-ML algorithm are compared on the second scenario. The numbers of hypotheses in the proposed JMDA4MS algorithm without the gating method (named I-JMDA4MS) and the JMF-MDA algorithm without the gating method (named I-JMF-MDA) are also analyzed. All simulation results are averaged over 100 Monte Carlo runs.

Table 2.1: Clock offsets of sensors with respect to reference sensor (sensor 1)

Bias coefficient (s)	b_2	b_3	b_4	b_5
$1 \cdot 10^{-6}$	$-1 \cdot 10^{-6}$	$1 \cdot 10^{-6}$	$2 \cdot 10^{-6}$	$5 \cdot 10^{-6}$
$1 \cdot 10^{-5}$	$-1 \cdot 10^{-5}$	$1 \cdot 10^{-5}$	$2 \cdot 10^{-5}$	$5 \cdot 10^{-5}$
$1 \cdot 10^{-4}$	$-1 \cdot 10^{-4}$	$1 \cdot 10^{-4}$	$2 \cdot 10^{-4}$	$5 \cdot 10^{-4}$
$1 \cdot 10^{-3}$	$-1 \cdot 10^{-3}$	$1 \cdot 10^{-3}$	$2 \cdot 10^{-3}$	$5 \cdot 10^{-3}$
$1 \cdot 10^{-2}$	$-1 \cdot 10^{-2}$	$1 \cdot 10^{-2}$	$2 \cdot 10^{-2}$	$5 \cdot 10^{-2}$
$1 \cdot 10^{-1}$	$-1 \cdot 10^{-1}$	$1 \cdot 10^{-1}$	$2 \cdot 10^{-1}$	$5 \cdot 10^{-1}$

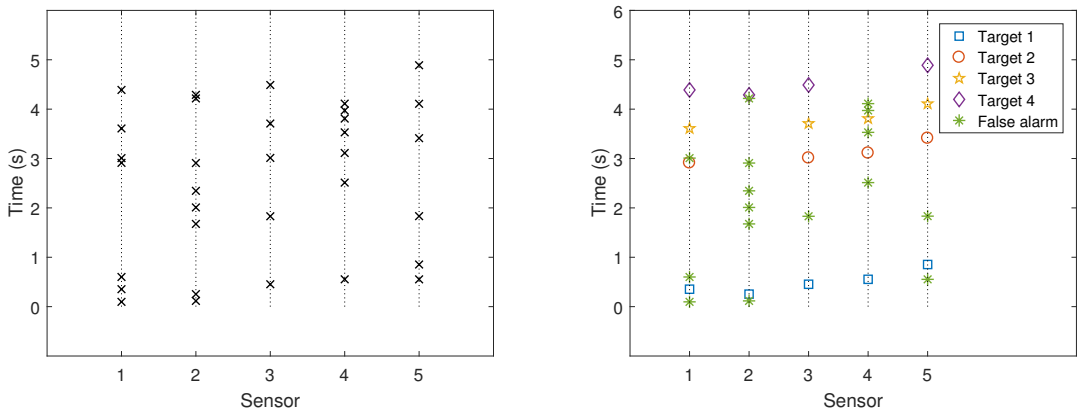

(a) (b)

Figure 2.1: Illustration of TOA measurements from five sensors in one frame. (a) TOA measurements, (b) Measurement origins.

To quantify the data association performances of the proposed algorithms, we define some metrics first. Given an association tuple, it falls into one of the following two categories: 1) Completely correct (CC) association: the association tuple consists of all measurements that originated from the same target; 2) Incompletely correct (IC) association: the association tuple does not include all measurements from the same origin but includes the measurements from other signal, false alarms or dummy measurement (i.e., missed detection). Then, the completely correct association rate (CCAR) is defined by

$$\text{CCAR} = \frac{N_{CC}}{N_{CC} + N_{IC}} \tag{2.7.1}$$

where N_{CC} is the number of completely correct association tuples and N_{IC} is the number of incompletely correct tuples.

As shown in Table 2.2, the CCAR results of the proposed JMDA4MS algorithm are much better than those of the standard MDA algorithm [56] for all parameter sets in the first scenario. This is because sensor clock offsets affect association performance

if they are not properly handled in data association. The E-JMDA4MS algorithm also yields improved association performance over the standard MDA algorithm. Table 2.3 shows the CCAR values of the JMF-MDA algorithm, the E-JMF-MDA algorithm and the MDA algorithm in the second scenario, leading to similar conclusions.

Table 2.2: Completely correct association rates of algorithms in scenario 1

Bias coefficient (s)	JMDA4MS	E-JMDA4MS	MDA
$1 \cdot 10^{-6}$	99.74%	97.25%	27.50%
$1 \cdot 10^{-5}$	99.85%	96.55%	23.11%
$1 \cdot 10^{-4}$	98.46%	97.32%	22.50%
$1 \cdot 10^{-3}$	99.03%	95.41%	24.50%
$1 \cdot 10^{-2}$	99.25%	97.68%	25.00%
$1 \cdot 10^{-1}$	98.25%	96.67%	15.42%

Table 2.3: Completely correct association rates of algorithms in scenario 2

Bias coefficient (s)	JMF-MDA	E-JMF-MDA	MDA
$1 \cdot 10^{-6}$	99.72%	98.08%	31.25%
$1 \cdot 10^{-5}$	99.04%	97.58%	27.75%
$1 \cdot 10^{-4}$	99.50%	96.87%	23.50%
$1 \cdot 10^{-3}$	98.75%	95.08%	25.96%
$1 \cdot 10^{-2}$	99.46%	97.72%	25.00%
$1 \cdot 10^{-1}$	98.96%	96.87%	12.50%

Next, the sensor synchronization performances of the proposed algorithms are evaluated. The JMDA4MS and JMF-MDA algorithms perform data association, target localization and sensor synchronization simultaneously, while the MDA algorithm solves the data association problem and estimates the target positions ignoring the clock offsets of sensors. The MDA-ML algorithm estimates the clock offsets based on the association results obtained from the MDA algorithm. Fig. 2.2 and Fig. 2.3 show the root mean square error (RMSE) values of sensor clock offset estimates obtained by different algorithms in scenarios 1 and 2, respectively. As the benchmark,

the $\sqrt{\text{CRLB}}$ values of clock offsets are also plotted. The JMDA4MS and JMF-MDA algorithms yield much better sensor synchronization performance than the MDA-ML algorithm, especially in the scenario where the sensor clock offsets are large. The main reason for this is that association errors degrade sensor synchronization performance in the MDA-ML algorithm. The proposed algorithms alleviate this problem by performing data association and sensor clock alignment simultaneously.

To illustrate target localization performance, the position estimates of different algorithms are compared next. Fig. 2.4 and Fig. 2.5 show the RMSE values of the target position estimates obtained by the proposed algorithms, the standard MDA algorithm and the MDA-ML algorithm in scenarios 1 and 2, respectively. The corresponding $\sqrt{\text{CRLB}}$ values of target positions are calculated for comparison as well. It is observed that the position RMSE values of the proposed algorithms are much lower than those of the MDA algorithm and the MDA-ML algorithm, and are very close to the $\sqrt{\text{CRLB}}$ values. Moreover, the target localization accuracies of the proposed algorithms do not change as the sensor clock offsets increase. With the MDA algorithm and the MDA-ML algorithm, however, the association errors and sensor clock offset estimation errors degrade the localization performance because they are performed separately. It can be seen from the Fig. 2.4 that the RMSE values of target 4 and the corresponding CRLB values are higher than those of other three targets, which confirms that localization accuracies get worse as targets move away from the region surrounded by the sensors.

To analyze the effectiveness of the gating method and the N_{s_0}-D+Seq(2-D) approach, we compare the numbers of hypotheses and the computation times of the

algorithms with and without using these methods. All algorithms are coded in MATLAB and run on an Intel i7 2.80 GHz laptop. The numbers of hypotheses and the computation times are averaged over 100 Monte Carlo runs as shown in Tables 2.4 and 2.5. In the gating method, $b_{\max}$ is set as the maximum clock offset according to Table 2.1 and d_{max} is equal to 1500m. It can be seen that the numbers of hypotheses in the I-JMDA4MS and I-JMF-MDA algorithms are very large, but they are significantly reduced by using the gating technique and further decreased by the N_{s_0}-D+Seq(2-D) method. The execution times of the algorithms after utilizing these two methods are acceptable for practical applications. Moreover, as shown in Figs. 2.2–2.5, the E-JMDA4MS and E-JMF-MDA algorithms yield accurate target localization and sensor synchronization results, which are comparable to those of the JMDA4MS and JMF-MDA algorithms. Due to the large numbers of hypotheses, the I-JMDA4MS and I-JMF-MDA algorithms are not implemented.

Table 2.4: Numbers of hypotheses and computation times of algorithms in scenario 1

Bias	Number of hypotheses			Computation time (s)	
coefficient (s)	I-JMDA4MS	JMDA4MS	E-JMDA4MS	JMDA4MS	E-JMDA4MS
$1 \cdot 10^{-6}$	$9.24 \cdot 10^{14}$	788.72	152.72	5.92	0.46
$1 \cdot 10^{-5}$	$5.48 \cdot 10^{14}$	1191.38	173.34	8.72	0.48
$1 \cdot 10^{-4}$	$7.84 \cdot 10^{14}$	1077.54	187.44	8.41	0.57
$1 \cdot 10^{-3}$	$1.31 \cdot 10^{15}$	935.68	183.94	7.02	0.64
$1 \cdot 10^{-2}$	$6.08 \cdot 10^{14}$	918.34	188.54	7.94	0.89
$1 \cdot 10^{-1}$	$4.27 \cdot 10^{14}$	2836.66	591.29	21.29	3.07

2.8 Conclusions

This paper formulated the problems of target localization, sensor synchronization and data association within a unified framework where these three problems were

Table 2.5: Numbers of hypotheses and computation times of algorithms in scenario 2

Bias	Number of hypotheses			Computation time (s)	
coefficient (s)	I-JMF-MDA	JMF-MDA	E-JMF-MDA	JMF-MDA	E-JMF-MDA
$1 \cdot 10^{-6}$	$6.21 \cdot 10^{10}$	568.46	137.68	4.42	0.44
$1 \cdot 10^{-5}$	$6.02 \cdot 10^{10}$	862.36	168.48	6.45	0.52
$1 \cdot 10^{-4}$	$3.62 \cdot 10^{10}$	962.84	157.84	7.27	0.49
$1 \cdot 10^{-3}$	$6.50 \cdot 10^{10}$	865.66	166.16	6.54	0.52
$1 \cdot 10^{-2}$	$4.18 \cdot 10^{10}$	1057.28	191.04	8.99	1.06
$1 \cdot 10^{-1}$	$5.72 \cdot 10^{9}$	642.50	243.38	8.37	2.38

solved simultaneously. In the proposed JMDA4MS algorithm and the JMF-MDA algorithm, the generalized likelihood of each hypothesis was calculated considering the fact that TDOA measurements are correlated and that sensors are unsynchronized. The association result was the hypothesis with the maximum generalized likelihood. The estimates of target positions and sensor clock offsets were obtained using an ML estimator based on the association result. Simulation results showed that the proposed algorithms outperform the standard MDA algorithm and the MDA-ML algorithm in terms of correct association rate, target position and sensor clock offset estimation accuracies when sensors are unsynchronized. The main reason for this is that the interdependence between data association and parameter estimation is handled correctly in the proposed algorithms. In addition, a gating method was utilized to prune unlikely association and the N_{s_0}-D+Seq(2-D) method was applied in large-scale sensor networks. It was shown through simulations that the proposed methods reduce both the number of hypotheses and computation times, improving the efficiency of the algorithms and maintaining the estimation accuracies and the association correctness.

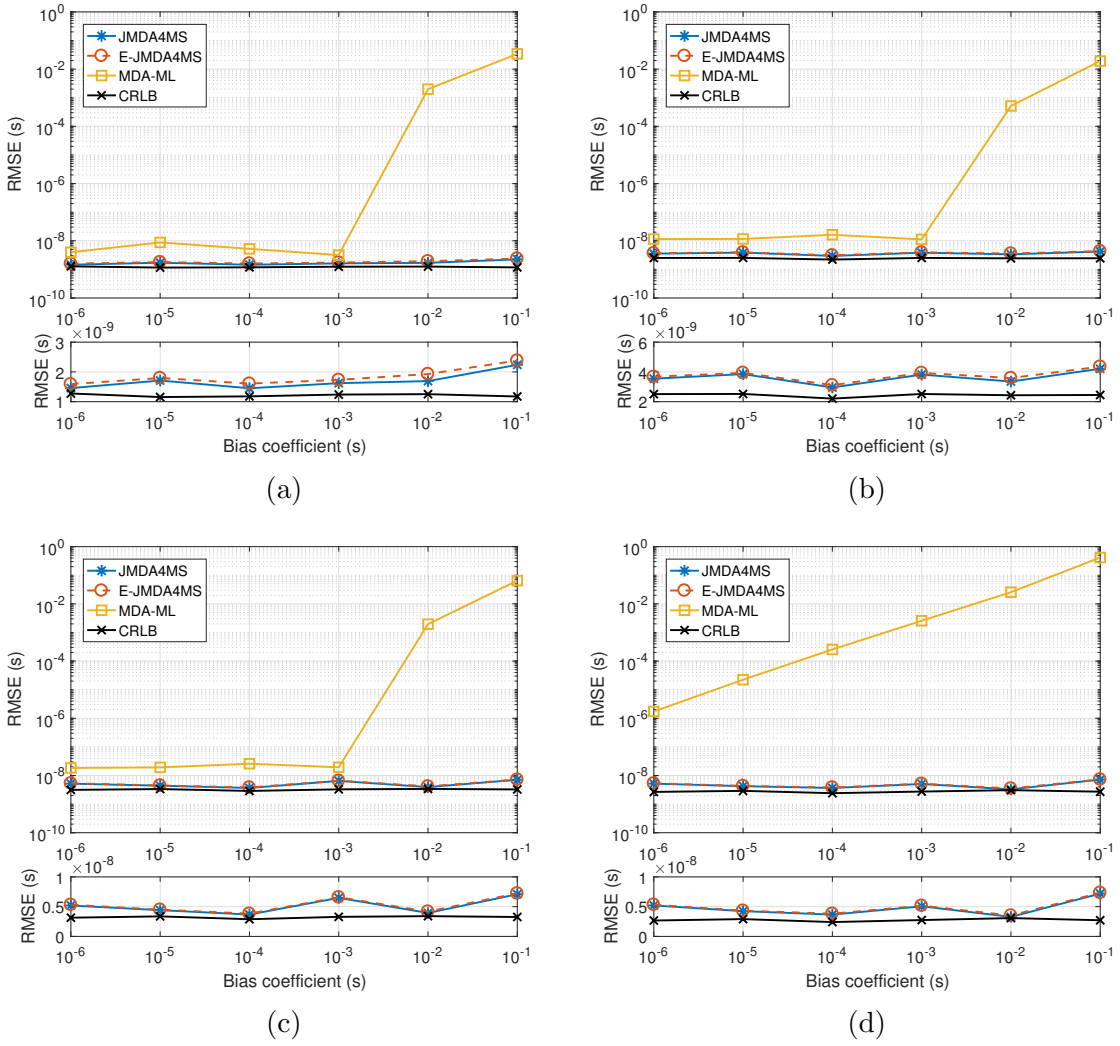

Figure 2.2: Comparison of sensor clock offset RMSE by different algorithms in scenario 1. (a) RMSE of clock offset estimate on b_2, (b) RMSE of clock offset estimate on b_3, (c) RMSE of clock offset estimate on b_4, (d) RMSE of clock offset estimate on b_5.

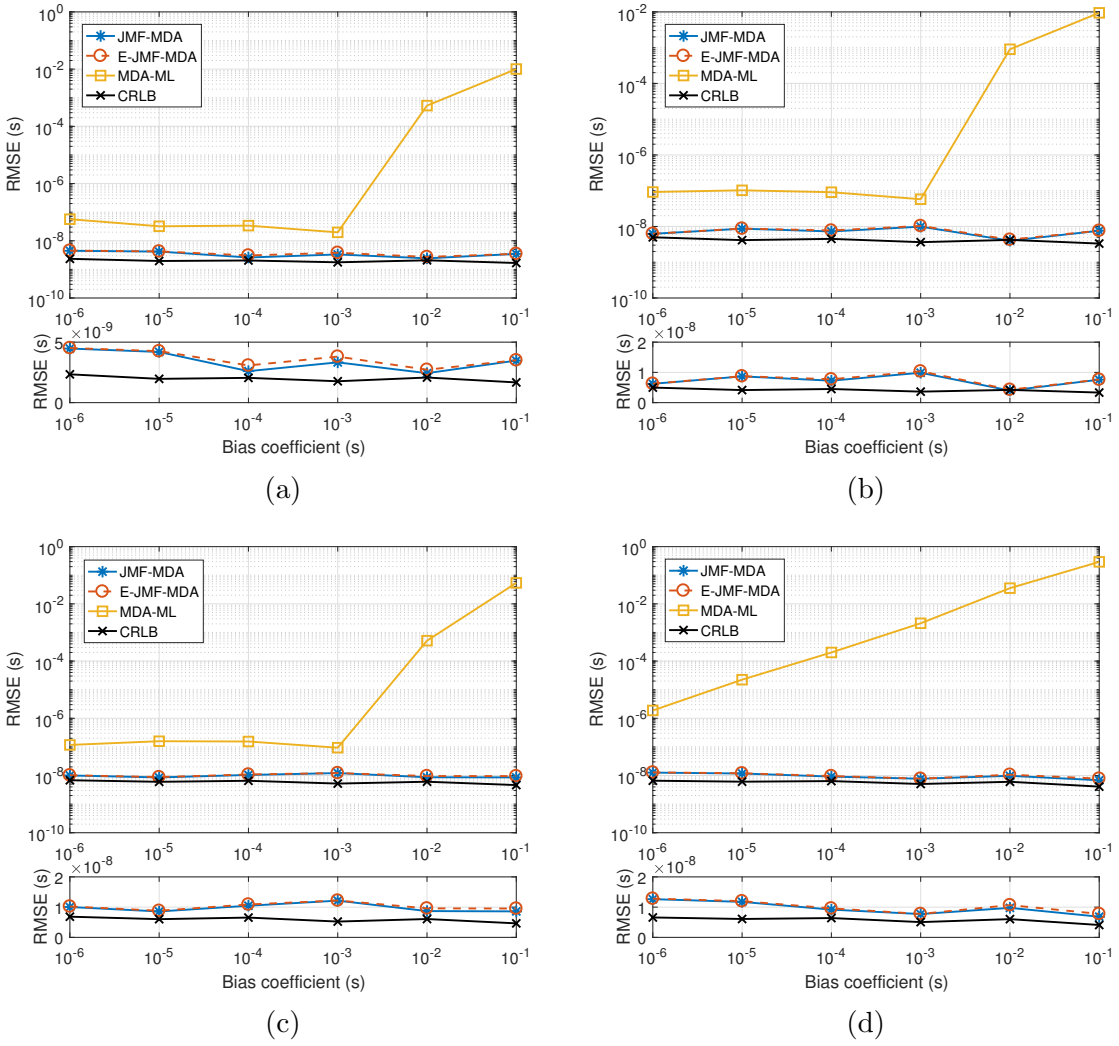

Figure 2.3: Comparison of sensor clock offsets RMSE by different algorithms in scenario 2. (a) RMSE of clock offset estimate on b_2, (b) RMSE of clock offset estimate on b_3, (c) RMSE of clock offset estimate on b_4, (d) RMSE of clock offset estimate on b_5.

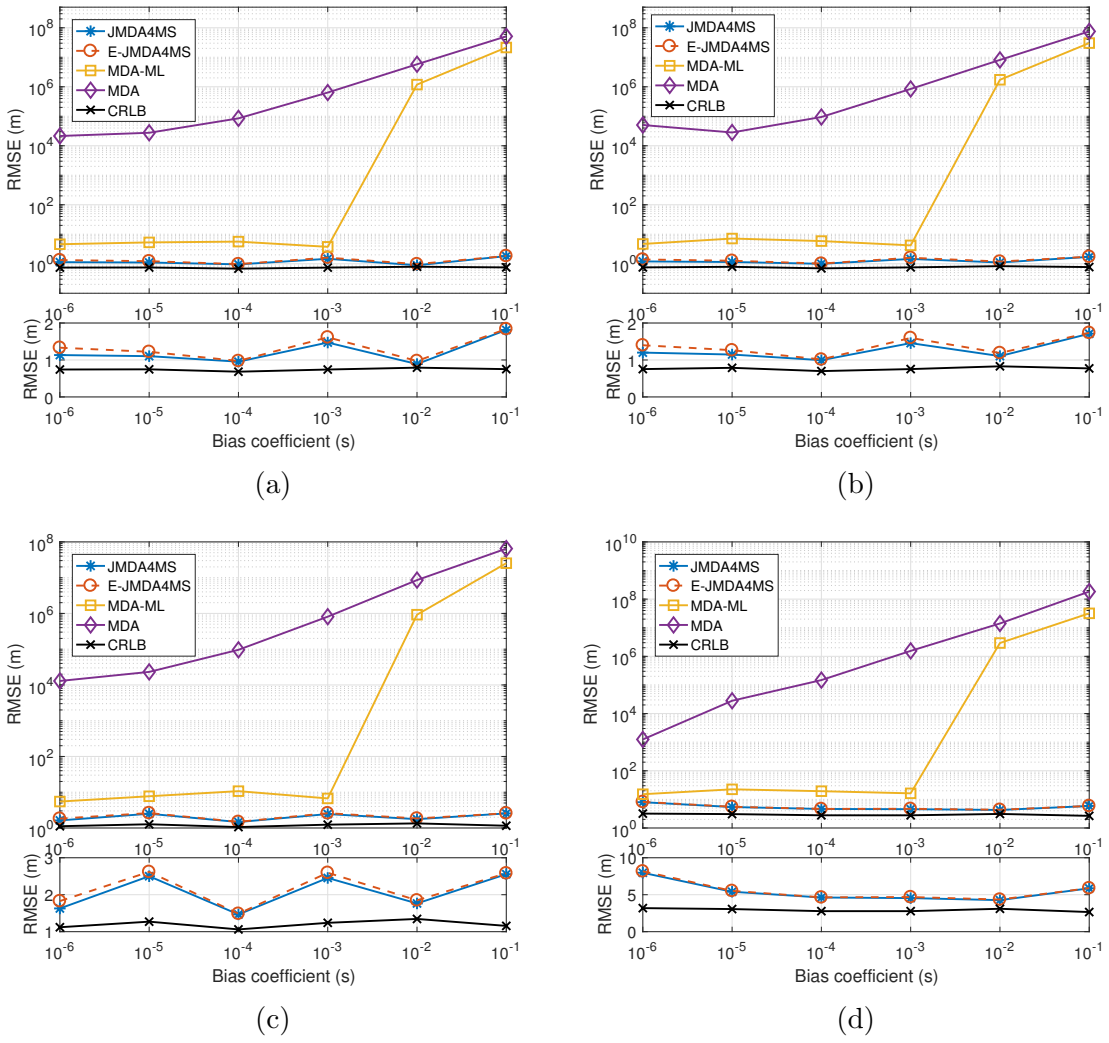

Figure 2.4: Comparison of position RMSE by different algorithms in scenario 1. (a) Position RMSE of target 1, (b) Position RMSE of target 2, (c) Position RMSE of target 3, (d) Position RMSE of target 4.

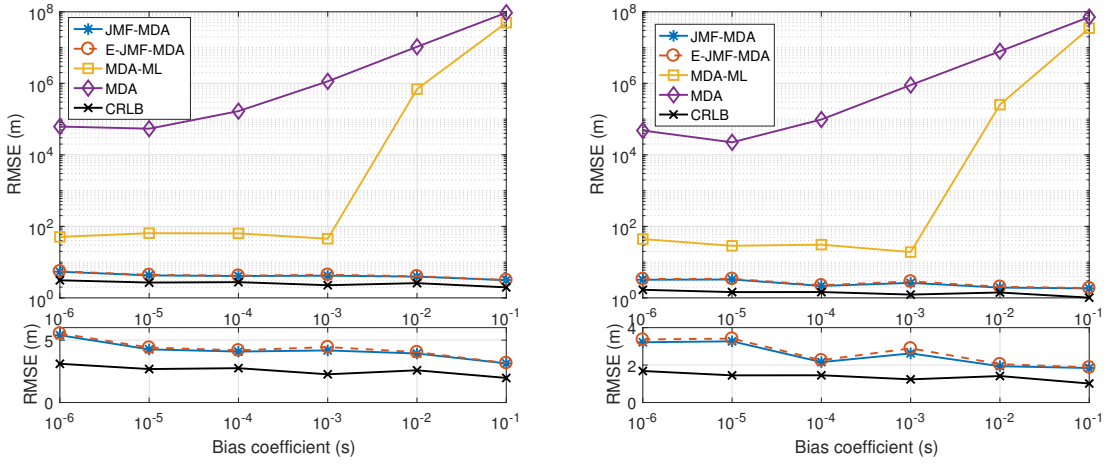

Figure 2.5: Comparison of position RMSE by different algorithms in scenario 2. (a) Position RMSE of target 1, (b) Position RMSE of target 2.

The following chapter is a reproduction of a peer-reviewed article submitted to the IEEE::

T.Ge, R. Tharmarasa, M. Bradford, T. Kirubarajan, "Sequence-Aided Data Association for Tracking Multiple On-road Targets With Unknown Interactions", Submitted to *IEEE Transactions on Aerospace and Electronic Systems*, May 2020.

Chapter 3

Sequence-Aided Data Association for Tracking Multiple On-road Targets With Unknown Interactions

3.1 Abstract

This paper considers the problem of tracking multiple on-road targets. Traditionally, multitarget tracking algorithms assume that targets move independently of one another or that targets move dependently where the interaction between targets can be described accurately with empirical motion behavior models. In practice, in the case of ground targets, the interactions are usually unknown and time-varying due

to complex road conditions and changes in traffic volume, making multitarget tracking more challenging. In general, on-road targets tend to move in an orderly manner along the centerline of each lane of the roads except for occasional lane changes. However, this characteristic is not exploited in target tracking literature. Therefore, this paper proposes a novel sequence-aided data association algorithm that incorporates target position sequence information into data association to enhance association and tracking performances, especially in the case of unknown target interactions. To address the uncertainty in target position sequence, a sequence-aided data association based multiple-hypothesis tracking algorithm is developed. The conditional posterior Cramér-Rao lower bound is derived as the theoretical performance benchmark. Simulation results show that the proposed algorithms achieve better performance than traditional tracking methods that do not make use of on-road target interactions.

3.2 Introduction

On-road target tracking plays an important role in many applications, ranging from ground surveillance to intelligent transportation systems and autonomous driving [69, 70, 71, 72]. The objective of this paper is to exploit the motion characteristics of on-road targets to improve multiple target tracking accuracy and reliability.

Road maps represent one of the most important prior information sources for on-road target tracking since they significantly reduce target motion uncertainties by constraining the motion of targets moving along roads. Many different approaches for using map information in target tracking, which can be divided into two categories according to their assumptions of target dynamics model, have been studied in the

literature. In the first category, the target motions are modeled in the ground coordinates with different options to incorporate road constraints. Directional process noise is one method that guides target states evolving along the direction of the road over time [19, 20], but this method cannot guarantee that target state estimates are positioned on the roads all the time. Road map information represented as state constraint can be incorporated into the Kalman filter (KF) and into the extended Kalman filter (EKF) with various options, such as the model reduction method [21], the pseudo-measurements method [22, 23], and the estimate projection method [24]. In the particle filter (PF), the road constraints are enforced on state estimates by discarding off-road particles to correct the state probability density function [73, 74, 75]. In the second category of approaches that make use of road map information, the target motions are described in the road coordinates using a target kinematic state consisting of the traveled distance, displacement from lane centerline, and their derivatives [26, 27, 28, 76, 77]. In [76], a single target is tracked in one-dimensional (1-D) road coordinate using the Kalman filter and the particle filter. With application to the multi-lane road case, the target longitudinal and lateral maneuvering behaviors are modeled in 2-D road coordinates and estimated by the Interacting Multiple Model (IMM) estimators using three different schemes, namely, centralized, distributed and sequential, to fuse radar data and image-sensor based measurements in [77].

On-road targets usually interact with their neighbors while moving along roads because of the limits imposed by traffic volume and road conditions [26]. These interactions between targets are usually handled using dependent motion models in most existing works. The social force model (SFM) proposed is utilized in [78] to describe the interactions between pedestrians and surrounding objects (e.g., buildings

and walls) using the forces introduced by a potential field. In [25], a modified SFM is proposed to model on-road target dynamics and combined with a moving horizon estimator (MHE) for target tracking. In [70], the group behavior model (GBM) describing the joint behavior of multiple vehicles using a traffic force is proposed for video-based target tracking. As another option for motion modeling, the car-following models (CFMs) describe the on-road target dynamics as a process of each target following its preceding one in traffic flow. In [26], the CFM is used to track multiple targets on single-lane roads assuming that a certain target sequence is maintained during the observation period. To extend this approach to the multi-lane case, the microscopic traffic model consisting of the CFM and lane-changing model is utilized and integrated with the unscented Kalman filter (UKF) in [27] and with the particle filter in [28] for multiple vehicle tracking. In most approaches using dependent motion models, multiple target states are estimated jointly in stacked form, which results in high computational cost. In practice, it is also difficult to obtain the prior knowledge about the exact behavior models and the corresponding model parameters to accurately describe target dynamics at all times because of the unknown and varying inter-target relationships. The overall tracking performance can degrade when mismatched model and/or model parameters are used. Therefore, the algorithms relying on an empirical dynamic model is unable to handle the interactions between on-road targets effectively.

In multitarget tracking (MTT) problems, one fundamental challenge is to determine the target from which a certain measurement originated in the presence of missed detections and false alarms, which is referred to as the data association problem [47]. In [26, 27], a 2-D assignment between one track list and one measurement list is used

to resolve the measurement origin uncertainty in vehicle tracking. In [16], target kinematic and class information is integrated into 2-D and multiframe (i.e., one track list and multiple measurement lists over time) assignments to improve association and tracking performances such that the accuracy of the target classifier is modeled by a confusion matrix. A feature-augmented multidimensional association algorithm is proposed in [79] for tracking ground vehicles using passive acoustic sensor arrays. The multiple hypothesis tracking (MHT) algorithm [15], a highly effective but computationally expensive technique considering data association across multiple scans, is used in [25] to track multiple on-road targets.

In a constrained operational area, such as highways, the idiosyncrasies of on-road target dynamics make the on-road tracking problems distinct from the standard (unconstrained and independent) multitarget tracking problem. The unknown and time-varying interactions among targets are still a challenge for target tracking as discussed above. Another characteristic of on-road motion is that, in general, targets tend to move in an orderly manner along the centerline of each lane of the roads except for occasional lane changes. To the best of our knowledge, this phenomenon of target position sequence has not yet been exploited by the algorithms for tracking multiple on-road targets, especially in the data association process. Moreover, different from feature-aided and classification-aided data association where additional explicit measurements of target feature or classes are available, the target sequence information is implicitly embedded in target kinematic states and is difficult to extract and utilize as an additional source of measurement. All these observations provide the motivation for the work in this paper.

There are three main contributions in this paper. First, we propose a novel data

association algorithm, called the sequence-aided 2D assignment (SA-2DA) algorithm, which incorporates the information of target position sequence into data association to obtain improved association and tracking performances, especially in the case of unknown target interactions. Second, the multiple-hypothesis framework integrated with the SA-2DA algorithm is developed to handle unknown and time-varying target sequences in each lane. In the process of hypothesis evaluation, the uncertainty in target sequence is resolved according to the hypothesis with the highest probability at each time step. Without any assumption on target behavior models, the proposed algorithm is robust and reliable in real scenarios where target interactions are unknown. Third, the conditional posterior Cramér-Rao lower bound (PCRLB) is derived to quantify the performance of the proposed sequence-aided tracking algorithm.

The remainder of the paper is organized as follows. In Section II, the target motion models and the measurement model in 2-D road coordinates are introduced. In Section III, the motion estimators (i.e., the longitudinal motion filter and the lane filter) and the standard 2-D assignment algorithm for data association are reviewed. The sequence-aided data association algorithm is proposed in Section IV. Considering the target-sequence uncertainty, the SA-2DA-based multiple hypothesis tracking algorithm (SA-2DA-MHT) is proposed in Section V. The conditional PCRLB is derived in Section VI. Simulation results are presented in Section VII along with discussions on the advantages of the proposed algorithm over other existing multiple target tracking algorithms. Finally, conclusions are discussed in Section VIII.

3.3 Background

3.3.1 Two-Dimensional Road Representation

With digitized vector road maps, a road can be approximated with sufficient accuracy by a set of consecutive linear segments [76]. Denote the ith segment of the road as s_i. The centerline of segment s_i is represented by its starting point $X_i^c = [x_i, y_i]^T$ and its direction angle θ_i with respect to the X-axis direction of 2-D Cartesian coordinates. The normalized direction vector of the segment s_i is $e_i^r = [\cos(\theta_i), \sin(\theta_i)]^T$ and the normalized displacement vector from the left boundary to the right boundary of the segment is $e_i^d = [\sin(\theta_i), -\cos(\theta_i)]^T$, where $e_i^r \perp e_i^d$. The centerline length of the segment s_i is defined as $\lambda_i = \left\| X_{i+1}^c - X_i^c \right\|$, where X_{i+1}^c is the centerline endpoint of segment s_i and the centerline starting point of segment s_{i+1}.

Each point on the road can be represented as $X_p = (r_p, d_p)$ in 2-D road coordinates, where r_p is the arc length from the road starting point X_1^c to the projection point of X_p in the mileage coordinate and d_p is the signed displacement of X_p from the road centerline in the displacement coordinate. Through the road-to-Cartesian coordinate transformation, the coordinate of point p in 2-D Cartesian coordinates, denoted as $X_p^c = (x_p, y_p)$, can be uniquely represented as

$$X_p^c = X_i^c + (r_p - r_i)e_i^r + d_p e_i^d, \quad r_i < r_p < r_{i+1} \tag{3.3.1}$$

where the arc length of segment starting point X_i^c is expressed as $r_i = \sum_{i=1}^{i-1} \lambda_i$.

3.3.2 Target Motion Models in 2-D Road Coordinates

The motion of an on-road target is described more naturally and conveniently in the road coordinates than in the Cartesian coordinates [77]. Target motions can be decomposed into the along-road motion and the across-road motion according to the two dimensions of the road coordinates [27].

The longitudinal state of the target t at time step k is defined by

$$X_t^r(k) = [r_t(k), \dot{r}_t(k)]^T \tag{3.3.2}$$

where $r_t(k)$ and $\dot{r}_t(k)$ are the position and velocity of the target t at time step k measured in terms of the arc length on the road, respectively. The longitudinal dynamics of on-road targets depend on both road condition and driver behaviors [77]. Due to the large distance between targets on the road with low traffic volume, targets are more likely to move independently without interaction. In this case, the independent motion models can be used to describe the target dynamics, such as the discrete nearly constant velocity model [80], i.e.,

$$X_t^r(k+1) = F_{cv} X_t^r(k) + G w_t(k) \tag{3.3.3}$$

where the state transition matrix F_{cv} and noise gain G are

$$F_{cv} = \begin{bmatrix} 1 & T \\ 0 & 1 \end{bmatrix}, \; G = \begin{bmatrix} T^2/2 \\ T \end{bmatrix} \tag{3.3.4}$$

where T is the sampling interval, and $w_t(k)$ is a zero-mean Gaussian white process

noise with standard deviation σ_{w_t} considered as a noisy acceleration component to describe uncertainties of driver behaviors. Other independent motion models are summarized in [80].

When a target moves on the road network with high traffic volume and complex road conditions, its longitudinal dynamics are influenced by the interactions between the target and its preceding objects. Generally, the interactions can be described as an additional acceleration term denoted as a_t and incorporated into the dynamic motion model as,

$$X_t^r(k+1) = F_{cv} X_t^r(k) + G(a_t(k) + w_t(k)) \tag{3.3.5}$$

According to the car-following theory, the acceleration (or deceleration) of a target is a response of the stimulus from the surrounding [81]. The formulations of car-following models vary according to the definitions of the stimulus. In the case of the General Motors driver-behavior models [82], the acceleration of each target is defined as a function of its longitude state relative to its preceding target. An example of the General Motors models is the linear Helly model [83], where

$$a_t(k) = c_1 \Delta r(k) + c_2 \Delta \dot{r}(k) + c_3 \dot{r}_t(k) + c_4 \tag{3.3.6}$$

where $\Delta r(k)$ and $\Delta \dot{r}(k)$ are the relative distance and velocity between the target t and its preceding target, respectively, while c_1, c_2, c_3 and c_4 are the parameters that are obtained by experiments [84].

Assuming that targets move along the centerline of each lane, the lateral state of

the target t at time step k is defined by

$$X_t^d(k) = d(l_t(k)) \tag{3.3.7}$$

where $d(l_t(k))$ is the displacement of the centerline of lane $l_t(k)$ in which target t is currently located. When the road segment has L lanes and the width of each lane is $2\delta_d$, the displacement of the centerline of the l-th lane is given by $d(l) = (2l - L - 1)\delta_d, l = 1, ..., L$. Assuming that the lane-changing process happens instantaneously, the lateral dynamics (i.e., the lane sequence $\{l(k), k = 1, ..., K\}$) is modeled as a homogeneous Markov chain with a known transition probability matrix (TPM) $\Pi = [\pi_{ij}]_{i,j=1}^{L}$ and an initial probability vector $u(0) = [u_1(0), ..., [u_L(0)]^T$, where

$$\begin{aligned} \pi_{ij} &= P(l(k) = j | l(k-1) = i), \quad i, j = 1..., L \\ u_i(0) &= P(l(0) = i), \quad i = 1..., L \end{aligned} \tag{3.3.8}$$

3.3.3 Measurement Model

Sensors, such as ground moving target indicator (GMTI) radar and camera [76, 77], can be used for on-road target localization and tracking. Position measurements are the most basic information provided by most of sensors and used in tracking algorithms [26]. Without loss of generality and for simplicity, it is assumed that position measurements are available in or have been transformed into the 2-D road coordinates. For details of measurement projection process with original measurements being in non-road coordinates, the reader is referred to [21, 24].

In the presence of noise, clutter and multipath in real environments, the received measurements are inaccurate and may suffer from missed detections and false alarms

[47]. The measurement that originated from target t and detected by the sensor with probability P_d at time step k is defined as

$$Z(k) = HX_t(k) + v(k)$$
$$\begin{bmatrix} Z^r(k) \\ Z^d(k) \end{bmatrix} = \begin{bmatrix} 1 & 0 & 0 \\ 0 & 0 & 1 \end{bmatrix} \begin{bmatrix} X_t^r(k) \\ X_t^d(k) \end{bmatrix} + \begin{bmatrix} v^r(k) \\ v^d(k) \end{bmatrix} \tag{3.3.9}$$

where $Z^r(k)$ and $Z^d(k)$ denote the mileage and displacement measurements, respectively; $v^r \sim N(0, \sigma_{v^r}^2)$ and $v^d \sim N(0, \sigma_{v^d}^2)$ are mutually uncorrelated Gaussian white-noise processes. False alarms are assumed to be uniformly distributed in the volume of measurement space and their number has a Poisson distribution with parameter λ [47], i.e.,

$$p(n_{fa}) = e^{-\lambda} \frac{\lambda^{n_{fa}}}{n_{fa}!},\ n_{fa} = 0, 1, ... \tag{3.3.10}$$

The set of measurements reported at time step k is denoted as

$$Z(k) = \{Z_m(k), m = 1, ..., M(k)\} \tag{3.3.11}$$

where $Z_m(k)$ is the m-th measurement and $M(k)$ denotes the number of received measurements, The cumulative set of measurements available up to time step K is denoted as

$$Z^K = \{Z(k), k = 1, ..., K\} \tag{3.3.12}$$

3.4 2-D Assignment Based Multitarget Tracking in Road Coordinates

The motion estimators consisting of a longitudinal state estimator and a lane filter and the data association algorithm as the two major components in a standard on-road multitarget tracking algorithm [1, 47], are reviewed in this section.

3.4.1 Motion Estimator

Based on the assumed longitudinal motion models, such as the nearly constant velocity (NCV) model (3.3.3) and the car-following model (3.3.5), the longitudinal states can be updated recursively using the Kalman filter when both the motion model and the measurement model are linear or using the extended Kalman filter when the models are nonlinear. For details about the KF and EKF, the reader is referred to [48].

The target's lateral states can be estimated over time by the lane filter (LF) [27]. Denoting the probability of the target in lane i at time step $k-1$ given Z^{k-1} as

$$u_i(k-1) = p(l(k-1) = i|Z^{k-1}), \quad i = 1, ..., L \tag{3.4.1}$$

the predicted probability of the target in lane j at time step k is expressed as

$$\begin{aligned} u_j(k|k-1) &= p(l(k) = j|Z^{k-1}) \\ &= \sum_{i=1}^{L} \pi_{ij} u_i(k-1) \end{aligned} \tag{3.4.2}$$

When a new measurement is available at time step k, the probability $u_j(k)$ is updated

by

$$\begin{aligned} u_j(k) &= p(l(k) = j|Z^k) \\ &= \frac{1}{c}\Lambda_j^d(k)u_j(k|k-1) \end{aligned} \tag{3.4.3}$$

where the normalization factor c is given by

$$c = \sum_{j=1}^{L} \Lambda_j^d(k)u_j(k|k-1) \tag{3.4.4}$$

and the likelihood function $\Lambda_j^d(k)$ is defined as

$$\begin{aligned} \Lambda_j^d(k) &= p(Z^d(k)|d(j)) \\ &= N(Z^d(k); d(j), \sigma_{v^d}^2) \end{aligned} \tag{3.4.5}$$

3.4.2 Data Association for Multitarget Tracking

In a multitarget tracking scenario, one fundamental issue is to determine from which target a certain measurement originated in the presence of missed detections and false alarms, which is referred to as the data association problem [47]. The assignment algorithm, where the data association problem is formulated as a constrained discrete optimization problem, has been widely used in the multitarget tracking systems due to its efficiency and effectiveness [16].

In 2-D assignment, the association is performed between the latest list of measurements and the list of established tracks, where each measurement-to-track association candidate is assigned a cost. The objective is to find the optimal assignment $A^*(k)$

which minimizes the global association cost given by [16]

$$C(k|A(k)) = \sum_{m=0}^{M(k)} \sum_{t=0}^{N(k)} c(k,m,t)a(k,m,t) \tag{3.4.6}$$

where $M(k)$ and $N(k)$ are the number of measurements and the number of tracks, respectively. That is,

$$A^*(k) = \arg\min_{A(k)} C(k|A(k)) \tag{3.4.7}$$

This 2-D assignment problem can be solved in polynomial time using the Auction algorithm [64]. The assignment result is subject to the one-to-one constraints that each track is assigned to at most one measurement and that each measurement is assigned to at most one track and the non-empty association constraint that the dummy measurement cannot be assigned to the dummy track [16], i.e.,

$$\begin{aligned} &\sum_{m=0}^{M(k)} a(k,m,t) = 1, \quad t = 1,2,...,N(k) \\ &\sum_{t=0}^{N(k)} a(k,m,t) = 1, \quad m = 1,2,...,M(k) \end{aligned} \tag{3.4.8}$$

where $a(k,m,t)$ is a binary indicator function defined as

$$a(k,m,t) = \begin{cases} 1 & \text{if measurment } Z_m(k) \text{ is assigned to track } X_t(k) \\ 0 & \text{otherwise} \end{cases} \tag{3.4.9}$$

and $A(k)$ is a set of complete assignments denoted as

$$A(k) = \{a(k,m,t),\ t = 0,1,...,N(k),\ m = 0,1,...,M(k)\} \tag{3.4.10}$$

The assignment $a(k,0,t)$ denotes that track t is not associated with any measurement. Similarly, $a(k,m,0)$ corresponds to the event that the mth measurement is not associated with any existing track.

The measurement-to-track association cost $c(k,m,t)$ in (3.4.6) is defined as the negative log-likelihood ratio [16]

$$c(k,m,t) = -\log \frac{\Lambda(Z_m(k)|X_t(k))}{\Lambda(Z_m(k)|t=0)} \tag{3.4.11}$$

where the likelihood that measurement $Z_m(k)$ originated from track t is given by

$$\Lambda(Z_m(k)|X_t(k)) = (1-P_d)^{1-u(m)}(P_d \cdot p\left(Z_m(k)|X_t(k)\right))^{u(m)} \tag{3.4.12}$$

and the likelihood that the measurement is a false alarm is given by

$$\Lambda(Z_m(k)|t=0) = \lambda^{u(m)} \tag{3.4.13}$$

where $u(m)$ is a binary indicator function defined as

$$u(m) = \begin{cases} 0 & m = 0 \\ 1 & m \neq 0 \end{cases}. \tag{3.4.14}$$

With the assumption that longitudinal and lateral measurement noises are mutually uncorrelated, the conditional probability density function (pdf) in (3.4.12) can be expressed as

$$p\left(Z_m(k)|X_t(k)\right) = p\left(Z_m^r(k)|X_t^r(k)\right) p\left(Z_m^d(k)|X_t^d(k)\right) \tag{3.4.15}$$

where

$$\begin{aligned} p\left(Z_m^r(k)|X_t^r(k)\right) &= N\left(Z_m^r(k); \hat{Z}_t^r(k|k-1), S_t^r(k)\right) \\ p\left(Z_m^d(k)|X_t^d(k)\right) &= \sum_{i=1}^{L} u_{t,i}(k|k-1) N\left(Z_m^d(k); d(i), \sigma_{v^d}^2\right) \end{aligned} \tag{3.4.16}$$

where $\hat{Z}_t^r(k|k-1)$ and $S_t^r(k)$ are the predicted mileage measurement of track t at time step k and its associated variance, respectively, and $u_{t,i}(k|k-1)$ is the predicted probability of track t given by (3.4.2).

Note that the predicted mileage measurement and its associated variance are determined by the assumed longitudinal motion model. In practice, the motion model used to describe the longitudinal dynamics is not accurate since the motion interactions between on-road targets are unknown and time-varying. Specifically, target longitudinal dynamics may transform from an independent mode to an interacting mode when it moves from a road with low traffic volume to one with high traffic volume and vice versa. The exact transition times in these cases are usually unknown. When targets move inter-dependently, the interaction model and the corresponding model parameters that may vary with different road conditions are not accurately known. Moreover, the dependent relationship between targets changes as their position sequence changes. Mismatched model and/or model parameters may lead to inaccurate predicted mileage measurements and the correspondingly incorrect likelihood values, which may result in wrong association and degraded overall tracking performance. To overcome this problem, additional implicit or explicit information based on the understanding of the idiosyncrasies of the on-road target tracking problem needs to be exploited to improve data association performance, especially in the

case of inaccurate motion model.

3.5 Target Sequence-Aided Data Association

One of the distinguishing features of on-road target motion is that each target moves approximately along the centerline of the lane by following any preceding target. Target positions in each lane is ordered in mileage road coordinate and this sequence does not change over a short period of time. The objective here is to present a novel sequence-aided data association algorithm that utilizes the information of target position sequence to improve data association and tracking performances, especially when target motion model is inaccurate.

Assuming that target position order in each lane at time step k is known and can be expressed as

$$I(k) = \{I_l(k), l = 1, ..., L\} \tag{3.5.1}$$

where $I_l(k)$, target position order in lane l, is defined as

$$\begin{gathered} I_l(k) = \left(t_1^l, t_2^l, ..., t_{N_t^l(k)}^l\right) \\ \text{subject to } \; r_{t_i^l}(k) > r_{t_{i+1}^l}(k), \; i = 1, \ldots, N_l(k) \end{gathered} \tag{3.5.2}$$

where $r_{t_i^l}(k)$ and $r_{t_{i+1}^l}(k)$ are the mileage positions of the t_i^l-th target and the t_{i+1}^l-th target in ordered set $I_l(k)$, respectively; $N_l(k)$ is the number of tracks in lane l and $N(k) = \sum_{l=1}^{L} N_l(k)$. The assumption that target position sequence is known will be relaxed in the following Section. Here, we denote ordered set by $(\cdot)$ and unordered set by $\{\cdot\}$.

According to the Bayes' theorem [1], the posterior probability of association event

$A_i(k)$ conditioned on target position sequence and all measurements available up to time step k is given by

$$p\left(A_i(k)|I(k),Z^k\right)=\frac{p\left(I(k)|A_i(k),Z^k\right)p\left(A_i(k)|Z^k\right)}{p\left(I(k)|Z^k\right)} \tag{3.5.3}$$

Since $p\left(I(k)|Z^k\right)$, the probability of target position sequence, is the same for all association events, we have

$$p\left(A_i(k)|I(k),Z^k\right)\propto p\left(I(k)|A_i(k),Z^k\right)p\left(A_i(k)|Z^k\right) \tag{3.5.4}$$

where $p\left(I(k)|A_i(k),Z^k\right)$ is the posterior probability of target position sequence $I(k)$ given association event $A_i(k)$ and all available measurements Z^k, and $p\left(A_i(k)|Z^k\right)$, the probability of association event $A_i(k)$ given all measurements Z^k, can be expressed as

$$p\left(A_i(k)|Z^k\right)\propto p\left(Z(k)|A_i(k),Z^{k-1}\right)p(A_i(k)) \tag{3.5.5}$$

where the independence of the association event $A_i(k)$ from Z^{k-1} is made use of. Note that the unconditional probability of $A_i(k)$ can be expressed in terms of the target detection probabilities and the number of false alarm measurements for this association event, both of which are assumed to be independent of the past [14]. Thus, the probability $p\left(A_i(k)|Z^k\right)$ is evaluated by [1]

$$p\left(A_i(k)|Z^k\right)\propto\prod_{m=1}^{M(k)}\left(\frac{1}{\lambda}\cdot p\left(Z_m(k)|X_{t_m}(k)\right)\right)^{\tau_m}\prod_{t=1}^{N(k)}(P_d)^{u_t}(1-P_d)^{1-u_t} \tag{3.5.6}$$

where the indicator variable τ_m denotes that the m-th measurement originated from a target, the indicator variable u_t denotes that the t-th target is associated with one

measurement, and $p\left(Z_m(k)|X_{t_m}(k)\right)$, the measurement likelihood function of associating t_m-th target to $Z_m(k)$ as indicated by $A_i(k)$, is given by (3.4.15).

Given an association event and the measurements at time step k, the updated target longitudinal states $\hat{X}_t^r(k|k) = [\hat{r}_t(k|k), \hat{\dot{r}}_t(k|k)]^T$ and associated covariance $P_t(k|k)$ can be obtained from the longitudinal motion estimator as discussed in Section III.A. Then, the mileage position component of target t is distributed as $N(r_t(k); \hat{r}_t(k|k), P_t^r(k|k))$, where $P_t^r(k|k)$ is the variance of the position component. Denoting the mileage distance between target t_i^l and target t_{i+1}^l by $\Delta r_i^l(k) = r_{t_i^l}(k) - r_{t_{i+1}^l}(k)$, $i = 1, .., N_l(k) - 1$, the pdf of the stacked vector consisting of the mileage distances $R^l(k) = [\Delta r_1^l(k), \Delta r_2^l(k), ..., \Delta r_{N_l(k)-1}^l(k)]^T$ is given by

$$p\left(R^l(k)|Z^k\right) = N\left(R^l(k); \hat{R}^l(k|k), P_{R^l}(k|k)\right) \tag{3.5.7}$$

with

$$\hat{R}^l(k|k) = \begin{bmatrix} \hat{r}_{t_1^l}(k|k) - \hat{r}_{t_2^l}(k|k) \\ \hat{r}_{t_2^l}(k|k) - \hat{r}_{t_3^l}(k|k) \\ \vdots \\ \hat{r}_{t_{N_l(k)-1}^l}(k|k) - \hat{r}_{t_{N_l(k)}^l}(k|k) \end{bmatrix} \tag{3.5.8}$$

and

$$\begin{aligned} P_{R^l}(k|k) &= \left[P_{R^l,ij}(k|k)\right],\ i,j = 1, ..., N_l(k) - 1 \\ P_{R^l,ij}(k|K) &= \begin{cases} -P_{t_j^l}^r(k|k) & i = j - 1 \\ P_{t_i^l}^r(k|k) + P_{t_{i+1}^l}^r(k|k) & i = j \\ -P_{t_i^l}^r(k|k) & i = j + 1 \\ 0 & \text{otherwise} \end{cases} \end{aligned} \tag{3.5.9}$$

The information of target position sequence indicates that the mileage distance between any two neighboring targets in the same lane should not be less than zero. If the knowledge of the safe-following distance to avoid collision ($\Delta r_{safe} \geq 0$) is known a priori, the mileage distance difference should satisfy

$$\Delta r_i^l(k) \geq \Delta r_{safe},\ i = 1, ..., N_l(k) - 1 \tag{3.5.10}$$

Thus, the posterior probability of target sequence $I(k)$ can be evaluated by

$$p\left(I(k)|A_i(k), Z^k\right) = \prod_{l=1}^{L} \left(P(R^l(k) > \Delta R_{safe}^l | Z^k) \prod_{i=1}^{N_l(k)} p(l_{t_i^l}(k) = l | Z^k) \right) \tag{3.5.11}$$

where $p(l_{t_i^l}(k) = l|Z^k)$, the probability of track t_i^l in lane l at time step k, is given by (3.4.3), and

$$P(R^l(k) > \Delta R_{safe}^l | Z^k) = 1 - \Phi\left(\frac{\Delta R_{safe}^l - \hat{R}^l(k|k)}{\sqrt{P_{R^l}(k|k)}} \right) \tag{3.5.12}$$

where ΔR_{safe}^l is a column vector with $N_l(k) - 1$ elements of Δr_{safe}, and $\Phi(\cdot)$ is the cumulative distribution function of the standard Gaussian distribution.

The posterior probability of each association event A_i can be evaluated by substituting (3.5.6) and (3.5.11) into (3.5.4). Then, the best association event is the one with the maximum posterior probability, that is,

$$A_I^*(k) = \arg\max_{A_i(k)} p\left(A_i(k)|I(k), Z^k\right) \tag{3.5.13}$$

The number of association events increases as the number of measurements and the

number of tracks increase. To improve algorithm efficiency, the Murty's algorithm [85] is used to generate the K-best assignments. Only these association events are evaluated as above at each time step.

3.6 SA-2DA-Based Multiple-Hypothesis Tracking

The information of target position sequences can improve data association and the overall tracking performance. The sequence of target position, however, is not known a priori and varies over time in real scenarios. The multi-target tracking algorithm proposed in this Section explicitly considers target sequence uncertainty by integrating the sequence-aided data association algorithm into the multiple-hypothesis framework.

3.6.1 Hypothesis Generation

When a target moves from its current lane to the destination lane, its position in the destination lane is determined not only by its current dynamics but also the dynamics and behaviors of the possible following target in the destination lane, which results in the uncertainty of target sequence in the destination lane. The hypothesis $H_j(k)$, corresponding to one possibility of target sequences $I_j(k)$, consisting of both the information of the lane each target is in, $I_j^l(k)$, and the information of target position sequence in each lane, $I_j^s(k)$. When the sensor sampling interval is short enough, it is reasonable to assume that each target can only change to one neighboring lane at a time. That is, assuming that target t travels in lane $l_t(k-1)$ at time step $k-1$, the possible lanes for the target to be in at time step k are $l_t(k) \in$

$\{l_t(k-1)-1, l_t(k-1), l_t(k-1)+1\}$ if lanes $l_t(k-1)-1$ and $l_t(k-1)+1$ exist. Note that it is assumed that the uncertainty in target position sequences only occurs through the lane-changing process. That is, the relative sequence of the targets in the common lane in the mileage coordinate remains unchanged if they do not change lanes.

3.6.2 Hypothesis Evaluation

Given the available measurements up to time step k, the probability of each hypothesis $H_j(k)$ is evaluated by

$$p(H_j(k)|Z^k) = \frac{1}{c} p(Z(k)|H_j(k), Z^{k-1}) p(H_j(k)|Z^{k-1}) \tag{3.6.1}$$

where $p(H_j(k)|Z^{k-1})$ is the prior probability of hypothesis $H_j(k)$, $p(Z(k)|H_j(k), Z^{k-1})$ is the likelihood function of hypothesis $H_j(k)$, and c is the normalization factor given by

$$c = \sum_j p(Z(k)|H_j(k), Z^{k-1}) p(H_j(k)|Z^{k-1}) \tag{3.6.2}$$

The prior probability of hypothesis $H_j(k)$ can be expressed as

$$p\left(H_j(k)|Z^{k-1}\right) = p\left(I_j^s(k)|I_j^l(k), Z^{k-1}\right) p\left(I_j^l(k)|Z^{k-1}\right) \tag{3.6.3}$$

where $p(I_j^l(k)|Z^{k-1})$ is the predicted lane-changing probability of hypothesis $H_j(k)$ given by

$$p(I_j^l(k)|Z^{k-1}) = \prod_{t=1}^{N(k)} p\left(l_t(k|H_j(k))|Z^{k-1}\right) \tag{3.6.4}$$

with $l_t(k|H_j(k))$ being the lane-changing decision of target t indicated by the hypothesis $H_j(k)$ and $p\left(l_t(k|H_j(k))|Z^{k-1}\right)$ being the corresponding probability given in (3.4.2). Here, $p(I_j^s(k)|I_j^l(k), Z^{k-1})$ is the predicted target sequence probabilities given the target lane-changing decisions $I_j^l(k)$ evaluated as

$$\begin{aligned} p(I_j^s(k)|I_j^l(k), Z^{k-1}) &= \prod_{l=1}^{L} P(R^l(k) > \Delta R_{safe}^l | Z^{k-1}) \\ &= \prod_{l=1}^{L} \left(1 - \Phi\left(\frac{\Delta R_{safe}^l - \hat{R}^l(k|k-1)}{\sqrt{P_{R^l}(k|k-1)}}\right)\right) \end{aligned} \tag{3.6.5}$$

where

$$\hat{R}^l(k|k-1) = \begin{bmatrix} \hat{r}_{t_1^l}(k|k-1) - \hat{r}_{t_2^l}(k|k-1) \\ \hat{r}_{t_2^l}(k|k-1) - \hat{r}_{t_3^l}(k|k-1) \\ \vdots \\ \hat{r}_{t^l_{N_l(k)-1}}(k|k-1) - \hat{r}_{t^l_{N_l(k)}}(k|k-1) \end{bmatrix} \tag{3.6.6}$$

and

$$\begin{aligned} P_{R^l}(k|k-1) &= \left[p_{ij}(k|k-1)\right],\ i,j = 1, ..., N_l(k) - 1 \\ p_{ij}(k|K) &= \begin{cases} -P^r_{t_j^l}(k|k-1) & i = j-1 \\ P^r_{t_i^l}(k|k-1) + P^r_{t_{i+1}^l}(k|k-1) & i = j \\ -P^r_{t_i^l}(k|k-1) & i = j+1 \\ 0 & \text{otherwise} \end{cases} \end{aligned} \tag{3.6.7}$$

with $\hat{r}_{t_i^l}(k|k-1)$ and $P^r_{t_i^l}(k|k-1)$ being the predicted longitudinal position of target t_i^l and its associated variance, respectively.

The sequence-aided 2D assignment algorithm proposed in the previous Section is applied to each hypothesis $H_j(k)$ to obtain the optimal association result $A^*_{I_j}(k)$. Once the measurement-to-track association is obtained, the likelihood function $p(Z(k)|H_j(k), Z^{k-1})$

can be evaluated as

$$p\left(Z(k)|H_j(k),Z^{k-1}\right) \propto \prod_{m=1}^{M(k)} \left(\frac{1}{\lambda}\cdot p_{H_j}\left(Z_m(k)|X_{t_m}(k)\right)\right)^{\tau_m(A^*_{I_j})} \times \prod_{t=1}^{N(t)} \left(P_d\right)^{u_t(A^*_{I_j})}\left(1-P_d\right)^{1-u_t(A^*_{I_j})} \tag{3.6.8}$$

where the values of the indicator variables $\tau_m(A^*_{I_j})$ and $u_t(A^*_{I_j})$ are decided by the corresponding association result $A^*_{I_j}(k)$, and $p_{H_j}\left(Z_m(k)|X_{t_m}(k)\right)$ is given by

$$\begin{aligned} p_{H_j}\left(Z_m(k)|X_{t_m}(k)\right) =& N\left(Z^r_m(k);\hat{Z}^r_{t_m}(k|k-1),S^r_{t_m}(k)\right) \\ & \times N\left(Z^d_m(k);d(l_{t_m}(k|H_j(k))),\sigma^2_{v^d}\right) \end{aligned} \tag{3.6.9}$$

Thus, the probability of each hypothesis is obtained by substituting (3.6.3) and (3.6.8) into (3.6.1). To enhance the algorithm efficiency, only the hypotheses with prior probability greater than the given threshold (i.e., $p\left(H_j(k)|Z^{k-1}\right) > p_{th}$) are considered in the process of hypotheses evaluation.

3.6.3 Algorithm Overall Structure

The overall structure of the SA-2DA-based multiple-hypothesis tracking algorithm is summarized in this Section with the block diagram shown in Fig. 3.1.

Measurement Validation

The gating method [47] is used to reduce the number of possible assignment events before applying the data association algorithm. A validation gate is calculated for each established track based on its predicted measurement at each time step. Only the

measurements falling within the gate are considered for association with this track. Specifically, the m-th measurement is valid for associating with the n-th track only if the Mahalanobis distance between them is less than the gate threshold γ [47], i.e.,

$$\Big(Z_m(k) - \hat{Z}_t(k|k-1)\Big)^T S_t(k)^{-1} \Big(Z_m(k) - \hat{Z}_t(k|k-1)\Big) \leq \gamma \tag{3.6.10}$$

where $\hat{Z}_t(k|k-1) = [\hat{Z}_t^r(k|k-1), \hat{Z}_t^d(k|k-1)]^T$ is the predicted measurement for the n-th track at time step k with covariance matrix $S_t(k) = \text{diag}(S_t^r(k), S_t^d(k))$, where $\text{diag}(\cdot)$ denotes the (block) diagonal matrix construction operator. The predicted lateral measurement and corresponding variances are given by

$$\begin{aligned} \hat{Z}_t^d(k|k-1) &= \sum_{l=1}^{L} d(l) u_{t,l}(k|k-1) \\ S_t^d(k) &= \sigma_{v^d}^2 + \sum_{l=1}^{L} u_{t,l}(k|k-1) \varepsilon_l(k) \varepsilon_l(k)^T \end{aligned} \tag{3.6.11}$$

where $\varepsilon_l(k) = d(l) - \hat{Z}_t^d(k|k-1)$.

Hypothesis Generation and Evaluation

The uncertainty in target sequence is resolved using the multiple-hypothesis method. Specifically, the sequence hypotheses are generated at the beginning of each time step as discussed in Section V.A. Then, the probability of each hypothesis is evaluated, based on the track state estimates given by the motion estimator and the SA-2DA algorithm, as explained in Section V.B. According to the hypothesis with the maximum probability at each time step, namely,

$$H^*(k) = \arg\max_{H_j(k)} p(H_j(k)|Z^k) \tag{3.6.12}$$

the target sequence $I^*(k)$ and the corresponding data association result $A_I^*(k)$ are determined.

Track Management

This process is implemented based on the data association results considering three possible track management stages (i.e., initialization, confirmation and termination). Existing tracks are updated with assumed models and associated measurements. The measurements that are not associated with any existing track are initialized as tentative tracks. The logic-based method [47] is applied to confirm tentative tracks and terminate dead ones.

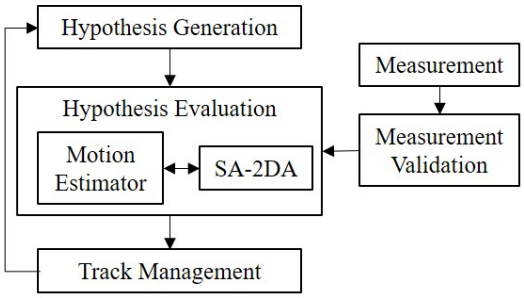

Figure 3.1: Block diagram of the proposed SA-2DA-based multiple-hypothesis tracking algorithm.

3.7 Conditional PCRLB for MTT

The posterior Cramér-Rao lower bound is commonly used as a powerful tool for both predicting and assessing the performances of target tracking algorithms [86, 87, 88]. For a hybrid estimation problem consisting of both continuous and discrete states, however, the regularity conditions required by the PCRLB are not satisfied [88, 89].

Furthermore, when the longitudinal dynamics consist of a few segments of interleaved independent and interacting motion, the model sequence is also an unknown discrete-valued variable. One alternative is to derive the conditional PCRLB for target longitudinal states given the true lateral states and the sequence of longitudinal motion models of the targets [28, 90]. Here, we use the conditional PCRLB as the theoretical metric. Conditional PCRLB can be overly optimistic since it assumes that the exact model sequence and lateral states are known.

The PCRLB, which is defined to be the inverse of the Fisher information matrix (FIM) $J(k)$ [48], gives a lower bound on the minimum mean square error (MSE) for unbiased dynamic estimators, i.e.,

$$P(k) = E\left\{\left(\hat{X}^r(k) - X^r(k)\right)\left(\hat{X}^r(k) - X^r(k)\right)^T\right\} \geq J(k)^{-1} \tag{3.7.1}$$

where $X^r(k)$ and $\hat{X}^r(k)$ are the longitudinal state vector and its estimate based on Z^k, respectively, at time step k. A recursive formula for efficient evaluation of the posterior FIM is developed in [86]:

$$J(k+1) = J_X(k+1) + J_Z(k+1) \tag{3.7.2}$$

where

$$\begin{aligned} J_X(k+1) &= D_k^{22} - D_k^{21}(J(k) + D_k^{11})^{-1} D_k^{12} \\ D_k^{11} &= E\{-\Delta_{X^r(k)}^{X^r(k)} \ln p(X^r(k+1)|X^r(k))\} \\ D_k^{12} &= E\{-\Delta_{X^r(k)}^{X^r(k+1)} \ln p(X^r(k+1)|X^r(k))\} \\ D_k^{21} &= (D_k^{12})^T \\ D_k^{22} &= E\{-\Delta_{X^r(k+1)}^{X^r(k+1)} \ln p(X^r(k+1)|X^r(k))\} \\ J_Z(k+1) &= E\{-\Delta_{X^r(k+1)}^{X^r(k+1)} \ln p(Z^r(k+1)|X^r(k+1))\} \end{aligned} \tag{3.7.3}$$

For multitarget tracking, the longitudinal state vector $X^r(k)$ is obtained by stacking the longitudinal states of all targets [87], that is, $X^r(k) = \left[X_1^r(k)^T, X_2^r(k)^T, ..., X_N^r(k)^T\right]^T$. When the targets are moving independently, the overall state motion model based on (3.3.3) is given by

$$X^r(k+1) = \bar{F}_{cv} X^r(k) + \bar{G} W(k) \tag{3.7.4}$$

where

$$\begin{aligned} \bar{F}_{cv} &= \text{diag}(F_{cv}, F_{cv}, ..., F_{cv}) \\ \bar{G} &= \text{diag}(G, G, ..., G) \\ W(k) &= [w_1(k), w_2(k), ..., w_N(k)]^T \end{aligned} \tag{3.7.5}$$

When the targets are moving inter-dependently with the car-following model given in (3.3.5)–(3.3.6), the overall state equation can be written as [26]

$$X^r(k+1) = \bar{F}_{CF} X^r(k) + \bar{G}(\bar{C} + W(k)) \tag{3.7.6}$$

where

$$\bar{F}_{CF} = \bar{F}_{cv} + \bar{G}\bar{A}$$

$$\bar{A} = \begin{bmatrix} 0 & & & & & \\ f_1 & f_2 & & & & \\ & f_1 & f_2 & & & \\ & & \ddots & \ddots & & \\ & & & & f_1 & f_2 \end{bmatrix} \tag{3.7.7}$$

$$f_1 = [c_1, c_2]$$

$$f_2 = [-c_1, -c_2 + c_3]$$

$$\bar{C} = [c_4, c_4, ..., c_4]^T$$

Substituting the overall longitudinal state equation into (3.7.3) and using the matrix inversion lemma [48], $J_X(k+1)$ can be evaluated as [87]

$$J_X(k+1) = \left[\bar{F}J(k)^{-1}\bar{F}^T + \bar{G}\bar{Q}\bar{G}^T\right]^{-1} \tag{3.7.8}$$

where $\bar{F}$ is replaced by $\bar{F}_{cv}$ when targets move independently or by $\bar{F}_{CF}$ when targets move with the CFM, and $\bar{Q} = \text{diag}(\sigma^2_{w_{x,1}}, \sigma^2_{w_{x,2}}, ..., \sigma^2_{w_{x,N}})$. The $J_Z(k+1)$ for multitarget tracking problem can be evaluated using the method developed in [87].

3.8 Simulations

In this Section, the performance of the proposed SA-2DA-based multiple-hypothesis tracking algorithm is compared with those of several existing multitarget tracking algorithms in terms of track purity, track accuracy, track continuity and computation times based on two simulated scenarios. Scenario I, where three targets move along a

single-lane road without changing their position sequence, is aimed at demonstrating the benefits of the proposed sequence-aided data association method. Scenario II, where position sequences change when targets change lanes, is used to illustrate the superiority of the proposed SA-2DA-based multiple-hypothesis tracking algorithm. In the simulations, target positions are measured in 2-D road coordinates every 2 seconds with $\sigma_v^r = 10$m and $\sigma_v^d = 2$m. The target detection probability $P_d = 0.95$ and the spatial density of false alarms $\lambda = 1.0^{-6}/\text{m}^2$. The performances of the various algorithms with consideration are evaluated over 200 Monte Carlo runs.

3.8.1 Scenario I

In this scenario, three targets travel along the centerline of a single-lane road from their starting points located at 200m, 150m and 50m in the mileage coordinate, respectively. In the initial stage, targets move independently with nearly constant velocities of 15 m/s, 20 m/s and 25 m/s, respectively, where the standard deviation of process noise is set as $\sigma_w = 0.1$ m/s^2. When the mileage distance between the first two targets is less than 30m, they move dependently following the linear Helly model (3.3.5)–(3.3.6), where $c_1 = 0.125$, $c_2 = 0.5$, $c_3 = -0.125$, $c_4 = -3.5$ are used as the values given in [83]. Then, the third target approaches the second one at about time 12s and all three targets move as a group where their dynamic motions are also described by the linear Helly model.

The proposed SA-2DA-MHT algorithm integrated with the NCV model (identified as NCV-SA-2DA-MHT in the tables and figures) is compared with the multitarget

tracking algorithm using NCV model and 2D assignment association method (NCV-2DA) proposed in [76], the CFM-based algorithm with 2D assignment method (CFM-2DA) developed in [26] and the algorithm using NCV model with ideal (i.e., perfect but unobtainable) data association results (NCV-IDA). It is required in the CFM-based algorithm that all model parameters be exactly known, which is difficult to achieve in real situations. In order to assess the impact of small parameter deviations on algorithm performance, mismatched CFM model based algorithm, in which the parameter c_3 is randomly generated with the uniform distribution in the interval $[-0.225, -0.025]$, is also used for comparison.

Track purity ϕ_{ij}, which is defined as the fraction of measurements from target i associated with track j, is a primary measure of the performances of data association algorithms [16]. The track purity matrices $[\phi_{ij}]$, where the rows correspond to the targets in the scenario and the columns correspond to the tracks maintained by the trackers, obtained by different tracking algorithms are shown in Table 3.1. Ideally, ϕ_{ij} is 1.0 for $i = j$ and 0.0 for $i \neq j$. However, when target trajectories are close to one another, the measurements from one target may be associated across multiple tracks, which results in track impurity. This phenomenon is especially pronounced when the motion model used in the tracker does not match the actual model, because inaccurate predicted-measurements make it less likely for the correct measurements to be associated, as shown in Table 3.1 by the purity matrix of the NCV-2DA algorithm. By utilizing the target sequence information, the proposed SA-2DA-MHT algorithm significantly improves track purity by reducing cross-association and overcomes the adverse effects of model mismatch to some extent. The proposed algorithm achieves almost the same performance as the matched-CFM-based algorithm and has higher

purity than the mismatched-CFM-based algorithm.

Table 3.1: Target-to-track association purity matrices in Scenario I

NCV-2DA	NCV-SA-2DA-MHT
$\begin{bmatrix} 0.6858 & 0.1817 & 0.1448 \\ 0.1415 & 0.5888 & 0.2451 \\ 0.1728 & 0.2295 & 0.6101 \end{bmatrix}$	$\begin{bmatrix} 0.9932 & 0.0080 & 0 \\ 0.0068 & 0.9731 & 0.0221 \\ 0 & 0.0189 & 0.9779 \end{bmatrix}$
Matched-CFM-2DA	**Mismatched-CFM-2DA**
$\begin{bmatrix} 0.9837 & 0.0023 & 0 \\ 0.0161 & 0.9806 & 0.0023 \\ 0.0002 & 0.0171 & 0.9977 \end{bmatrix}$	$\begin{bmatrix} 0.9741 & 0.0176 & 0.0013 \\ 0.0254 & 0.9409 & 0.0245 \\ 0.0005 & 0.0415 & 0.9743 \end{bmatrix}$

The Root Mean Square Error (RMSE) is one of the commonly used track accuracy metrics in the literature [87, 91]. Fig. 3.2 shows the RMSE values of the target state estimates obtained by different algorithms and the corresponding PCRLB values calculated using the method presented in Section VI. It can be seen that the position RMSE values between 6s and 40s given by the NCV-2DA algorithm are significantly higher than those of all other algorithms. Due to the inappropriate motion model, the NCV-2DA algorithm cannot correctly predict measurements or correctly associate measurements when the target motion transitions from independent motion mode to interacting mode. This is significantly improved by the NCV-SA-2DA-MHT algorithm which utilizes the information of target position sequence to aid the association process and correspondingly enhances track accuracy. Furthermore, the proposed algorithm reaches the steady state faster than the NCV-2DA algorithm. The NCV-IDA algorithm based on the ideal (i.e., perfect but unrealistic) association results represents the best performance that can be achieved by the NCV model based algorithms.

It can be observed that the RMSE values of the proposed algorithm is very close to the corresponding values of the NCV-IDA method, which indicates that the proposed SA-2DA algorithm yields accurate data association results. The performance of the CFM-basd algorithm is close to the PCRLB only when the correct parameter values are used in the model. That is, small parameter deviations can significantly degrade the algorithm's track accuracy. To be specific, the mismatched-CFM-2DA algorithm yields higher RMSE values during model transition periods compared to the matched-CFM-2DA algorithm and has higher steady state errors than all other NCV model based algorithms.

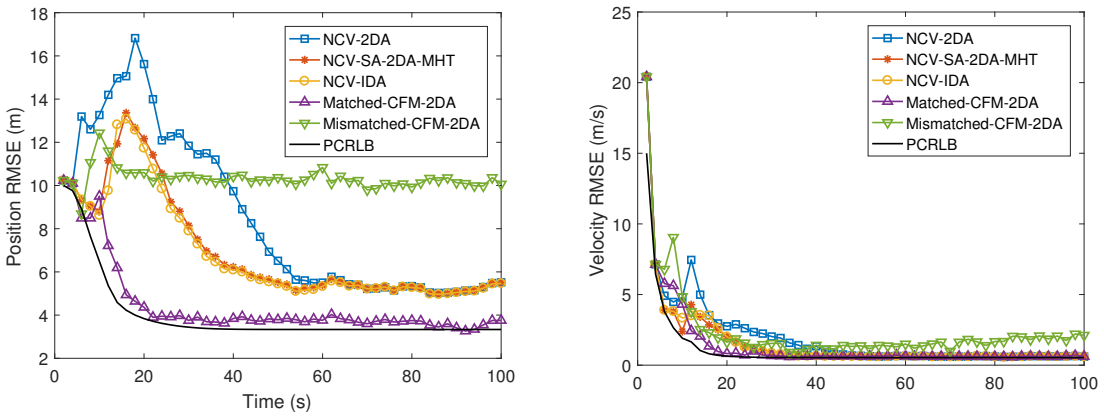

(a) (b)

Figure 3.2: Comparison of RMSE of different algorithms in Scenario I. (a) Longitudinal position RMSE and PCRLB, (b) Longitudinal velocity RMSE and PCRLB.

The RMSE values are evaluated based on track-to-truth association results. Since it is possible for multiple tracks to be assigned to one target or for no track to be assigned to a target at some time steps, the RMSE metric itself is insufficient to demonstrate the performances of tracking algorithms. Algorithms need to be further evaluated from the aspect of track continuity. The average number of swaps N_{swap}

and the average number of breaks N_{break} in tracks are defined by [91]

$$\begin{aligned} N_{swap} &= \frac{1}{N_M \cdot N_t} \sum_{m}^{N_M} \sum_{t}^{N_t} n_{t,m}^{s} \\ N_{break} &= \frac{1}{N_M \cdot N_t} \sum_{m}^{N_M} \sum_{t}^{N_t} n_{t,m}^{b} \end{aligned} \tag{3.8.1}$$

where $n_{t,m}^{s}$ and $n_{t,m}^{b}$ are the number of swaps and the number of breaks for target t at the mth Monte Carlo run, respectively; N_M and N_t are the number of Monte Carlo runs and the number of targets, respectively. The continuity measure for the target t at the mth run is defined by [91]

$$Tc_{t,m} = \frac{1}{n_{t,m}^{a}} \sum_{n=1}^{n_{t,m}^{a}} \frac{\Delta k_{t,n}}{\Delta k_t} \tag{3.8.2}$$

where $n_{t,m}^{a}$ is the number of tracks assigned to target t, Δk_t and $\Delta k_{t,n}$ are the duration of target t and the duration of the nth track assigned to target, respectively. It can be seen that the track continuity includes the information of both swaps and breaks. The track continuities averaged over Monte Carlo runs are shown in Table 3.4. As shown in Table 3.2–3.4, compared with the NCV-2DA algorithm and the mismatched-CFM-2DA algorithm, the proposed NCV-SA-2DA-MHT algorithm yields fewer swaps and breaks and better track continuity, achieving almost the same performance as the matched-CFM-2DA method. The swap ratios, defined as the ratio of the number of swaps at each time step to the number of all runs, are shown in Fig. 3.3. It can be seen that the NCV-2DA algorithm results in significantly more swaps from time 8s to 36s when target motion models change and the mismatched-CFM-2DA algorithm has high swap ratios over the whole simulation time, whereas the proposed algorithm significantly reduces swap ratios but with performance similar to that of

the matched-CFM-2DA algorithm.

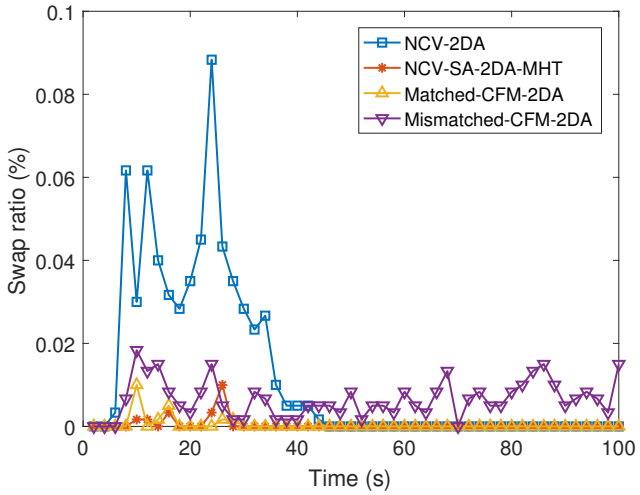

Figure 3.3: Comparison of swap ratios by different algorithms in Scenario I.

Table 3.2: Average number of swaps in Tracks in Scenario I

	Target 1	Target 2	Target 3	Average
NCV-2DA	0.480	0.780	0.565	0.608
NCV-SA-2DA-MHT	0.005	0.025	0.030	0.020
Matched-CFM-2DA	0.030	0.015	0.015	0.020
Mismatched-CFM-2DA	0.245	0.295	0.445	0.328

3.8.2 Scenario II

In order to evaluate the capability of the proposed SA-2DA-MHT algorithm to adapt to the changes in target sequence, a more complex scenario is considered here. The road has $L = 2$ lanes and each lane has a width of $2\delta_d = 4$m. In the initial stage, three targets travel along the centerline of the left lane and have the same longitudinal dynamics as in in Scenario I (i.e., from moving independently with the NCV model to inter-dependently with the CFM). To evaluate the performances of various algorithms

Table 3.3: Average number of breaks in Tracks in Scenario I

	Target 1	Target 2	Target 3	Average
NCV-2DA	0.185	0.570	1.165	0.640
NCV-SA-2DA-MHT	0.000	0.005	1.040	0.348
Matched-CFM-2DA	0.005	0.000	0.435	0.147
Mismatched-CFM-2DA	0.360	0.035	1.400	0.598

Table 3.4: Average Track Continuity in Scenario I

	Target 1	Target 2	Target 3	Average
NCV-2DA	0.802	0.716	0.699	0.739
NCV-SA-2DA-MHT	0.998	0.987	0.934	0.973
Matched-CFM-2DA	0.989	0.992	0.983	0.988
Mismatched-CFM-2DA	0.919	0.912	0.807	0.879

in the case of smaller distances between targets, the parameter c_4 indicating the behavioral aggressiveness is increased to -2. The first target changes to the right lane when it arrives at 700m at time 35s. Then, the second target accelerates with $a = 0.5$ m/s^2 and then changes lane and overtakes the first target at about time 45s. Finally, the first two targets move as a group following the linear Helly model with switched position sequence in the right lane while the third target moves independently in the left lane. An example of target longitudinal velocities is shown in Fig. 3.4. The same tracking algorithms as in Scenario I are used here for comparison. In the longitudinal motion estimator, the standard deviation of process noise is set as a larger value $\sigma_w = 2$ m/s^2 to take into account more maneuvering. In the lane filter, the initial probability vector is $u(0) = [0.5, 0.5]^T$ and the TPM is

$$\Pi = \begin{bmatrix} 0.9 & 0.1 \\ 0.1 & 0.9 \end{bmatrix} \tag{3.8.3}$$

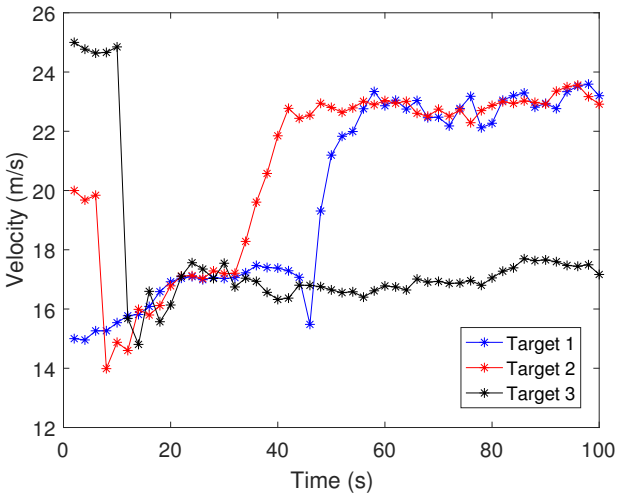

Figure 3.4: The longitudinal velocities of the three targets in Scenario II.

The track purity matrices shown in Table 3.5 indicate that the proposed NCV-SA-2DA-MHT algorithm yields the best performance. It can be seen that all tracks obtained by the proposed algorithm are much purer than those by the NCV-2DA algorithm. By integrating the SA-2DA method into the multiple-hypothesis framework, the proposed tracking algorithm can correctly handle the uncertainty and variability of target lanes and position sequences, and bring the track purity to acceptable levels without changing the motion model. Since the CFM-based algorithm is sensitive to the changes in inter-target relationship and the mismatch between the actual model and the assumed model, it results in much more cross-associations in the first two tracks than the proposed algorithm. This also indicates that the proposed algorithm yields good performance under both independent motion and interacting motion conditions.

The longitudinal position and velocity RMSEs with their corresponding PCRLBs are shown in Fig. 3.5. The figures indicate that the NCV-2DA algorithm yields the

Table 3.5: Target-to-track association purity matrices in Scenario II

NCV-2DA	NCV-SA-2DA-MHT	Matched-CFM-2DA
$\begin{bmatrix} 0.4736 & 0.2960 & 0.2329 \\ 0.2904 & 0.4371 & 0.2756 \\ 0.2360 & 0.2669 & 0.4915 \end{bmatrix}$	$\begin{bmatrix} 0.9217 & 0.0545 & 0.0256 \\ 0.0566 & 0.8723 & 0.0711 \\ 0.0217 & 0.0732 & 0.9033 \end{bmatrix}$	$\begin{bmatrix} 0.5320 & 0.4490 & 0.0191 \\ 0.4680 & 0.5147 & 0.0132 \\ 0 & 0.0363 & 0.9677 \end{bmatrix}$

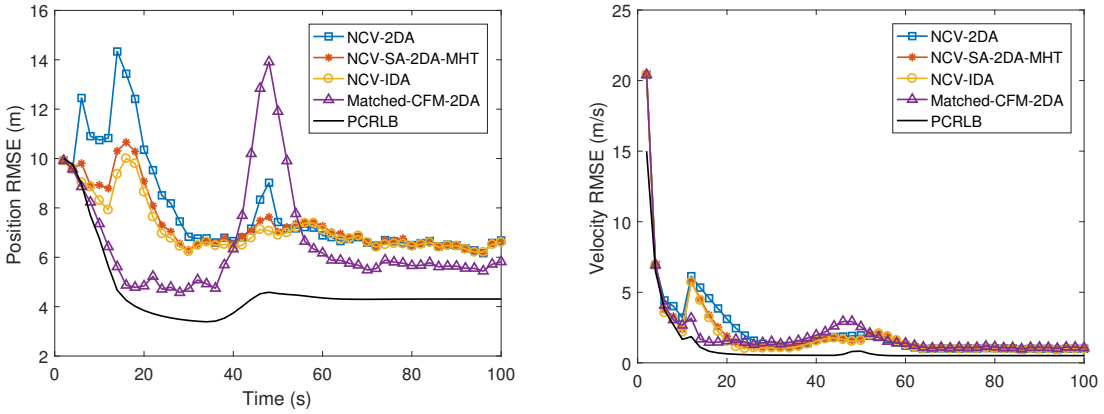

(a) (b)

Figure 3.5: Comparison of RMSE of different algorithms in Scenario II. (a) Longitudinal position RMSE and PCRLB, (b) Longitudinal velocity RMSE and PCRLB.

highest RMSE values between time 6s and 30s as it ignores the interactions among targets, and that the CFM-2DA algorithm has the largest estimation error from time 42s to 54s because of the incorrect dependent-motion assumption. The proposed algorithm yields moderate RMSE values over all time steps, since its significantly improved data association results enhance tracking accuracy. Note that the conditional PCRLB is an overly optimistic bound with lower limits than achievable RMSEs since it assumes that the exact target lateral states and motion model sequences are known.

The probability of the correct lane, defined as the ratio of the number of correct

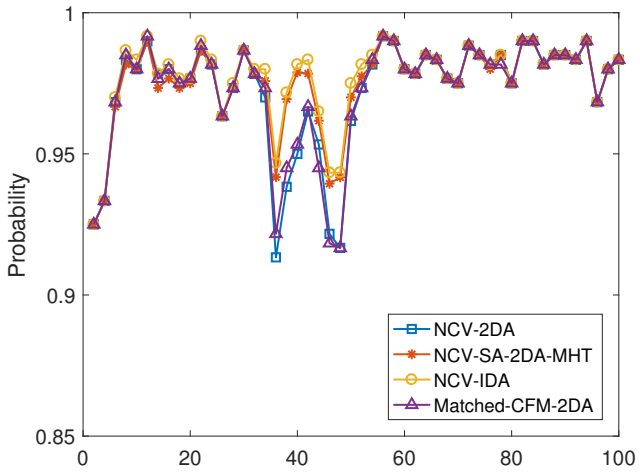

Figure 3.6: Comparison of probability of correct lane by difference algorithms in Scenario II.

estimate lane to the number of runs in which a track is associated with the target at each time [27], is used to evaluate the accuracy of the lateral state estimates. As shown in Fig. 3.6, the probability of the correct lane of the proposed algorithm is better than those of the NCV-2DA algorithm and the CFM-2DA algorithm at the valleys corresponding to the lane-changing times.

The average number of swaps and the average number of breaks are shown in Table 3.6 and 3.7, respectively, and the track continuity values of different algorithms are compared in Table 3.8. The tables indicate that the NCV-SA-2DA-MHT algorithm yields the smallest number of swaps and breaks with the best performance on track continuity than the NCV-2DA algorithm and the CFM-2DA algorithm as a result of improved association. Similarly, the proposed algorithm has lower swap ratios than the other two algorithms during all time steps as shown in Fig. 3.7.

The average computational times per run over 200 Monte Carlo runs are compared in Table 3.9. All tracking algorithms are coded in MATLAB and run on a 2.80 GHz

Table 3.6: Average number of swaps in Tracks in Scenario II

	Target 1	Target 2	Target 3	Average
NCV-2DA	1.070	1.695	0.615	1.127
NCV-SA-2DA-MHT	0.240	0.345	0.105	0.230
Matched-CFM-2DA	0.875	0.910	0.065	0.617

Table 3.7: Average number of breaks in Tracks in Scenario II

	Target 1	Target 2	Target 3	Average
NCV-2DA	0.005	0.010	0.020	0.012
NCV-SA-2DA-MHT	0.000	0.000	0.015	0.005
Matched-CFM-2DA	0.000	0.005	0.015	0.007

Intel i7 PC. In comparison with the 2D assignment based algorithms, the proposed algorithm has higher computational cost especially in Scenario II because multiple hypotheses are generated and evaluated at each time step. However, the computational efficiency can be improved if the algorithm is implemented in the C/C++ language and executed in a computer with higher computational capability. Since the execution ratio (i.e., computational time/duration of each run) is less than 1, even the MATLAB implementation itself is real-time feasible.

3.9 Conclusions

A novel SA-2DA-based multiple-hypothesis tracking algorithm was proposed in this paper for tracking multiple on-road targets. The proposed algorithm utilized the estimated target sequence to improve the measurement-to-track association performance. To be specific, the target sequence uncertainty was resolved using multiple-hypothesis method and the information of target sequence at each lane was exploited in the sequence-aided data association approach. Without assuming any particular

Table 3.8: Average Track Continuity in Scenario II

	Target 1	Target 2	Target 3	Average
NCV-2DA	0.598	0.498	0.702	0.599
NCV-SA-2DA-MHT	0.928	0.896	0.987	0.937
Matched-CFM-2DA	0.570	0.563	0.972	0.701

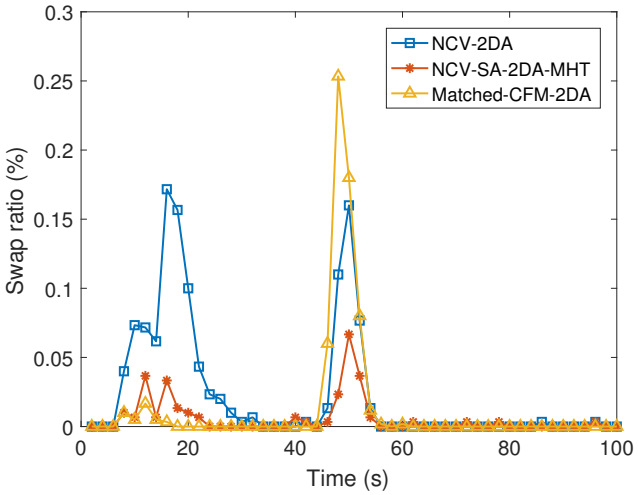

Figure 3.7: Comparison of swap ratios by different algorithms in Scenario II.

inter-dependent motion model between targets, the proposed algorithm is especially suitable for scenarios with unknown target interactions. Simulation results showed that the proposed algorithms outperform the NCV-based 2D assignment algorithm and CFM-based 2D assignment algorithms in terms of track purity, track accuracy and track continuity, especially in the scenario of varying target interactions and sequences.

Table 3.9: Average Computational Times (s)

	Scenario I	Scenario II
NCV-2DA	0.047	0.050
NCV-SA-2DA-MHT	0.242	1.434
Matched-CFM-2DA	0.127	0.196
Mismatched-CFM-2DA	0.122	–

The following chapter is a reproduction of a peer-reviewed article submitted to the IEEE::

T.Ge, R. Tharmarasa, M. Bradford, T. Kirubarajan, "Sequence-Aided Joint Probabilistic Data Association for Multiple On-road Target Tracking", Submitted to *IEEE Transactions on Intelligent Transportation Systems*, May 2020.

Chapter 4

Sequence-Aided Joint Probabilistic Data Association for Multiple On-road Target Tracking

4.1 Abstract

In this paper, the problem of tracking multiple targets on multi-lane roads using sensors such as radars and cameras is addressed. The motion of an on-road target is constrained by traffic rules and limited lane capacity. With multiple targets, the extra information implied in target position sequence along a lane can be exploited to improve tracking performance, but existing works do not enforce position sequence constraints in the data association or the state estimation stages of target tracking. Given this gap in the literature, two novel data association algorithms are proposed in this paper. The sequence-aided joint probabilistic data association (JPDA) algorithm utilizes target position sequence information to re-weight the probabilities

of association hypotheses, resulting in enhanced association between measurements and tracks and more accurate tracks. To track multiple maneuvering targets, the sequence information is integrated into the tracking framework consisting of the interacting multiple model (IMM) estimator and the JPDA algorithm. Besides, a track segment association algorithm is proposed to handle target lane-changing behaviors, yielding more continuous tracks. The conditional posterior Cramér-Rao lower bound is also derived as a theoretical performance benchmark for this problem. The performance of the proposed sequence-aided data association algorithms is compared with those of existing algorithms that do not utilize the target position sequence information. Numerical results show that the proposed algorithms yield more continuous and accurate ground target tracks.

4.2 Introduction

On-road target tracking is an important component in various civil and military applications, such as traffic monitoring [70, 71] and ground surveillance [19, 76, 92]. Because of the unique target motion characteristics that are influenced by the road network [93], ground target tracking sill remains a challenging problem in spite of significant research into this area.

As targets move along roads, their motion is subjected to the constraints imposed by the roads. One of the efficient ways to ingest the road-map information into a tracker is to track targets directly in the 2-D road coordinates by decomposing the target motion into the longitudinal motion in the mileage coordinate and the lateral motion in the displacement coordinate [77]. Then, the constrained state estimation problem becomes the standard unconstrained estimation problem. A comprehensive

literature review on road-map assisted ground target tracking is available in [24, 69]. Due to limited road resources, neighboring targets usually interact with one another while moving along roads. Dependent motion models are often used to characterize the interactions among targets. For example, in [25], a modified social force model (SFM) is used for ground target tracking where the interactions between a target and its neighbors are described by virtual forces among them but such force-based modeling lacks any direct physical meaning. The longitudinal dynamics of on-road targets are modeled using the linear Helly car-following model [83] in [26] and the intelligent drive model [94] in [27]. It is difficult to define the parameters in these two empirical car-following models so as to ensure that the models are consistent with actual target motion. In [77], the target lateral motion is modeled as a homogeneous Markov chain with a known transition probability matrix (TPM) and an initial probability vector, ignoring the effects of the motions of targets in the vicinity of the target under consideration. To overcome this limitation, the incentive-based Minimizing Overall Braking Induced by Lane-change (MOBIL) lane-changing model [95] is used to describe target lateral dynamics across multiple lanes in [27, 28]. However, it is not possible to obtain accurate lateral state estimates when the target longitudinal state estimates are not accurate. This is because the test statistics used in the MOBIL model are determined by the target longitudinal states as well. Another distinguishing characteristic of on-road target motion is that the targets in the same lane tend to move in an orderly manner along the centerline of each lane because of traffic rules and limited lane width. In practice, no prior knowledge or the direct measurements of the target position sequence in each lane are available. As a result, to the best of our knowledge, the target position sequence information has not yet been well studied or

exploited in target tracking literature.

The objective of multitarget tracking (MTT) is to simultaneously estimate the number of targets and their states [1]. Data association as a key task addressing the measurement origin uncertainty problem in MTT systems is particularly challenging in on-road target tracking due to the interactions and close distances among targets. The common approaches for data association in the literature are the nearest neighbor (NN) [13], joint probabilistic data association (JPDA) [14], multiple hypothesis tracking (MHT) [15] and the multidimensional assignment (MDA) algorithm [16]. The JPDA algorithm is the focus of this paper because of its balance between estimation accuracy and computational cost [96]. Extensions of our work to the MHT and the association-free random finite set (RFS) [97, 98] frameworks are the topics for our future works. Track management techniques, such as the quality-based method and the logic-based method, are usually combined with the JPDA algorithm to handle track birth and termination [47]. The combination of the interacting multiple model (IMM) estimator and the JPDA algorithm has been proposed for tracking multiple closely-spaced maneuvering targets in the presence of clutter and possibly missed detections [99, 100, 101]. An accelerated IMMJPDA algorithm based on K-best assignment [102] approaches instead of enumerating all feasible hypotheses is proposed in [103]. To avoid the track coalescence that ensues in tracking closely spaced targets using the standard JPDA, the scaled JPDA algorithm, where the likelihood of the most likely association hypothesis is re-weighted by multiplying by an arbitrary positive scaling factor, is proposed in [104]. However, the performance of this algorithm is largely influenced by the value of the scaling factor. Another option is the JPDA* algorithm proposed in [105] that utilizes an additional hypothesis pruning strategy

to avoid track coalescence.

Track segment association (TSA) is a common technique to improve track continuity by stitching the track segments that are possibly from the same target [106, 107]. In TSA, two track segment candidates are propagated to the common time for association. The techniques used for track state propagation and common time selection vary with different TSA algorithms. In [108], a TSA approach with application for an airborne early warning (AEW) system with long sampling intervals propagates young (i.e., newly initialized) tracks back to the times when the old (i.e., previously terminated) tracks had their last measurement-associated update. In the case of tracking ground moving targets that often use evasive move-stop-move maneuvers to avoid detection by a ground moving target indicator (GMTI) radar, a TSA algorithm that uses an IMM estimator with state-dependent mode transition probabilities for track segment prediction and chooses the middle point between the end of old track and the start of young track as the common time is proposed in [109]. In these TSA approaches, the common times are selected based on the assumption that young tracks are always initialized after the termination of old tracks, which is not always true in real situations where an old track may prolong due to association with false alarms or detections from other targets or a young track may be initialized with a false measurement before its corresponding old one is terminated. To overcome this limitation, an algorithm that applies an extra step to release associated measurements by going backward and forward in time along the old and young track segments, respectively, before performing prediction and backpropagation in TSA is proposed in [106]. However, this algorithm is computationally expensive and cannot be used to address the track swaps due to target lane changes, where a young track and its corresponding

old track have different lateral states.

While the use of road-map information and the modeling of the interaction motion among targets have been explored in the literature, the information of target position sequence along a road lane has not yet been well-addressed. To the best of our knowledge, the sequence-aided 2D assignment (SA-2DA) algorithm proposed in our previous work [110] is the first attempt to integrate target sequence information into a tracker. In [110], a homogeneous Markov chain model with a known TPM is used to characterize target lane-changing behavior.

In this follow-up paper, no empirical model is assumed in the longitudinal or lateral motion of the target, which makes the algorithms proposed in our current work more robust and reliable in real scenarios. Besides, the target position sequence information is further exploited within the JPDA framework, making it suitable for high false alarm rate or high association ambiguity scenarios. There are four main contributions in this paper. First, we propose a new sequence-aided JPDA (SA-JPDA) algorithm that utilizes target position sequence information to re-weight the probabilities of association hypotheses, yielding improved association between measurements and tracks. As a result, not only are more accurate tracks obtained, but also the track coalescence problem inherent in the JPDA algorithm is mitigated. Second, the sequence-aided IMMJPDA (SA-IMMJPDA) algorithm is developed for tracking multiple maneuvering on-road targets. Third, a novel track segment association algorithm is proposed to handle the swaps in tracks due to the lane changes by targets. More continuous and accurate tracks are obtained by combining the proposed sequence-aided measurement-to-track association algorithms with the proposed TSA algorithm. Finally, the conditional posterior Cramér-Rao lower bound (PCRLB)

quantifying the best possible estimation accuracy achievable by any algorithm is derived for this problem.

The rest of the paper is structured as follows. The target dynamics and the measurement model in 2-D road coordinates are introduced in Section II. In Section III, the proposed SA-JPDA algorithm and the SA-IMMJPDA algorithm are described in detail. The TSA algorithm for on-road target tracking is developed in Section IV. The conditional PCRLB is derived in Section V. In Section VI, simulation results and comparisons with existing algorithms for tracking multiple targets on multi-lane roads are preformed. Conclusions are given in Section VII.

4.3 Background

4.3.1 Target Kinematics in 2-D Road Coordinates

By modeling roads as a sequence of connected linear segments, the kinematics of on-road targets can be represented in 2-D road coordinates consisting of the mileage and displacement coordinates [77]. Corresponding to the motions in these two coordinates, the target kinematic state is decomposed into the longitudinal state $X_t^r(k) = [r_t(k), \dot{r}_t(k), \ddot{r}_t(k)]^T$ and the lateral state $l_t(k)$, where the continuous-valued variables $r_t(k)$, $\dot{r}_t(k)$ and $\ddot{r}_t(k)$ are the position, velocity and the acceleration of target t measured in the mileage coordinate, respectively, and the discrete-valued variable $l_t(k)$ denotes the lane target t located on at time step k.

4.3.2 Target Longitudinal Motion Models

The longitudinal motion model describes the target longitudinal states evolving along the centerline of the current lane. The discrete-time model in a generic form is given by

$$X_t^r(k+1) = FX_t^r(k) + Gw(k) \tag{4.3.1}$$

where $w(k)$ is a zero-mean white Gaussian process noise with standard deviation σ_w while F and G are the model dependent system matrices. The nearly constant velocity (NVC) model, based on the discrete white-noise acceleration model [48], is intended to describe non-maneuvering target motion with matrices

$$F = \begin{bmatrix} 1 & T & 0 \\ 0 & 1 & 0 \\ 0 & 0 & 0 \end{bmatrix}, \; G = \begin{bmatrix} T^2/2 \\ T \\ 0 \end{bmatrix} \tag{4.3.2}$$

where T is the sampling interval. The nearly constant acceleration (NCA) model, based on the discrete Wiener process acceleration model [48], is intended to describe maneuvers with a nearly constant acceleration using matrices

$$F = \begin{bmatrix} 1 & T & T^2/2 \\ 0 & 1 & T \\ 0 & 0 & 1 \end{bmatrix}, \; G = \begin{bmatrix} T^2/2 \\ T \\ 1 \end{bmatrix} \tag{4.3.3}$$

These two models are used in this paper. The reader is referred to [80] for a comprehensive survey on dynamic models and any model therein can be used within our solution framework.

4.3.3 Measurement Model

Without loss of generality and for simplicity, the road-coordinates-based position measurement model [27, 28] is used in this paper. Targets are observed by the sensor with detection probability P_d in each scan. The target-originated measurement is not accurate due to the limited accuracy of a sensor and can be expressed as

$$\begin{bmatrix} Z_t^r(k) \\ Z_t^d(k) \end{bmatrix} = \begin{bmatrix} HX_t^r(k) \\ d(l_t(k)) \end{bmatrix} + \begin{bmatrix} v^r(k) \\ v^d(k) \end{bmatrix} \tag{4.3.4}$$

where $Z_t^r(k)$ and $Z_t^d(k)$ are the mileage and displacement measurements, respectively; $X_t^r(k)$ and $l_t(k)$ are target longitudinal and lateral states, respectively; $v^r \sim N(0, \sigma_{v^r}^2)$ and $v^d \sim N(0, \sigma_{v^d}^2)$ are mutually uncorrelated white Gaussian noise processes. In (4.3.4), $H = [1, 0, 0]$ and the displacement of the centerline of lane $l_t(k)$ is given by $d(l_t(k)) = (2l_t(k) - L - 1)\delta_d$, $l_t(k) = 1, ..., L$, where L is the number of lanes and the width of each lane is $2\delta_d$. It is assumed that false alarms are uniformly distributed in the field of view of the sensor with a Poisson-distributed cardinality given by

$$p(n_{fa}) = e^{-\lambda} \frac{\lambda^{n_{fa}}}{n_{fa}!}, \; n_{fa} = 0, 1, ... \tag{4.3.5}$$

Let $Z(k) = \{Z_m(k), m = 1, ..., M(k)\}$ denote the set of measurements received at time step k and $Z^K = \{Z(k), k = 1, ..., K\}$ denote the cumulative set of measurements available up to time step K, where $Z_m(k)$ is the m-th measurement and $M(k)$ is the number of received measurements.

4.4 Sequence-aided Data Association Algorithms

It is observed that the targets in the same lane tend to move in an orderly manner along the centerline of each lane except for occasional lane changes. Due to traffic rules and limited lane capacity, it is reasonable to assume that the sequences of target mileage positions change only when a target makes lane changes. In this Section, the sequence information is exploited and integrated into the JPDA and IMMJPDA algorithms to obtain improved measurement-to-track association results and to better update target longitudinal states. The changes in target lateral states due to target lane-changing behaviors are addressed in the next Section.

4.4.1 Definition of Target Sequences

For a set of targets moving along lane l at time step k, the sequence is defined according to their mileage positions [110], i.e.,

$$\begin{gathered} I_l(k) = \left(t_1^l, t_2^l, ..., t_{N_t^l(k)}^l\right) \\ \text{subject to } \; r_{t_i^l}(k) > r_{t_{i+1}^l}(k), \; i = 1, \ldots, N_t^l(k) \end{gathered} \tag{4.4.1}$$

where $r_{t_i^l}(k)$ is the mileage positions of the t_i^l-th target and $r_{t_{i+1}^l}(k)$ is that of the t_{i+1}^l-th target in set $I_l(k)$, and the number of targets in lane l is $N_t^l(k)$. The set of target position sequences in each lane at time step k is denoted by [110]

$$I(k) = \{I_l(k), l = 1, ..., L\} \tag{4.4.2}$$

Let $(\cdot)$ and $\{\cdot\}$ denote the ordered set and the unordered set, respectively. In the tracking algorithms, the target longitudinal states are random variables and can be

represented as $X_t^r(k) \sim N\left(\hat{X}_t^r(k|k), P_t(k|k)\right)$, $t = 1, \ldots, N_t(k)$, $k = 1, \ldots, K$. The sequence of target positions in lane l is defined based on their mileage position estimates [110], i.e.,

$$\begin{gathered} I_l(k) = \left(t_1^l, t_2^l, ..., t_{N_t^l(k)}^l\right) \\ \text{subject to } \hat{r}_{t_i^l}(k|k) > \hat{r}_{t_{i+1}^l}(k|k),\ \hat{l}_{t_i^l}(k) = l,\ i = 1, \ldots, N_l(k) \end{gathered} \tag{4.4.3}$$

where $\hat{r}_{t_i^l}(k|k)$ and $\hat{r}_{t_{i+1}^l}(k|k)$ are the mileage position estimates of the t_i^l-th track and the t_{i+1}^l-th track in the set $I_l(k)$, respectively, and $\hat{l}_{t_i^l}(k)$ is the lane that track t_i^l moving along.

4.4.2 Sequence-aided JPDA Algorithm

Using the Bayesian framework [47], the joint probabilistic data association algorithm uses only the latest scan data from a sensor [1]. The JPDA algorithm relies on a few assumptions [14]:

1. The number of established targets in the presence of clutter is known.

2. Each target produces at most one measurement, and each measurement either originates from one target or from clutter.

3. Measurements from one target may fall within the validation regions of neighboring targets.

4. Under the Markovian assumption, the past of the system is summarized by an approximate sufficient statistic consisting of state estimates, which are given by approximate conditional means, along with covariance for each state estimate.

5. The states are assumed to be Gaussian distributed.

The key task of the JPDA algorithm is to evaluate the conditional probability of the joint association event:

$$A_i(k) = \bigcap_{m=1}^{M(k)} \theta_{mt_m}(k), \quad i = 1, ..., N_A(k) \tag{4.4.4}$$

where $\theta_{mt_m}(k)$ is the event that the m-th measurement at time step k originated from target t_m, $m = 1, \ldots, M(k)$, $t_m = 1, .., N_t(k)$, and $N_A(k)$ denotes the number of all possible joint association events at time step k.

The probability of event $A_i(k)$ conditioned on target sequence information $I(k)$ and measurements Z^k can be evaluated using the Bayes' theorem [110], i.e.,

$$p\left(A_i(k)|I(k), Z^k\right) = \frac{1}{c} p\left(A_i(k)|Z^k\right) p\left(I(k)|A_i(k), Z^k\right) \tag{4.4.5}$$

where $c = p\left(I(k)|Z^k\right)$ is the same for all association events. In the above, the probability of association event $A_i(k)$ given measurements Z^k can be expressed as [14]

$$p\left(A_i(k)|Z^k\right) \propto \prod_{m=1}^{M(k)} \left(\frac{1}{\lambda} \cdot p\left(Z_m(k)|X_{t_m}(k)\right)\right)^{\tau_m} \prod_{t=1}^{N_t(k)} (P_d)^{u_t} (1 - P_d)^{1-u_t} \tag{4.4.6}$$

where τ_m and u_t are both binary indicators given by

$$\tau_m = \begin{cases} 1 & \text{the } m\text{-th measurement originated from a target} \\ 0 & \text{otherwise} \end{cases} \tag{4.4.7}$$

and

$$u_t = \begin{cases} 1 & \text{the } t\text{-th target is associated with one measurement} \\ 0 & \text{otherwise} \end{cases} \tag{4.4.8}$$

respectively; $p\left(Z_m(k)|X_{t_m}(k)\right)$ is the measurement likelihood function of associating t_m-th target to $Z_m(k)$ as indicated by $A_i(k)$, i.e.,

$$p\left(Z_m(k)|X_t(k)\right) = N\left(Z_m(k); \hat{Z}_t(k|k-1), S_t(k)\right) \tag{4.4.9}$$

where $\hat{Z}_t(k|k-1) = \left[\hat{Z}_t^r(k|k-1), d(\hat{l}_t(k))\right]^T$ is the predicted measurement for target t with associated covariance matrix $S_t(k) = \text{diag}(S_t^r(k), \sigma_{v^d}^2)$, where $S_t^r(k)$ denotes the innovation covariance of the predicted longitudinal measurement $\hat{Z}_t^r(k|k-1)$. Here, $\text{diag}(\cdot)$ denotes the (block) diagonal matrix construction operator.

Given an association event and the measurements in the latest scan, the target longitudinal state estimates and the associated covariance can be obtained. Let $\Delta r_i^l(k) = r_{t_i^l}(k) - r_{t_{i+1}^l}(k)$ denote the mileage distance between target t_i^l and target t_{i+1}^l and $R^l(k) = [\Delta r_1^l(k), \Delta r_2^l(k), ..., \Delta r_{N_t^l(k)-1}^l(k)]^T$ denote the stacked vector consisting of all mileage distances between two neighboring targets. The probability density function (pdf) of $R^l(k)$ conditioned on Z^k is given by [110]

$$p\left(R^l(k)|Z^k\right) = N\left(R^l(k); \hat{R}^l(k|k), P_{R^l}(k|k)\right) \tag{4.4.10}$$

with

$$\hat{R}^l(k|k) = \begin{bmatrix} \hat{r}_{t_1^l}(k|k) - \hat{r}_{t_2^l}(k|k) \\ \hat{r}_{t_2^l}(k|k) - \hat{r}_{t_3^l}(k|k) \\ \vdots \\ \hat{r}_{t^l_{N_t^l(k)-1}}(k|k) - \hat{r}_{t^l_{N_t^l(k)}}(k|k) \end{bmatrix} \tag{4.4.11}$$

and

$$\begin{aligned} P_{R^l}(k|k) &= \left[P_{R^l,ij}(k|k)\right],\ i,j = 1,...,N_t^l(k)-1 \\ P_{R^l,ij}(k|K) &= \begin{cases} -P^r_{t_j^l}(k|k) & i = j-1 \\ P^r_{t_i^l}(k|k) + P^r_{t_{i+1}^l}(k|k) & i = j \\ -P^r_{t_i^l}(k|k) & i = j+1 \\ 0 & \text{otherwise} \end{cases} \end{aligned} \tag{4.4.12}$$

where $\hat{r}_t(k|k)$ and $P_t^r(k|k))$ are the mileage position estimate and the corresponding covariance for target t, respectively. Then, the probability of target position sequence $I(k)$ conditioned on association event $A_i(k)$ and measurement Z^k can be evaluated by

$$\begin{aligned} p\left(I(k)|A_i(k), Z^k\right) &= \prod_{l=1}^{L}\left(P(R^l(k) > \Delta R^l_{safe}|Z^k)\right) \\ &= \prod_{l=1}^{L}\left(1 - \Phi\left(\frac{\Delta R^l_{safe} - \hat{R}^l(k|k)}{\sqrt{P_{R^l}(k|k)}}\right)\right) \end{aligned} \tag{4.4.13}$$

where ΔR^l_{safe} is a threshold column vector with $N_l(k)-1$ elements of Δr_{safe} ($\Delta r_{safe} \geq 0$), where Δr_{safe} is the parameter indicating the safe-following distance among targets, and $\Phi(\cdot)$ is the cumulative distribution function of the standard Gaussian distribution.

Measurement validation is performed for each target to preclude the association events with low probabilities. The validation region for target t is an ellipsoid defined as

$$\Big(Z_m(k) - \hat{Z}_t(k|k-1)\Big)^T S_t(k)^{-1} \Big(Z_m(k) - \hat{Z}_t(k|k-1)\Big) \leq \gamma \tag{4.4.14}$$

where $\gamma = \chi^2_{n_z}(1-q)$ is the threshold determining the gate volume with n_z denoting the dimension of the measurement vector and q denoting the tail probability [47]. Here, $\chi^2_{n_z}$ denotes the chi-square distribution with n_z degrees of freedom [48]. Once the probabilities of joint association events have been evaluated by substituting (4.4.6) and (4.4.13) into (4.4.5), the JPDA algorithm computes the marginal association probability $p\left(\theta_{mt}(k)|I(k), Z^k\right)$. This is achieved by summing the probabilities for all joint events in which the marginal event of interest θ_{mt} occurs, i.e.,

$$\begin{aligned} \beta_{mt} &\triangleq p\left(\theta_{mt}(k)|I(k), Z^k\right) \\ &= \sum_{A:\theta_{mt}\in A} p\left(A(k)|I(k), Z^k\right) \end{aligned} \tag{4.4.15}$$

The calculated marginal probabilities then serve as the probabilistic weights used in the probabilistic data association filter (PDAF) to update the longitudinal state estimate for each target. One cycle of the PDAF algorithm is summarized as follows.

1. *Prediction:* The longitudinal state estimate and the associated covariance matrix for target t are predicted as

$$\begin{aligned} \hat{X}^r_t(k|k-1) &= F\hat{X}^r_t(k-1|k-1) \\ P_t(k|k-1) &= FP_t(k-1|k-1)F^T + Q \end{aligned} \tag{4.4.16}$$

where $Q = G\sigma_w^2 G^T$. The predicted longitudinal measurement and the corresponding innovation covariance matrix are

$$\begin{aligned} \hat{Z}_t^r(k|k-1) &= H\hat{X}_t^r(k|k-1) \\ S_t^r(k) &= HP_t^r(k|k-1)H^T + R \end{aligned} \tag{4.4.17}$$

where $R = \sigma_{v^r}^2$.

2. *Update:* The updated longitudinal state and the associated covariance matrix for target t are

$$\begin{aligned} \hat{X}_t^r(k|k) &= \hat{X}_t^r(k|k-1) + W(k)v(k) \\ P_t(k|k) &= \beta_{0t}P_t(k|k-1) + (1-\beta_{0t})P_t^c(k|k) + \tilde{P}_t(k) \end{aligned} \tag{4.4.18}$$

where

$$\begin{aligned} v_m(k) &= Z_m^r(k) - \hat{Z}_t^r(k|k-1) \\ v(k) &= \sum_{m=1}^{M(k)} \beta_{mt} v_m(k) \\ W(k) &= P_t(k|k-1)H(k)^T S_t^r(k)^{-1} \\ P_t^c(k|k) &= P_t(k|k-1) - W(k)S_t^r(k)W(k)^T \\ \tilde{P}_t(k) &= W(k)\left[\sum_{m=1}^{M(k)} \beta_{mt} v_m(k)v_m(k)^T - v(k)v(k)^T\right] W(k)^T \end{aligned} \tag{4.4.19}$$

4.4.3 Sequence-aided IMMJPDA Algorithm

The combination of the IMM estimator and the JPDA algorithm has been proven to be effective in tracking multiple maneuvering targets in the presence of clutter and possibly missed detections [99]. In this Section, the target sequence information is integrated into the IMMJPDA approach.

The longitudinal motion mode of target t at time k is denoted by $m_{t,j}(k)$, $j = 1, .., N_m$, where N_m is the number of motion modes. The mode sequence is assumed to be a homogeneous Markov chain with a known TPM $\Pi = [\pi_{ij}]_{i,j=1}^{N_m}$ and an initial probability vector $u(0) = [u_1(0), \ldots [u_{N_m}(0)]^T$, where

$$\begin{aligned} \pi_{ij} &\triangleq P\left(m(k) = j | m(k-1) = i\right) \\ u_i(0) &\triangleq P(m(0) = i), \quad i = 1, \ldots, N_m \end{aligned} \tag{4.4.20}$$

The IMM estimator recursion at time step k starts with the longitudinal state estimate $\hat{X}_{t,j}^r(k-1|k-1)$, the associated covariance matrix $P_{t,j}(k-1|k-1)$ and the mode probability $u_{t,j}(k-1) \triangleq P(m_{t,j}(k-1)|Z^{k-1})$ at time step $k-1$ for each mode $j = 1, \ldots, N_m$ and each target $t = 1, \ldots, N_t(k-1)$.

Interaction

Given the predicted mode probabilities:

$$\begin{aligned} u_{t,j}(k|k-1) &\triangleq P\left(m_{t,j}(k)|Z^{k-1}\right) \\ &= \sum_{i=1}^{N_m} \pi_{ij} u_{t,i}(k-1) \end{aligned} \tag{4.4.21}$$

and the mixing probabilities:

$$\begin{aligned} u_{t,i|j}(k-1) \triangleq & P\left(m_{t,i}(k-1)|m_{t,j}(k)\right) \\ = & \frac{\pi_{ij} u_{t,i}(k-1)}{u_{t,j}(k|k-1)} \end{aligned} \tag{4.4.22}$$

the mixed longitudinal state estimate and the associated covariance matrix for mode j are

$$\begin{aligned} \hat{X}^r_{t,0j}(k-1|k-1) = & \sum_{i=1}^{N_m} \hat{X}^r_{t,i}(k-1|k-1) u_{t,i|j}(k-1) \\ P_{t,0j}(k-1|k-1) = & \sum_{i=1}^{N_m} \Big[P_{t,i}(k-1|k-1) + \Big(\hat{X}^r_{t,i}(k-1|k-1) - \hat{X}^r_{t,0j}(k-1|k-1) \Big) \\ & \times \Big(\hat{X}^r_{t,i}(k-1|k-1) - \hat{X}^r_{t,0j}(k-1|k-1) \Big)^T \Big] u_{t,i|j}(k-1) \end{aligned} \tag{4.4.23}$$

Prediction

The predicted longitudinal states for mode j are

$$\begin{aligned} \hat{X}^r_{t,j}(k|k-1) &= F_j \hat{X}^r_{t,0j}(k-1|k-1) \\ P_{t,j}(k|k-1) &= F_j P_{t,0j}(k-1|k-1) F_j^T + Q_j \end{aligned} \tag{4.4.24}$$

where $Q_j = G_j \sigma_w^2 G_j^T$, F_j and G_j are defined by mode j. The predicted longitudinal measurements for mode j are

$$\hat{Z}^r_{t,j}(k|k-1) = H \hat{X}^r_{t,j}(k|k-1) \tag{4.4.25}$$

with the corresponding covariance of the measurement residual:

$$S^r_{t,j}(k) = HP_{t,j}(k|k-1)H^T + R \tag{4.4.26}$$

Measurement validation

The validation region for target t is taken to be the same for all models [47]. Letting

$$\hat{j}_t = \arg\max_j |S^r_{t,j}(k)| \tag{4.4.27}$$

the measurement $Z_m(k)$ is validated if and only if

$$\left(Z_m(k) - \hat{Z}_{t,\hat{j}_t}(k|k-1)\right)^T \left(S_{t,\hat{j}_t}(k)\right)^{-1} \left(Z_m(k) - \hat{Z}_{t,\hat{j}_t}(k|k-1)\right) \leq \gamma \tag{4.4.28}$$

where $\hat{Z}_{t,\hat{j}_t}(k|k-1) = \left[\hat{Z}^r_{t,\hat{j}_t}(k|k-1), d(\hat{l}_t(k))\right]^T$ and $S_{t,\hat{j}_t}(k) = \text{diag}(S^r_{t,\hat{j}_t}(k), \sigma^2_{v^d})$ are the predicted measurement and the corresponding covariance matrix for mode $\hat{j}_t$, respectively.

Data association

Different from the sequence-aided JPDA algorithm, the probability of the joint association event $A_i(k)$ given that target t in mode j needs to be evaluated, i.e.,

$$p\left(A_i(k)|m_{t,j}(k), I(k), Z^k\right) = \frac{1}{c} p\left(A_i(k)|m_{t,j}(k), Z^k\right) p\left(I(k)|m_{t,j}(k), A_i(k), Z^k\right) \tag{4.4.29}$$

where $c = p(I(k)|m_{t,j}(k), Z^k)$ is a normalized factor. The first term on the right-hand side of (4.4.29) can be written as [99]

$$p\left(A_i(k)|m_{t,j}(k), Z^k\right) = p\left(Z(k)|m_{t,j}(k), A_i(k), Z^{k-1}\right) p\left(A_i(k)|m_{t,j}(k), Z^{k-1}\right) \quad (4.4.30)$$

with

$$\begin{aligned} p\left(Z(k)|m_{t,j}(k), A_i(k), Z^{k-1}\right) = & \sum_{j_1=1}^{N_m} \cdots \sum_{j_{t-1}=1}^{N_m} \sum_{j_{t+1}=1}^{N_m} \cdots \sum_{j_{N_t(k)}=1}^{N_m} \\ & p\left(Z(k)|\{m_{t',j_{t'}}(k)\}_{t'=1}^{N_t(k)}, A_i(k), Z^{k-1}\right) \times \\ & p\left(\{m_{t',j_{t'}}(k)\}_{t'=1,t'\neq t}^{N_t(k)}|m_{t,j}(k), A_i(k), Z^{k-1}\right) \end{aligned} \quad (4.4.31)$$

$$p\left(A_i(k)|m_{t,j}(k), Z^{k-1}\right) \propto \prod_{t=1}^{N_t(k)} (P_d)^{u_t}(1-P_d)^{1-u_t} \quad (4.4.32)$$

It is assumed that the states and modes of the targets conditioned on the past measurements are mutually independent. Thus, the terms on the right-hand side of (4.4.31) can be evaluated by [99]

$$p\left(Z(k)|\{m_{t',j_{t'}}(k)\}_{t'=1}^{N_t(k)}, A_i(k), Z^{k-1}\right) = \prod_{t'=1}^{N_t(k)} \left(\frac{1}{\lambda} \cdot p\left(Z_{m_{t'}}(k)|X_{t',j_{t'}}(k)\right)\right)^{\tau_m} \quad (4.4.33)$$

$$p\left(\{m_{t',j_{t'}}(k)\}_{t'=1,t'\neq t}^{N_t(k)}|m_{t,j}(k), A_i(k), Z^{k-1}\right) = \prod_{t'=1,t'\neq t}^{N_t(k)} p\left(m_{t',j_{t'}}(k)|Z^{k-1}\right) \quad (4.4.34)$$

where $p\left(Z_{m_{t'}}(k)|X_{t',j_{t'}}(k)\right) = N\left(Z_{m_{t'}}(k); \hat{Z}_{t',j_{t'}}(k|k-1), S_{t',j_{t'}}(k)\right)$, in which the measurement $Z_{m_{t'}}(k)$ is indicated by the association event $A_i(k)$, and $p\left(m_{t',j_{t'}}(k)|Z^{k-1}\right)$,

the predicted mode probability, is given in (4.4.21).

Similarly, the second term on the right-hand side of (4.4.29) can be written as

$$\begin{aligned} p\left(I(k)|m_{t,j}(k), A_i(k), Z^k\right) = & \sum_{j_1=1}^{N_m} \cdots \sum_{j_{t-1}=1}^{N_m} \sum_{j_{t+1}=1}^{N_m} \cdots \sum_{j_{N_t(k)}=1}^{N_m} \\ & p\left(I(k)|\{m_{t',j_{t'}}(k)\}_{t'=1}^{N_t(k)}, A_i(k), Z^{k-1}\right) \times \\ & p\left(\{m_{t',j_{t'}}(k)\}_{t'=1,t'\neq t}^{N_t(k)}|m_{t,j}(k), A_i(k), Z^{k-1}\right) \end{aligned} \tag{4.4.35}$$

where $p\left(I(k)|\{m_{t',j_{t'}}(k)\}_{t'=1}^{N_t(k)}, A_i(k), Z^{k-1}\right)$, the probability of target position sequence given one possibility of target motion modes and an association event, can be evaluated as in (4.4.13), where the mean vector $\hat{R}^l(k|k)$ and associated covariance matrix $P_{R^l}(k|k)$ are calculated based on the mode-conditioned longitudinal states of the targets.

By substituting (4.4.30) and (4.4.35) into (4.4.29), the probabilities of joint events given that target t is in mode j are obtained. Then, the probabilities of the marginal association events conditioned on target t being in mode j can be evaluated as

$$\begin{aligned} \beta_{mt}(m_{t,j}(k)) &\triangleq p\left(\theta_{mt}(k)|m_{t,j}(k), I(k), Z^k\right) \\ &= \sum_{A:\theta_{mt}\in A} p\left(A(k)|m_{t,j}(k), I(k), Z^k\right) \end{aligned} \tag{4.4.36}$$

The marginal probabilities are calculated via (4.4.29)–(4.4.36) for each mode $j = 1, \ldots, N_m$ and each target $t = 1, \ldots, N_t(k)$.

Update

The mode probability is updated by

$$u_{t,j}(k) = P\left(Z(k)|m_{t,j}(k), Z^{k-1}\right) u_{t,j}(k|k-1) \tag{4.4.37}$$

where the likelihood function is given by

$$\begin{aligned} & P\left(Z(k)|m_{t,j}(k), Z^{k-1}\right) \\ = & \sum_{i=1}^{N_A(k)} P\left(Z(k)|m_{t,j}(k), A_i(k), Z^{k-1}\right) P\left(A_i(k)|m_{t,j}(k), Z^{k-1}\right) \end{aligned} \tag{4.4.38}$$

The mode-conditioned longitudinal state estimate $X^r_{t,j}(k|k)$ and the associated covariance $P_{t,j}(k|k)$ are updated via the PDAF steps in (4.4.16)–(4.4.19) with the marginal probabilities calculated in (4.4.36). The final longitudinal state estimate and the corresponding covariance matrix are given by

$$\begin{aligned} \hat{X}^r_t(k|k) = & \sum_{j=1}^{N_m} \hat{X}^r_{t,j}(k|k) u_{t,j}(k) \\ P_t(k|k) = & \sum_{j=1}^{N_m} \Big[P_{t,j}(k|k) + \left(\hat{X}^r_t(k|k) - \hat{X}^r_{t,j}(k|k)\right) \\ & \times \left(\hat{X}^r_t(k|k) - \hat{X}^r_{t,j}(k|k)\right)^T \Big] u_{t,j}(k) \end{aligned} \tag{4.4.39}$$

4.4.4 Track management

The logic-based track management method [47] is used to update the status of existing tracks and to initialize new tracks based on the data association results. There are three possibilities for the track status, namely, tentative, confirmed and terminated.

Out of N_{tent} scans, if in at least M_{tent} scans measurements are associated with a tentative track, that track status is promoted as confirmed. Otherwise, the track is terminated. For a confirmed track, if the number of the scans in which it is associated with measurements is less than M_{conf} in the past N_{conf} scans, it is terminated. The measurements that are not associated with any existing track are used to initialize new tentative tracks so that the fundamental JPDA assumption of a known number of targets is removed. The lateral state of the new track initialized by $Z_m(k)$ is given by

$$\begin{aligned} \hat{l}_t(k) &= \arg\max_{l} \Lambda\left(Z_m(k)|d(l)\right) \\ &= \arg\max_{l} N(Z_m(k); d(l), \sigma_{v^d}^2) \end{aligned} \tag{4.4.40}$$

When a target makes a lane change, moving from its previous lane to the current one, a new track might be initialized on the current lane with the lateral state given by (4.4.40). This phenomenon will be addressed by the track segment association algorithm proposed in the next Section.

4.5 Track Segment Association for Target Lane Changes

In order to handle the swaps in tracks due to target lane-changing behaviors, a new track segment association algorithm is developed here. By stitching the tracks that are potentially from the same target, the TSA algorithm significantly improves track continuity.

4.5.1 Track Segment Sets

Track segment association is performed between the following two track sets [108]:

- Old track segment set (T^o) – the set of track segments that have been terminated due to lack of assigned measurements, for example, as the corresponding targets perform lane changes or move out of the observation area;
- Young track segment set (T^y) – the set of track segments that have been recently started, which might be continuations of some of the targets whose tracks have been terminated.

The two track segment sets are updated using the following two steps [109]:

- Pre-update: At time step k, the statuses of tracks are updated through the track management process. The new non-terminated tracks, initialized in the interval $(k-\tau, k)$ and attaining a certain minimum age ϵ, are added to the set $T^y(k)$. The tracks terminated at time k are removed from the young track set $T^y(k)$ and added to the old track set $T^o(k)$. The tracks terminated before time step $k-\tau$ are removed from the set $T^o(k)$. The sliding window length τ and the minimum track age ϵ are user-defined parameters.
- Post-update: After the TSA process, the track pairs that have been associated are removed from the two track sets.

For track i in the set $T^o(k)$, its starting and ending time steps are denoted by $k^o_{s_i}$ and $k^o_{e_i}$, respectively. For track j in the set $T^y(k)$, its starting and ending time steps are denoted by $k^y_{s_j}$ and $k^y_{e_j}$, respectively. A valid track pair should satisfy the constraint $k^o_{s_i} < k^y_{s_j}$, which means that the old track i initialized earlier than the young

track j. Using the logic-based track management method, each track is terminated a few time steps later than the last time it was updated with a measurement. That is, the young track segment that is the continuation of an old track segment might be initialized before the termination of the old track, as shown in Fig. 4.1(a). This is in contrast to the assumption made in previous works on TSA. Thus, we have the constraint $|k^o_{e_i} - k^y_{s_j}| < \tau$ for a valid track segment pair. Let $l_i(k)$ and $l_j(k)$ denote the lanes track i and track j are evolving along, respectively. Assuming that targets can only change to their neighboring lanes, the track swaps caused by target lane-changing behaviors mean that the constraint $|l_i(k) - l_j(k)| = 1$ should be satisfied by a valid track pair.

4.5.2 Track Prediction and Retrodiction

Before performing track segment association, it is necessary to propagate a valid track pair to a common time step k_c. It is chosen as the starting time of the young track considering target lane changes.

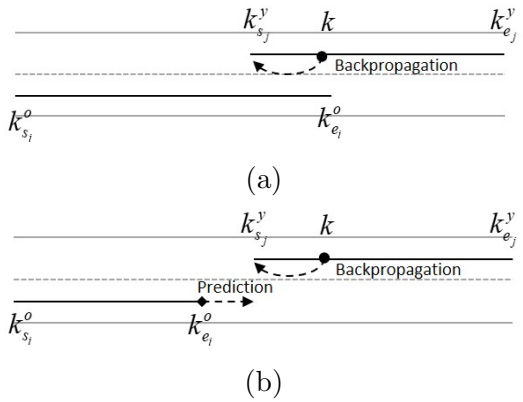

Figure 4.1: Illustration of track segment pair due to a target's lane-change.

For a given old track i, the common time step will be, typically, different as it is

associated with different young tracks. In case a young track is initialized before the termination of an old track (i.e., $k^y_{s_j} \leq k^o_{e_i}$), the longitudinal state estimate $\hat{X}^r_i(k_c|k_c)$ and the associated covariance matrix $P_i(k_c|k_c)$ are available, as shown in Fig. 4.1(a). Otherwise (i.e., $k^y_{s_j} > k^o_{e_i}$), the old track i is predicted from its end with the longitudinal state estimate $\hat{X}^r_i(k^o_{e_i}|k^o_{e_i})$ and the associated covariance matrix $P_i(k^o_{e_i}|k^o_{e_i})$ to the common time with the longitudinal state estimate $\hat{X}^r_i(k_c|k^o_{e_i})$ and the associated covariance matrix $P_i(k_c|k^o_{e_i})$, as shown in Fig. 4.1(b). This is achieved via (4.4.16) using the JPDA algorithm or via (4.4.23)–(4.4.24) using the IMMJPDA algorithm.

For the young track segment j, to reduce the error due to the track initialization method, it is backpropagated from the current time with the longitudinal state estimate $\hat{X}^r_j(k|k)$ and the associated covariance matrix $P_j(k|k)$ to its start with the smoothed longitudinal state estimate $\hat{X}^r_j(k^y_{s_j}|k)$ and the associated covariance matrix $P_j(k^y_{s_j}|k)$.

When the SA-JPDA algorithm is implemented into the tracking process, the Rauch-Tung-Striebel (RTS) smoothing approach [48] can be used. One iteration of the RTS algorithm is given by

$$\begin{aligned} \hat{X}^r_t(k'|k) &= \hat{X}^r_t(k'|k') + C(k')\left(\hat{X}^r_t(k'+1|k) - \hat{X}^r_t(k'+1|k')\right) \\ P_t(k'|k) &= P_t(k'|k') + C(k')\left(P_t(k'+1|k) - P_t(k'+1|k')\right)C(k')^T \end{aligned} \quad (4.5.1)$$

where $C(k')$ is the smoother gain given by

$$C(k') = P_t(k'|k')F^T(P_t(k'+1|k'))^{-1} \quad (4.5.2)$$

and $\hat{X}^r_t(k'|k')$, $\hat{X}^r_t(k'+1|k')$, $P_t(k'|k')$ and $P_t(k'+1|k')$ are stored in the filtering

process, where $k' = k^y_{s_j}, \ldots, k$.

When the SA-IMMJPDA algorithm is used for target tracking, the IMM backward smoothing algorithm proposed in [111] is used for TSA since it maintains the fundamental spirit of the IMM. Given the filtered results (i.e., state estimate, associated covariance and mode probability) at time step k' and the smoothed results at time step $k'+1$, the backward iteration can be summarized as follows [111]:

1. Calculation of the backward transition probability:
   $b_{t,ij} \triangleq p\left(m_{t,j}(k')|m_{t,i}(k'+1), Z^k\right)$, i.e.,

$$b_{t,ij} = \frac{1}{e_{t,i}} \pi_{ji} u_{t,j}(k') \tag{4.5.3}$$

   where $e_{t,i} = \sum_{j=1}^{N_m} \pi_{ji} u_{t,j}(k')$.

2. Calculation of the backward mixing probability:
   $\mu_{t,i|j}(k'+1) \triangleq P\left(m_{t,i}(k'+1)|m_{t,j}(k'), Z^k\right)$, i.e.,

$$\mu_{t,i|j}(k'+1) = \frac{1}{d_{t,j}} b_{t,ij} p(m_{t,i}(k'+1)|Z^k) \tag{4.5.4}$$

   where $d_{t,j} = \sum_{i=1}^{N_m} b_{t,ij} p(m_{t,i}(k'+1)|Z^k)$.

3. The mixed longitudinal state estimate and the associated covariance matrix for

the j-th mode-matched smoother are given by

$$\begin{aligned}\hat{X}^{r,s}_{t,0j}(k'+1|k) &= \sum_{i=1}^{N_m} \hat{X}^{r}_{t,i}(k'+1|k)\mu_{t,i|j}(k'+1) \\ P^{s}_{t,0j}(k'+1|k) &= \sum_{i=1}^{N_m} \Big[P_{t,i}(k'+1|k) + \Big(\hat{X}^{r,s}_{t,i}(k'+1|k) - \hat{X}^{r,s}_{t,0j}(k'+1|k)\Big) \\ &\quad \times \Big(\hat{X}^{r,s}_{t,i}(k'+1|k) - \hat{X}^{r,s}_{t,0j}(k'+1|k)\Big)^T\Big] \mu_{t,i|j}(k'+1)\end{aligned} \tag{4.5.5}$$

4. The smoothed longitudinal state estimate and the associated covariance matrix for mode j are given by

$$\begin{aligned}\hat{X}^{r}_{t,j}(k'|k) &= \hat{X}^{r}_{t,j}(k'|k') + C_{t,j}(k')\Big(\hat{X}^{r,s}_{t,0j}(k'+1|k) - \hat{X}^{r}_{t,j}(k'+1|k')\Big) \\ P_{t,j}(k'|k) &= P_{t,j}(k'|k') + C_{t,j}(k')\Big(P^{s}_{t,0j}(k'+1|k) - P_{t,j}(k'+1|k')\Big)C_{t,j}(k')^T\end{aligned} \tag{4.5.6}$$

where $\hat{X}^{r}_{t,j}(k'+1|k')$ and $P_{t,j}(k'+1|k')$ are the predicted mean and the associated covariance matrix corresponding to j-th mode, and $C_{t,j}(k')$ is the smoothing gain given by

$$C_{t,j}(k') = P_{t,j}(k'|k')F_j^T(P_{t,j}(k'+1|k'))^{-1} \tag{4.5.7}$$

where F_j is the transition matrix corresponding to mode j.

5. The smoothed mode probability, $\mu_{t,j}(k') = p(m_{t,j}(k')|Z^k)$, is given by

$$\mu_{t,j}(k') = \frac{1}{f}\Lambda_{t,j}(k'|k)\mu_{t,j}(k'|k') \tag{4.5.8}$$

where

$$\begin{aligned}\Lambda_{t,j}(k'|k) &= \sum_{i=1}^{N_m} \pi_{ji} N(\hat{X}^r_{t,i}(k'+1|k); \hat{X}^r_{t,i}(k'+1|k'), P_{t,i}(k'+1|k')) \\ f &= \sum_{j=1}^{N_m} \Lambda_{t,j}(k'|k)\mu_{t,j}(k'|k')\end{aligned} \tag{4.5.9}$$

6. The final longitudinal state estimate and corresponding covariance matrix are found using moment matching [48], i.e.,

$$\begin{aligned}\hat{X}^r_t(k'|k) &= \sum_{j=1}^{N_m} \hat{X}^r_{t,j}(k'|k) u_{t,j}(k') \\ P_t(k'|k) &= \sum_{j=1}^{N_m} \Big[P_{t,j}(k'|k) + \Big(\hat{X}^r_t(k'|k) - \hat{X}^r_{t,j}(k'|k)\Big) \\ &\quad \times \Big(\hat{X}^r_t(k'|k) - \hat{X}^r_{t,j}(k'|k)\Big)^T \Big] u_{t,j}(k')\end{aligned} \tag{4.5.10}$$

4.5.3 Track Segment Association

After propagating the track segments to the corresponding common times, the association can be carried out. Similar to the measurement-to-track association, the gating technique [47] is applied first to decide if a pair of track segments is valid for association. This is formulated as a hypothesis testing problem. Given a track pair $\{i, j\}$, their longitudinal state estimates and the associated covariances matrix at the common time are denoted by $\hat{X}^{r,o}_i$, $\hat{X}^{r,y}_j$ and P^o_i, P^y_j, ignoring time step index for simplicity, respectively. The difference between the two longitudinal state estimates is

$$\Delta\hat{X}^r_{ij} = \hat{X}^{r,o}_i - \hat{X}^{r,y}_j \tag{4.5.11}$$

with the associated covariance matrix given by

$$P_{ij} = P_i^o + P_j^y \tag{4.5.12}$$

Let H_{ij} denote the hypothesis that the track pair $\{i, j\}$ is from the same target and $\bar{H}_{ij}$ denotes the alternative hypothesis. Using the chi-square testing, hypothesis H_{ij} is accepted if

$$(\Delta\hat{X}_{ij}^r)^T(P_{ij})^{-1}\Delta\hat{X}_{ij}^r \leq \chi^2_{n_x}(1-q) \tag{4.5.13}$$

is true, where n_x denotes the dimension of the longitudinal state vector [48].

After gating, the association between the two track sets $T^o(k)$ and $T^y(k)$ is formulated as a 2-D assignment problem. Dummy tracks are added to both sets to represent non-association [109]; a track being associated with a dummy track means that the track did not originate from the same target with any other track. A binary assignment variable is defined as

$$a_{ij} = \begin{cases} 1 & \text{track } i \text{ and track } j \text{ are from the same target} \\ 0 & \text{otherwise} \end{cases} \tag{4.5.14}$$

The cost corresponding to assignment a_{ij} is given by the dimensionless negative log-likelihood ratio (NLLR) [108], i.e.,

$$c_{ij} = \begin{cases} -\ln\frac{N(\Delta\hat{X}_{ij}^r;0,P_{ij})}{\lambda} & i \neq 0, j \neq 0 \\ (1-P_d) & i = 0 \text{ or } j = 0 \end{cases} \tag{4.5.15}$$

where 0 denotes the dummy track. The goal is to find an optimal set of assignment

variable $\{a_{ij}\}$ to minimize the global cost

$$C = \sum_{i=0}^{N_t^o(k)} \sum_{j=0}^{N_t^y(k)} a_{ij} c_{ij} \tag{4.5.16}$$

subject to

$$\begin{aligned} \sum_{i=0}^{N_t^o(k)} a_{ij} &= 1, \quad j = 1, ..., N_t^y(k) \\ \sum_{j=0}^{N_t^y(k)} a_{ij} &= 1, \quad i = 1, ..., N_t^o(k) \end{aligned} \tag{4.5.17}$$

where $N_t^y(k)$ and $N_t^o(k)$ are the numbers of tracks in set $T^y(k)$ and $T^o(k)$, respectively. Generally, the cardinalities of two sets are not the same. This 2-D assignment problem can be solved efficiently using the Auction [64] or JVC algorithm [1]. Given TSA results, a common target's tracks on different lanes are connected to yield more continuous and pure tracks.

4.6 Conditional PCRLB for MTT

The PCRLB is commonly used as a lower bound to quantify the best possible accuracy of an unbiased state estimator [86, 87]. For the problem considered in this paper, the target states consist of both continuous-valued and discrete-valued variables, which makes that the regularity conditions required by the PCRLB violated [88, 89]. Besides, the actual motion model of a target is unknown to the motion estimator. Thus, the conditional PCRLB for target longitudinal state is derived in this Section as a trade-off [28, 90]. Since the lateral states and longitudinal motion models of targets are assumed to be known, the conditional PCRLB can be overly optimistic.

Let $\hat{X}^r(k)$ denote an unbiased estimate of $X^r(k)$ based on Z^k. Then,

$$P(k) = E\left\{\left(\hat{X}^r(k) - X^r(k)\right)\left(\hat{X}^r(k) - X^r(k)\right)^T\right\} \geq J(k)^{-1} \tag{4.6.1}$$

where $J(k)$ is the Fisher information matrix (FIM) for $X^r(k)$. The FIM $J(k)$ can be recursively evaluated as [86]

$$J(k+1) = J_X(k+1) + J_Z(k+1) \tag{4.6.2}$$

where

$$\begin{aligned}
J_X(k+1) &= D_k^{22} - D_k^{21}(J(k) + D_k^{11})^{-1}D_k^{12} \\
D_k^{11} &= E\{-\Delta_{X^r(k)}^{X^r(k)} \ln p(X^r(k+1)|X^r(k))\} \\
D_k^{12} &= E\{-\Delta_{X^r(k)}^{X^r(k+1)} \ln p(X^r(k+1)|X^r(k))\} \\
D_k^{21} &= (D_k^{12})^T \\
D_k^{22} &= E\{-\Delta_{X^r(k+1)}^{X^r(k+1)} \ln p(X^r(k+1)|X^r(k))\} \\
J_Z(k+1) &= E\{-\Delta_{X^r(k+1)}^{X^r(k+1)} \ln p(Z^r(k+1)|X^r(k+1))\}
\end{aligned} \tag{4.6.3}$$

In the MTT problem, the overall longitudinal state equation can be written as

$$X^r(k+1) = \bar{F}X^r(k) + \bar{G}W(k) \tag{4.6.4}$$

where $X^r(k) = \left[X_1^r(k)^T, X_2^r(k)^T, ..., X_{N_t}^r(k)^T\right]^T$ is the stacked vector consisting of the longitudinal states of all targets, and $\bar{F}$ and $\bar{G}$ are obtained by stacking the matrices F and G corresponding to each target. When targets move independently, $\bar{F}$ is a block diagonal matrix. Otherwise, the non-diagonal blocks in $\bar{F}$ represent the dependency between target motions. Substituting the (4.6.4) into (4.6.3) and using the matrix

inversion lemma [48], $J_X(k+1)$ can be evaluated as [87]

$$J_X(k+1) = \left[\bar{F}J(k)^{-1}\bar{F}^T + \bar{G}\bar{Q}\bar{G}^T\right]^{-1} \tag{4.6.5}$$

where $\bar{Q} = \text{diag}(\sigma_w^2, \sigma_w^2, \ldots, \sigma_w^2)$. The $J_Z(k+1)$ for multitarget tracking problem can be evaluated using the method in [87].

4.7 Simulations

The performance of the proposed algorithms is evaluated and compared with existing algorithms through Monte Carlo simulations in this Section.

4.7.1 Simulation Scenario

Four targets are simulated to move along a two-lane road where the width of each lane is $2\delta_d = 4$m. The targets start at 250m, 200m, 100m and 50m in the mileage coordinate, respectively. The simulation scenario duration is 100s and the durations the targets travel in each lane are shown in Table 4.1. Targets move independently with a nearly constant velocity when their inter-mileage distances are larger than 30m and the standard deviation of process noise is set as $\sigma_w = 0.1$ m/s^2. Otherwise, the motions of targets are inter-dependent and generated by the linear Helly model, one type of car-following models [83]:

$$\begin{aligned} X_t^r(k+1) &= FX_t^r(k) + G(a_t(k) + w(k)) \\ a_t(k) &= c_1\Delta r(k) + c_2\Delta\dot{r}(k) + c_3\dot{r}_t(k) + c_4 \end{aligned} \tag{4.7.1}$$

where $\Delta r(k) = r_{t^l}(k) - r_t(k)$ and $\Delta \dot{r}(k) = \dot{r}_{t^l}(k) - \dot{r}_t(k)$ are the relative mileage distance and the velocity between target t and its preceding (leading) target t^l, respectively, and the design parameters are set as $c_1 = 0.125$, $c_2 = 0.5$, $c_3 = -0.125$, $c_4 = -3.5$ according to [83]. As shown in Fig. 4.2, the target longitudinal speed changes significantly when the target motion switches from independent mode to car-following mode, i.e., time duration 2–4s for target 2, 64–66s for target 3, 4–6s and 52–54s for target 4. Target position measurements are generated every $T = 2$s according to (4.3.4) with $\sigma_v^r = 10$m and $\sigma_v^d = 2$m. The target detection probability is $P_d = 0.95$ and the spatial density of false alarms is $\lambda = 1.0^{-6}/\text{m}^2$. The performances of all algorithms are evaluated over 200 Monte Carlo runs.

Table 4.1: Lanes Targets are Traveling on in Simulations

	Duration (s)	
	Left-lane	Right-lane
Target 1	0–54	54–100
Target 2	0–100	–
Target 3	–	0–100
Target 4	20–100	0–20

4.7.2 Numerical Results

The SA-JPDA algorithm proposed in Section III.B and the SA-IMMJPDA algorithm developed in Section III.C are compared with the standard JPDA algorithm [14], the IMMJPDA algorithm proposed in [99], the 2D assignment (2DA) algorithm [16] and the sequence-aided 2D assignment (SA-2DA) algorithm proposed in [110]. Unlike the SA-JPDA algorithm, which updates tracks taking into account all association events, the SA-2DA algorithm provides the most likely association event, which has a maximum probability given by (4.4.5), to the Kalman filter (KF) for track update.

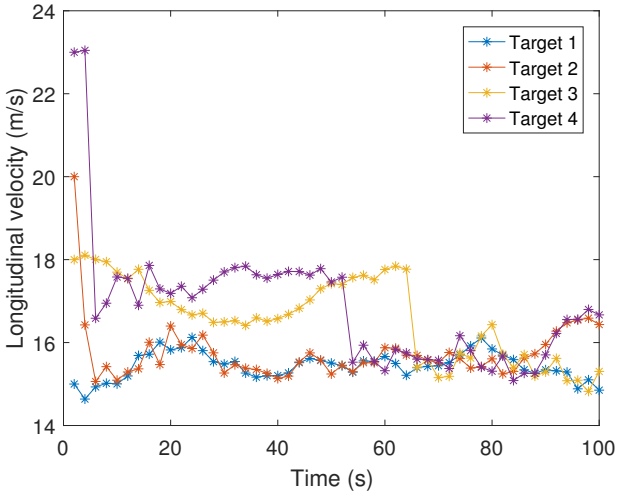

Figure 4.2: Target longitudinal velocities.

The NCV motion model is used in the PDAF and the KF where the standard deviation of process noise is set as $\sigma_w = 0.5$ m/s^2. In the IMM motion estimator, both the NCV model and the NCA model are used with the initial probability vector $u(0) = [0.5, 0.5]^T$ and the TPM given by

$$\Pi = \begin{bmatrix} 0.9 & 0.1 \\ 0.1 & 0.9 \end{bmatrix} \tag{4.7.2}$$

The standard deviation of the process noise in the NCA model is set as $\sigma_w = 1$ m/s^2. All the above data association algorithms are combined with the track segment association method developed in Section IV, where the sliding window length is $\tau =$ 30s and the track minimum age is $\epsilon = 10$s.

In the simulations, the performance of the multitarget tracking algorithms is evaluated based on the track-to-truth association results [91]. It is possible that different tracks are assigned to a certain target over time while a target is alive, especially in

the scenarios where targets are close to one another. The average number of swaps in the tracks for each target is shown in Table 4.2. It can be seen that, compared with the algorithms that do not utilize target position sequence information (i.e., JPDA, IMMJPDA and 2DA algorithms), the proposed sequence-aided data association algorithms (i.e., SA-JPDA, SA-IMMJPDA and SA-2DA algorithms) yield far fewer swaps in tracks, which means that more consistent tracking performance is obtained. Target 1 and 4 make lane changes during the simulation. After utilizing the track segment association algorithm, the numbers of swaps for both targets are reduced significantly. This is because the tracks that originated from the same target but generated on different lanes due to target lane changes are associated correctly.

Fig. 4.3 shows the track swap ratios (i.e., the ratio of the number of swaps at each time step to the number of Monte Carlo runs) by different algorithms. Referring to the target velocities shown in Fig. 4.2, it can be seen that the JPDA algorithm, IMMJPDA algorithm and the 2D assignment algorithm have much higher track swaps than the proposed sequence-aided data association algorithms during the periods that target velocities change significantly. Target 1 and 4 make lane changes at times 54s and 20s, respectively. By applying the TSA algorithm, the number of swaps at these times are reduced to an acceptable level. Specifically, the swap ratios at these times are below 0.1% in the sequence-aided data association algorithms.

It is also probable that there is no track assigned to a certain target over several time steps because there is no track close to the target. The average numbers of breaks for each target yielded by different algorithms are shown in Table 4.3. As the sequence information is utilized, the proposed data association algorithms yield fewer breaks because more accurate track are obtained. Besides, the IMMJPDA

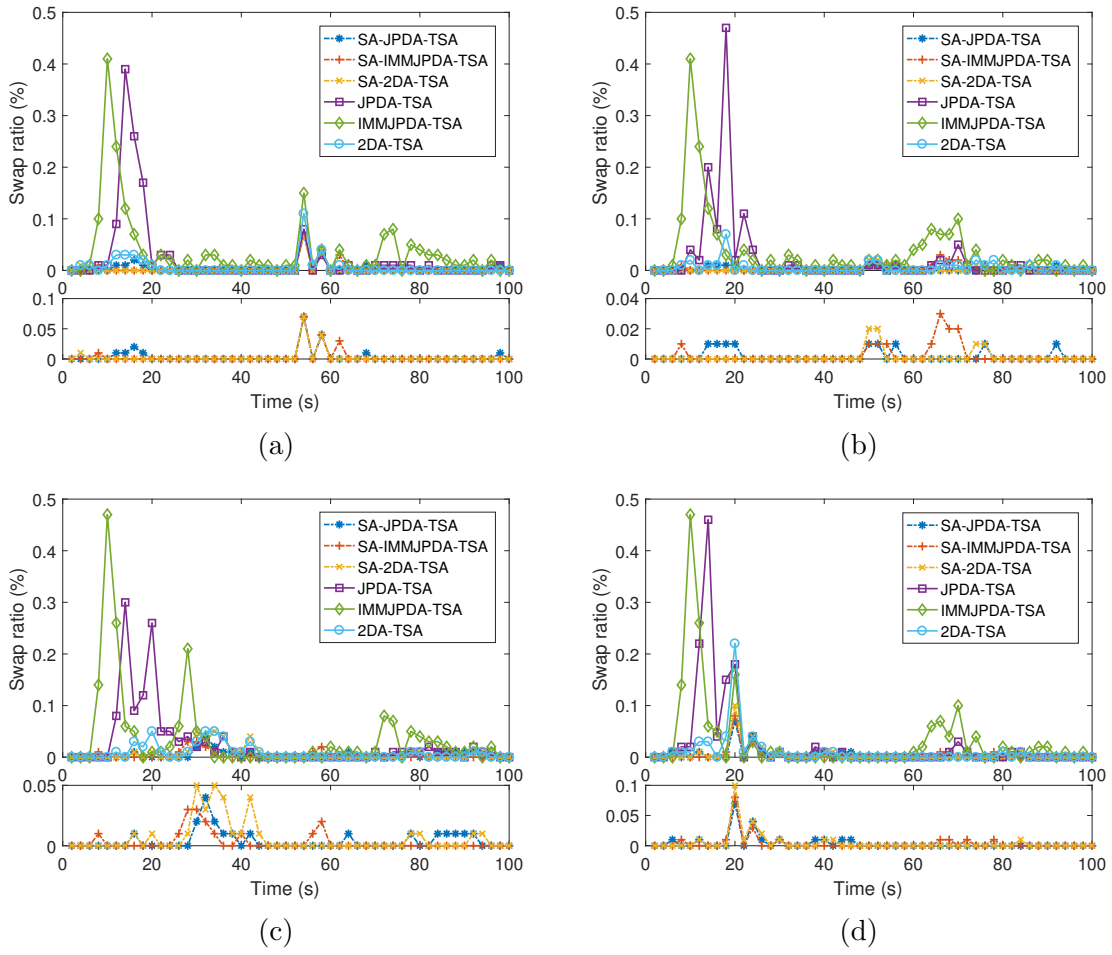

Figure 4.3: Comparison of swap ratios by different algorithms. (a) Target 1 (b) Target 2 (c) Target 3 (d) Target 4

and SA-IMMJPDA algorithms yield fewer breaks than other algorithms since both maneuvering and non-maneuvering modes are considered in the IMM estimator. Note that the TSA method is applied after tracking process to associate the tracks possibly originating from the same target. Thus, TSA makes no difference on the number of breaks.

The track continuity is a metric including the information of both swaps and

breaks. For target t in the mth run, it is defined as [91]

$$Tc_{t,m} = \frac{1}{n^a_{t,m}} \sum_{n=1}^{n^a_{t,m}} \frac{\Delta k_{t,n}}{\Delta k_t} \tag{4.7.3}$$

where $n^a_{t,m}$ denotes the number of tracks assigned to target t while Δk_t and $\Delta k_{t,n}$ denote the whole duration of target t and the duration of the nth track assigned to target t, respectively. Table 4.4 compares the track continuities averaged over Monte Carlo runs by different tracking algorithms. It is observed that more continuous tracks are obtained by using the sequence-aided data association algorithms. Besides, the TSA algorithm further improves track continuity.

Table 4.2: Average Number of Track Swaps

	TSA	Target 1	Target 2	Target 3	Target 4	Average
JPDA	before	2.12	1.15	1.28	2.07	1.655
	after	1.20	1.15	1.28	1.27	1.225
SA-JPDA	before	1.11	0.09	0.19	1.11	0.625
	after	0.18	0.09	0.19	0.26	0.180
IMMJPDA	before	2.67	1.81	1.83	2.48	2.198
	after	1.85	1.81	1.83	1.64	1.782
SA-IMMJPDA	before	1.06	0.12	0.15	1.10	0.608
	after	0.15	0.12	0.15	0.23	0.163
2DA	before	1.20	0.27	0.40	1.24	0.778
	after	0.32	0.27	0.40	0.47	0.365
SA-2DA	before	1.05	0.06	0.31	1.15	0.643
	after	0.12	0.06	0.31	0.40	0.223

The Root Mean Square Error (RMSE) is used as an accuracy metric to evaluate the performance of tracking algorithms. The longitudinal position and velocity RMSEs with their corresponding conditional PCRLBs for each target are shown in Fig. 4.4 and Fig. 4.5, respectively. It can be seen that the RMSE values of the proposed SA-JPDA algorithm are much lower than those of the JPDA algorithm

Table 4.3: Average Number of Track Breaks

	Target 1	Target 2	Target 3	Target 4	Average
JPDA	0.50	0.83	0.85	0.57	0.688
SA-JPDA	0.14	0.03	0.09	0.12	0.095
IMMJPDA	0.20	0.11	0.28	0.09	0.170
SA-IMMJPDA	0.17	0.00	0.00	0.07	0.060
2DA	0.25	0.15	0.20	0.22	0.205
SA-2DA	0.12	0.00	0.12	0.12	0.090

Table 4.4: Average Track Continuity

	TSA	Target 1	Target 2	Target 3	Target 4	Average
JPDA	before	0.329	0.497	0.476	0.327	0.407
	after	0.496	0.497	0.476	0.459	0.482
SA-JPDA	before	0.485	0.972	0.927	0.484	0.717
	after	0.944	0.972	0.927	0.896	0.935
IMMJPDA	before	0.296	0.429	0.399	0.297	0.355
	after	0.424	0.429	0.399	0.420	0.418
SA-IMMJPDA	before	0.488	0.960	0.933	0.484	0.716
	after	0.938	0.960	0.933	0.907	0.934
2DA	before	0.465	0.885	0.820	0.464	0.659
	after	0.862	0.885	0.820	0.802	0.842
SA-2DA	before	0.491	0.980	0.870	0.483	0.706
	after	0.958	0.980	0.870	0.846	0.913

and the RMSE values of the proposed SA-IMMJPDA algorithm are much lower than those of the IMMJPDA algorithm. This improvement is especially obvious when the targets undergo large velocity changes. The main reason for this is that improved measurement-to-track association results yield more accurate tracks. Specifically, the correct measurements are assigned with larger weights when the information of target position sequence is considered. This also mitigates the track coalescence problem that is inherent in the JPDA algorithm. Besides, the SA-2DA algorithm outperforms the standard 2D assignment algorithm because the correct association events are more likely to be selected when the sequence information re-weights the probability

of each event. As shown in Fig. 4.5 (a) and (d), the velocity errors introduced by the one-point track initialization method at lane-changing times are reduced by the smoothing process in the TSA algorithm. As shown in Fig. 4.4–4.5, the conditional PCRLB is an overly optimistic bound with lower values than the empirical RMSEs since it is assumed in calculation the conditional PCRLB that the exact target lateral states and motion model sequences are known.

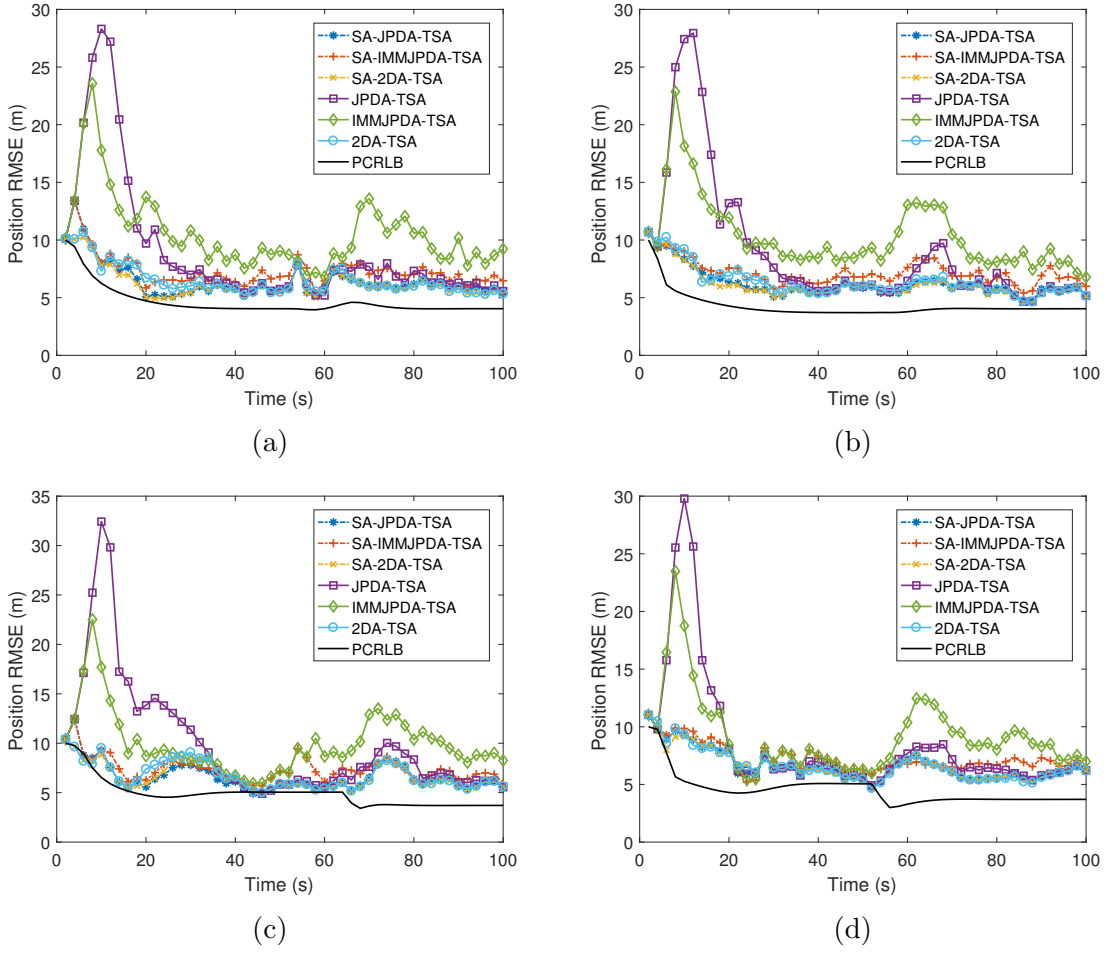

Figure 4.4: Comparison of longitudinal position RMSE by different algorithms. (a) Target 1 (b) Target 2 (c) Target 3 (d) Target 4

Table 4.5 shows the average computational times per run over 200 Monte Carlo

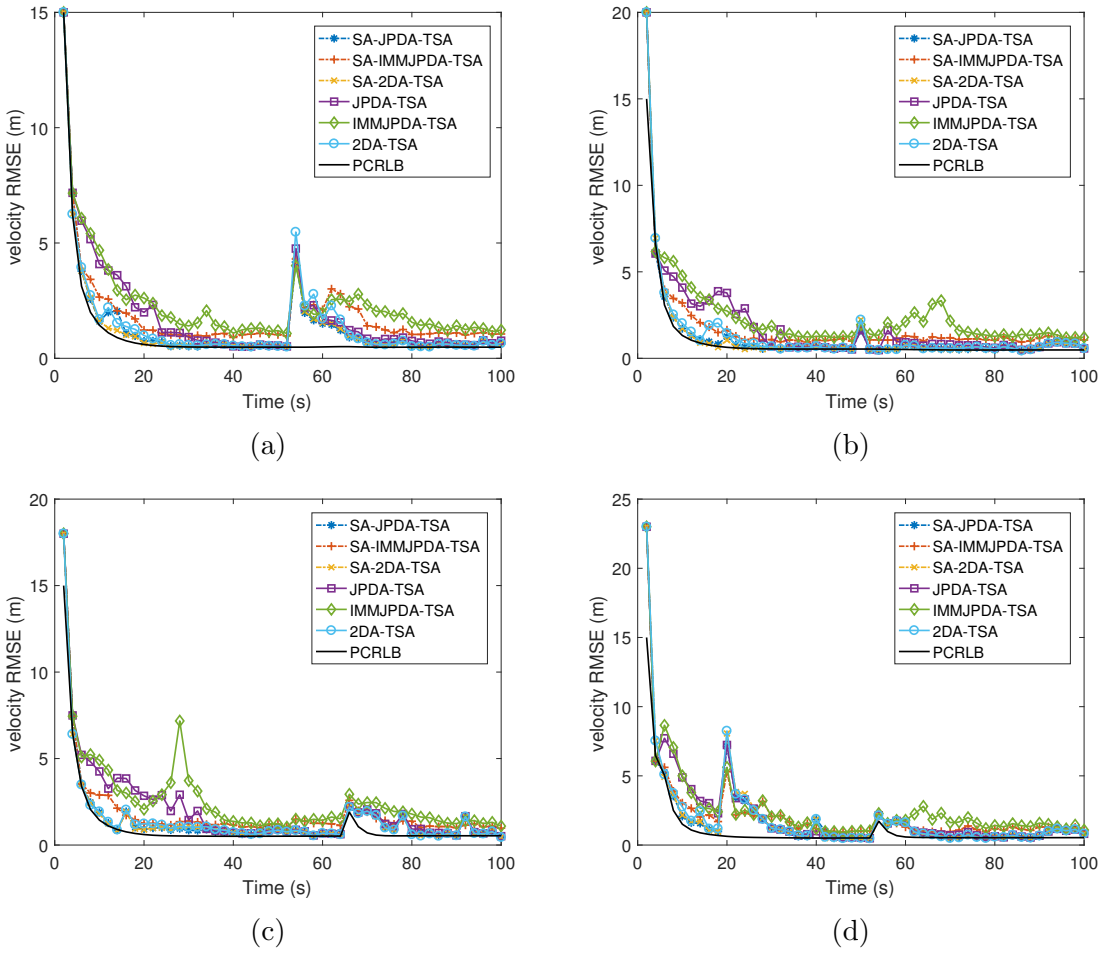

Figure 4.5: Comparison of longitudinal velocity RMSE by different algorithms. (a) Target 1 (b) Target 2 (c) Target 3 (d) Target 4

runs by different tracking algorithms. All tracking algorithms coded in MATLAB are executed on a 2.80 GHz Intel i7 PC. It is observed that the sequence-aided algorithms incur only slightly higher computational cost than the corresponding algorithms not using the sequence information. Moreover, the track segment association method adds almost no significant computational cost.

Table 4.5: Average Computational Times

	Without TSA (s)	With TSA (s)
JPDA	0.137	0.140
SA-JPDA	0.251	0.253
IMMJPDA	0.901	0.912
SA-IMMJPDA	1.309	1.325
2DA	0.045	0.048
SA-2DA	0.279	0.283

4.8 Conclusions

The problem of exploiting target position sequences in a road lane for tracking multiple on-road targets was addressed in this paper. In the proposed SA-JPDA and SA-IMMJPDA algorithms, the probability of each association hypothesis is re-weighted by the target sequence information and then used to calculate the marginal probability for each target. In the process of updating track states via the PDA filter, the more likely measurements have larger weights after considering the sequence information, which yields more accurate tracks. To address track terminations that result when a new track is initialized as a target changes lane, a track segment association algorithm was proposed to associate the old and new tracks that originated from the same target. The experiments show that the proposed algorithms yield better performance in terms of track accuracy and continuity than the existing algorithms that ignore target position sequence information. Besides, without having to describe target interactions by empirical car-following models, the proposed algorithms using position sequence information yield better performance regardless of whether targets move independently or inter-dependently. This enhances the robustness and reliability of the proposed algorithms in realistic ground target tracking scenarios.

Chapter 5

Conclusions and Future Works

5.1 Conclusions

Data association algorithms for multisensor-multitarget tracking were studied in this thesis.

First, a new multidimensional assignment algorithm using TDOA measurements for joint multitarget localization, multisensor synchronization and data association was proposed. The key step in the proposed algorithm was to evaluate of the generalized likelihood of each association hypothesis considering the fact that TDOA measurements are correlated and corrupted by sensor clock offsets. Given an association hypothesis, target positions and sensor clock offsets were unknown and estimated using a maximum likelihood estimator. To ensure the observability of the unknown parameters, the proposed algorithm was extended to use the measurements in multiple frames. Numerical results showed that the proposed algorithms achieved better association results and obtained more accurate estimates of target positions and sensor clock offsets than the standard multidimensional algorithm which do not

address the correlation between measurement-to-measurement association and sensor synchronization. It was also shown in numerical results that the gating method and multidimensional plus sequential two-dimensional association approach improve the efficiency of the proposed algorithms by pruning unlikely association hypotheses. The proposed algorithms are especially important in the initial period of multitarget tracking applications since it can calibrate sensors using the estimated sensor clock offsets and initialize tracks using the estimates of target positions.

Next, the data association algorithms for tracking multiple on-road targets were explored. Observing the phenomenon that targets usually move in an orderly manner on the road, a sequence-aided 2D assignment algorithm was proposed. By mathematically formulating target position sequences, this information was incorporated into the process of calculating the probability of an association event. The uncertainty in target position sequence was addressed by the proposed multiple-hypothesis algorithm that generates and evaluates possible sequence hypotheses. The conditional PCRLB for target longitudinal states given the true lateral states and longitudinal motion models of targets was derived as a performance benchmark.

Target position sequence information was further integrated into the standard JPDA algorithm and IMMJPDA algorithm. After utilizing sequence information, correct association events were assigned higher weights, which yields more accurate tracks and mitigates the track coalescence problem inherent in the JPDA algorithm. The track segment association algorithm was proposed to handle the swaps in tracks due to target lane changes, yielding more continuous tracks. Since no empirical model was assumed in the longitudinal or lateral motion of the target, the proposed algorithms were more robust and reliable in real scenarios. As shown in numerical results,

the proposed sequence-aided data association algorithms outperformed the existing on-road target tracking algorithms that ignore target position sequence information in terms of track accuracy and continuity.

5.2 Future Works

There are still a few limitations existing in this work, which can be addressed in future research. First, the algorithms proposed in this thesis are only evaluated and compared with existing algorithms through numerical simulations. Applying the proposed algorithms to real datasets is necessary for further algorithm validation. Second, efficiency is an important metric to determine whether the data association algorithm can be used in real scenarios. A few strategies have been developed to improve the efficiency of the proposed algorithms. To be specific, a gating method and a multi-dimensional plus sequential two-dimensional association approach are developed for joint multidimensional assignment algorithm in Chapter 2. The Murty's algorithm for generating the K-best assignments is integrated in the proposed sequence-aided data association algorithms in Chapter 3 and 4. To deploy the algorithm on real-time systems, more effective solutions need to be explored to further improve algorithm efficiency.

Bibliography

[1] Y. Bar-Shalom, P. K. Willett, and X. Tian, *Tracking and Data Fusion.* Storrs, CT, USA: YBS Publishing, 2011.

[2] X. Tian and Y. Bar-Shalom, "Track-to-track fusion configurations and association in a sliding window." *Journal of Advances in Information Fusion*, vol. 4, no. 2, pp. 146–164, 2009.

[3] X. Lin and Y. Bar-Shalom, "Multisensor target tracking performance with bias compensation," *IEEE Transactions on Aerospace and Electronic Systems*, vol. 42, no. 3, pp. 1139–1149, 2006.

[4] B. Friedland, "Treatment of bias in recursive filtering," *IEEE Transactions on Automatic Control*, vol. 14, no. 4, pp. 359–367, 1969.

[5] M. B. Ignagni, "Separate bias kalman estimator with bias state noise," *IEEE Transactions on Automatic Control*, vol. 35, no. 3, pp. 338–341, 1990.

[6] A. Alouani, P. Xia, T. Rice, and W. Blair, "On the optimality of two-stage state estimation in the presence of random bias," *IEEE Transactions on Automatic Control*, vol. 38, no. 8, pp. 1279–1283, 1993.

[7] D. C. Cowley and B. Shafai, "Registration in multi-sensor data fusion and tracking," in *1993 American Control Conference*. IEEE, 1993, pp. 875–879.

[8] Y. Zhou, H. Leung, and P. C. Yip, "An exact maximum likelihood registration algorithm for data fusion," *IEEE Transactions on Signal Processing*, vol. 45, no. 6, pp. 1560–1573, 1997.

[9] N. Okello and B. Ristic, "Maximum likelihood registration for multiple dissimilar sensors," *IEEE Transactions on Aerospace and Electronic Systems*, vol. 39, no. 3, pp. 1074–1083, 2003.

[10] D. F. Crouse, Y. Bar-Shalom, and P. Willett, "Sensor bias estimation in the presence of data association uncertainty," in *Signal and Data Processing of Small Targets 2009*, vol. 7445. International Society for Optics and Photonics, 2009, p. 74450P.

[11] N. N. Okello and S. Challa, "Joint sensor registration and track-to-track fusion for distributed trackers," *IEEE Transactions on Aerospace and Electronic Systems*, vol. 40, no. 3, pp. 808–823, 2004.

[12] Z. Li, S. Chen, H. Leung, and E. Bosse, "Joint data association, registration, and fusion using EM-KF," *IEEE Transactions on Aerospace and Electronic Systems*, vol. 46, no. 2, pp. 496–507, 2010.

[13] P. Konstantinova, A. Udvarev, and T. Semerdjiev, "A study of a target tracking algorithm using global nearest neighbor approach," in *Proceedings of the International Conference on Computer Systems and Technologies*, 2003, pp. 290–295.

[14] Y. Bar-Shalom, F. Daum, and J. Huang, "The probabilistic data association filter," *IEEE Control Systems Magazine*, vol. 29, no. 6, pp. 82–100, 2009.

[15] S. S. Blackman, "Multiple hypothesis tracking for multiple target tracking," *IEEE Aerospace and Electronic Systems Magazine*, vol. 19, no. 1, pp. 5–18, 2004.

[16] Y. Bar-Shalom, T. Kirubarajan, and C. Gokberk, "Tracking with classification-aided multiframe data association," *IEEE Transactions on Aerospace and Electronic Systems*, vol. 41, no. 3, pp. 868–878, 2005.

[17] Y. Bar-Shalom and H. Chen, "Track-to-track association for tracks with features and attributes," in *Signal and Data Processing of Small Targets 2005*, vol. 5913. International Society for Optics and Photonics, 2005, p. 59131A.

[18] X. Wang, B. La Scala, and R. Ellem, "Feature aided probabilistic data association for multi-target tracking," in *2008 11th International Conference on Information Fusion*. IEEE, 2008, pp. 1–7.

[19] T. Kirubarajan, Y. Bar-Shalom, K. R. Pattipati, and I. Kadar, "Ground target tracking with variable structure IMM estimator," *IEEE Transactions on Aerospace and Electronic Systems*, vol. 36, no. 1, pp. 26–46, 2000.

[20] P. J. Shea, T. Zadra, D. M. Klamer, E. Frangione, and R. Brouillard, "Improved state estimation through use of roads in ground tracking," in *Signal and Data Processing of Small Targets 2000*, vol. 4048. International Society for Optics and Photonics, 2000, pp. 321–332.

[21] D. Simon and T. L. Chia, "Kalman filtering with state equality constraints," *IEEE Transactions on Aerospace and Electronic Systems*, vol. 38, no. 1, pp. 128–136, 2002.

[22] Z. Duan and X. R. Li, "The role of pseudo measurements in equality-constrained state estimation," *IEEE Transactions on Aerospace and Electronic Systems*, vol. 49, no. 3, pp. 1654–1666, 2013.

[23] G. Zhou, K. Li, T. Kirubarajan, and L. Xu, "State estimation with trajectory shape constraints using pseudo-measurements," *IEEE Transactions on Aerospace and Electronic Systems*, vol. 5, no. 5, pp. 2395–2407, 2018.

[24] J. López-Araquistain, Á. J. Jarama, J. A. Besada, G. de Miguel, and J. R. Casar, "A new approach to map-assisted Bayesian tracking filtering," *Information Fusion*, vol. 45, pp. 79–95, 2019.

[25] R. Ding, M. Yu, H. Oh, and W.-H. Chen, "New multiple-target tracking strategy using domain knowledge and optimization," *IEEE Transactions on Systems, Man, and Cybernetics: Systems*, vol. 47, no. 4, pp. 605–616, 2017.

[26] D. Song, R. Tharmarasa, T. Kirubarajan, and X. N. Fernando, "Multi-vehicle tracking with road maps and car-following models," *IEEE Transactions on Intelligent Transportation Systems*, vol. 19, no. 5, pp. 1375–1386, 2018.

[27] D. Song, R. Tharmarasa, G. Zhou, M. C. Florea, N. Duclos-Hindie, and T. Kirubarajan, "Multi-vehicle tracking using microscopic traffic models," *IEEE Transactions on Intelligent Transportation Systems*, no. 99, pp. 1–13, 2018.

[28] D. Song, R. Tharmarasa, M. C. Florea, N. Duclos-Hindie, X. N. Fernando, and T. Kirubarajan, "Multi-vehicle tracking with microscopic traffic flow model-based particle filtering," *Automatica*, vol. 105, pp. 28–35, 2019.

[29] M. Erol-Kantarci, H. T. Mouftah, and S. Oktug, "A survey of architectures and localization techniques for underwater acoustic sensor networks," *IEEE Communications Surveys & Tutorials*, vol. 13, no. 3, pp. 487–502, 2011.

[30] M. Bayat, N. Crasta, A. P. Aguiar, and A. M. Pascoal, "Range-based underwater vehicle localization in the presence of unknown ocean currents: Theory and experiments," *IEEE Transactions on Control Systems Technology*, vol. 24, no. 1, pp. 122–139, 2016.

[31] J. Naganawa, H. Miyazaki, and H. Tajima, "Localization accuracy model incorporating signal detection performance for wide area multilateration," *IEEE Transactions on Aerospace and Electronic Systems*, 2018.

[32] A. Yassin, Y. Nasser, M. Awad, A. Al-Dubai, R. Liu, C. Yuen, R. Raulefs, and E. Aboutanios, "Recent advances in indoor localization: A survey on theoretical approaches and applications," *IEEE Communications Surveys & Tutorials*, vol. 19, no. 2, pp. 1327–1346, 2016.

[33] G. Han, J. Jiang, C. Zhang, T. Q. Duong, M. Guizani, and G. K. Karagiannidis, "A survey on mobile anchor node assisted localization in wireless sensor networks." *IEEE Communications Surveys & Tutorials*, vol. 18, no. 3, pp. 2220–2243, 2016.

[34] J. Yan, C. C. Tiberius, G. J. Janssen, P. J. Teunissen, and G. Bellusci, "Review

of range-based positioning algorithms," *IEEE Aerospace and Electronic Systems Magazine*, vol. 28, no. 8, pp. 2–27, 2013.

[35] S. Xu and K. Doğançay, "Optimal sensor placement for 3-D angle-of-arrival target localization," *IEEE Transactions on Aerospace and Electronic Systems*, vol. 53, no. 3, pp. 1196–1211, 2017.

[36] Y. Wang and K. Ho, "TDOA source localization in the presence of synchronization clock bias and sensor position errors," *IEEE Transactions on Signal Processing*, vol. 61, no. 18, pp. 4532–4544, 2013.

[37] Y.-C. Wu, Q. Chaudhari, and E. Serpedin, "Clock synchronization of wireless sensor networks," *IEEE Signal Processing Magazine*, vol. 28, no. 1, pp. 124–138, 2011.

[38] H. Wang, H. Zeng, M. Li, B. Wang, and P. Wang, "Maximum likelihood estimation of clock skew in wireless sensor networks with periodical clock correction under exponential delays," *IEEE Transactions on Signal Processing*, vol. 65, no. 10, pp. 2714–2724, 2017.

[39] M. Leng and Y.-C. Wu, "On clock synchronization algorithms for wireless sensor networks under unknown delay," *IEEE Transactions on Vehicular Technology*, vol. 59, no. 1, pp. 182–190, 2010.

[40] K. Römer and F. Mattern, "Towards a unified view on space and time in sensor networks," *Computer Communications*, vol. 28, no. 13, pp. 1484–1497, 2005.

[41] J. Zheng and Y.-C. Wu, "Joint time synchronization and localization of an

unknown node in wireless sensor networks," *IEEE Transactions on Signal Processing*, vol. 58, no. 3, pp. 1309–1320, 2010.

[42] M. R. Gholami, S. Gezici, and E. G. Strom, "TDOA based positioning in the presence of unknown clock skew," *IEEE Transactions on Communications*, vol. 61, no. 6, pp. 2522–2534, 2013.

[43] A. Ahmad, E. Serpedin, H. Nounou, and M. Nounou, "Joint node localization and time-varying clock synchronization in wireless sensor networks," *IEEE Transactions on Wireless Communications*, vol. 12, no. 10, pp. 5322–5333, 2013.

[44] D. Carevic, "Automatic estimation of multiple target positions and velocities using passive TDOA measurements of transients," *IEEE Transactions on Signal Processing*, vol. 55, no. 2, pp. 424–436, 2007.

[45] R. T. Rajan and A.-J. van der Veen, "Joint ranging and synchronization for an anchorless network of mobile nodes," *IEEE Transactions on Signal Processing*, vol. 63, no. 8, pp. 1925–1940, 2015.

[46] M. Leng, F. Quitin, W. P. Tay, C. Cheng, S. G. Razul, and C. M. S. See, "Anchor-aided joint localization and synchronization using SOOP: Theory and experiments," *IEEE Transactions on Wireless Communications*, vol. 15, no. 11, pp. 7670–7685, 2016.

[47] S. Blackman and R. Popoli, *Design and Analysis of Modern Tracking Systems*. Boston, MA, USA: Artech House, 1999.

[48] Y. Bar-Shalom, X. R. Li, and T. Kirubarajan, *Estimation with Applications*

to Tracking and Navigation: Theory Algorithms and Software. Hoboken, NJ, USA: Wiley, 2004.

[49] Q. Wang, Z. Chen, Z. Wang, Z. Zhao, and Z. Wu, "Clustering data association using data relevance in spatial domain for Doppler-only RSN localization," *IEEE Transactions on Aerospace and Electronic Systems*, vol. 54, no. 6, pp. 3018–3031, 2018.

[50] K. Pattipati and S. Deb, "Comparison of assignment algorithms with applications to the passive sensor data association problem," in *Control and Applications, 1989. Proceedings. ICCON'89. IEEE International Conference on.* IEEE, 1989, pp. 317–322.

[51] S. Deb, K. R. Pattipati, and Y. Bar-Shalom, "A multisensor-multitarget data association algorithm for heterogeneous sensors," *IEEE Transactions on Aerospace and Electronic Systems*, vol. 29, no. 2, pp. 560–568, 1993.

[52] R. L. Popp, K. R. Pattipati, and Y. Bar-Shalom, "M-best SD assignment algorithm with application to multitarget tracking," *IEEE Transactions on Aerospace and Electronic Systems*, vol. 37, no. 1, pp. 22–39, 2001.

[53] R. Tharmarasa, M. Subramaniam, N. Nadarajah, T. Kirubarajan, and M. McDonald, "Multitarget passive coherent location with transmitter-origin and target-altitude uncertainties," *IEEE Transactions on Aerospace and Electronic Systems*, vol. 48, no. 3, pp. 2530–2550, 2012.

[54] W. Dou, J. George, L. Kaplan, R. W. Osborne, and Y. Bar-Shalom, "Assignment and EM approaches for passive localization of multiple transient emitters,"

in *Signal Processing, Sensor/Information Fusion, and Target Recognition XXV*, vol. 9842. International Society for Optics and Photonics, 2016, p. 984206.

[55] T. Sathyan and A. Sinha, "A two-stage assignment-based algorithm for asynchronous multisensor bearings-only tracking," *IEEE Transactions on Aerospace and Electronic Systems*, vol. 47, no. 3, pp. 2153–2168, 2011.

[56] T. Sathyan, A. Sinha, and T. Kirubarajan, "Passive geolocation and tracking of an unknown number of emitters," *IEEE Transactions on Aerospace and Electronic Systems*, vol. 42, no. 2, pp. 740–750, 2006.

[57] T. Sathyan, A. Sinha, T. Kirubarajan, M. McDonald, and T. Lang, "MDA-based data association with prior track information for passive multitarget tracking," *IEEE Transactions on Aerospace and Electronic Systems*, vol. 47, no. 1, pp. 539–556, 2011.

[58] S. Deb, M. Yeddanapudi, K. Pattipati, and Y. Bar-Shalom, "A generalized SD assignment algorithm for multisensor-multitarget state estimation," *IEEE Transactions on Aerospace and Electronic Systems*, vol. 33, no. 2, pp. 523–538, 1997.

[59] M. R. Chummun, T. Kirubarajan, K. R. Pattipati, and Y. Bar-Shalom, "Fast data association using multidimensional assignment with clustering," *IEEE Transactions on Aerospace and Electronic Systems*, vol. 37, no. 3, pp. 898–913, 2001.

[60] S. Zhang and Y. Bar-Shalom, "Practical data association for passive sensors in 3D," *Journal of Advances Information Fusion*, vol. 9, no. 1, pp. 47–56, 2014.

[61] H. Chen, X. R. Li, and Y. Bar-Shalom, "On joint track initiation and parameter estimation under measurement origin uncertainty," *IEEE Transactions on Aerospace and Electronic Systems*, vol. 40, no. 2, pp. 675–694, 2004.

[62] X. R. Li, "Optimal Bayes joint decision and estimation," in *Information Fusion, 2007 10th International Conference on*. IEEE, 2007, pp. 1–8.

[63] D. Belfadel, R. Osborne, and Y. Bar-Shalom, "A robust approach for space based sensor bias estimation in the presence of data association uncertainty," in *Signal Processing, Sensor/Information Fusion, and Target Recognition XXIV*, vol. 9474. International Society for Optics and Photonics, 2015, p. 947407.

[64] D. P. Bertsekas, "The auction algorithm: A distributed relaxation method for the assignment problem," *Annals of Operations Research*, vol. 14, no. 1, pp. 105–123, 1988.

[65] K. R. Pattipati, S. Deb, Y. Bar-Shalom, and R. B. Washburn, "A new relaxation algorithm and passive sensor data association," *IEEE Transactions on Automatic Control*, vol. 37, no. 2, pp. 198–213, 1992.

[66] R. J. Kenefic, "Local and remote track file registration using minimum description length," *IEEE Transactions on Aerospace and Electronic Systems*, vol. 29, no. 3, pp. 651–655, 1993.

[67] H. Chen, Y. Bar-Shalom, K. Pattipati, and T. Kirubarajan, "MDL approach for multiple low observable track initiation," *IEEE Transactions on Aerospace and Electronic Systems*, vol. 39, no. 3, pp. 862–882, 2003.

[68] G. Mellen, M. Pachter, and J. Raquet, "Closed-form solution for determining emitter location using time difference of arrival measurements," *IEEE Transactions on Aerospace and Electronic Systems*, vol. 39, no. 3, pp. 1056–1058, 2003.

[69] H. Oh, S. Kim, and A. Tsourdos, "Road-map–assisted standoff tracking of moving ground vehicle using nonlinear model predictive control," *IEEE Transactions on Aerospace and Electronic Systems*, vol. 51, no. 2, pp. 975–986, 2015.

[70] Y. Yuan, Y. Lu, and Q. Wang, "Tracking as a whole: Multi-target tracking by modeling group behavior with sequential detection," *IEEE Transactions on Intelligent Transportation Systems*, vol. 18, no. 12, pp. 3339–3349, 2017.

[71] K. Jo, M. Lee, J. Kim, and M. Sunwoo, "Tracking and behavior reasoning of moving vehicles based on roadway geometry constraints," *IEEE Transactions on Intelligent Transportation Systems*, vol. 18, no. 2, pp. 460–476, 2016.

[72] X. Zhang, H. Xu, and J. Fang, "Multiple vehicle tracking in aerial video sequence using driver behavior analysis and improved deterministic data association," *Journal of Applied Remote Sensing*, vol. 12, no. 1, p. 016014, 2018.

[73] Y. Cheng and T. Singh, "Efficient particle filtering for road-constrained target tracking," *IEEE Transactions on Aerospace and Electronic Systems*, vol. 43, no. 4, pp. 1454–1469, 2007.

[74] Y. Fang, C. Wang, W. Yao, X. Zhao, H. Zhao, and H. Zha, "On-road vehicle tracking using part-based particle filter," *IEEE Transactions on Intelligent Transportation Systems*, vol. 20, no. 12, pp. 4538–4552, 2019.

[75] M. Ekman and E. Sviestins, "Multiple model algorithm based on particle filters for ground target tracking," in *2007 10th International Conference on Information Fusion*. IEEE, 2007, pp. 1–8.

[76] M. Ulmke and W. Koch, "Road-map assisted ground moving target tracking," *IEEE Transactions on Aerospace and Electronic Systems*, vol. 42, no. 4, pp. 1264–1274, 2006.

[77] Y. Chen, V. P. Jilkov, and X. R. Li, "Multilane-road target tracking using radar and image sensors," *IEEE Transactions on Aerospace and Electronic Systems*, vol. 51, no. 1, pp. 65–80, 2015.

[78] D. Helbing and P. Molnar, "Social force model for pedestrian dynamics," *Physical Review E*, vol. 51, no. 5, p. 4282, 1995.

[79] V. C. Ravindra, Y. Bar-Shalom, and T. Damarla, "Feature-aided localization of ground vehicles using passive acoustic sensor arrays," in *2009 12th International Conference on Information Fusion*. IEEE, 2009, pp. 70–77.

[80] X. R. Li and V. P. Jilkov, "Survey of maneuvering target tracking. Part I. Dynamic models," *IEEE Transactions on Aerospace and Electronic Systems*, vol. 39, no. 4, pp. 1333–1364, 2003.

[81] Y. Li and D. Sun, "Microscopic car-following model for the traffic flow: The state of the art," *Journal of Control Theory and Applications*, vol. 10, no. 2, pp. 133–143, 2012.

[82] R. E. Chandler, R. Herman, and E. W. Montroll, "Traffic dynamics: Studies in car following," *Operations Research*, vol. 6, no. 2, pp. 165–184, 1958.

[83] W. Helly, "Simulation of bottlenecks in single-lane traffic flow," Apr. 1959.

[84] T. H. Rockwell, R. L. Ernst, and A. Hanken, "A sensitivity analysis of empirically derived car-following models," *Transportation Research*, vol. 2, no. 4, pp. 363–373, 1968.

[85] K. G. Murthy, "An algorithm for ranking all the assignments in order of increasing costs," *Operations research*, vol. 16, no. 3, pp. 682–687, 1968.

[86] P. Tichavsky, C. H. Muravchik, and A. Nehorai, "Posterior Cramér-Rao bounds for discrete-time nonlinear filtering," *IEEE Transactions on Signal Processing*, vol. 46, no. 5, pp. 1386–1396, 1998.

[87] R. Tharmarasa, T. Kirubarajan, M. L. Hernandez, and A. Sinha, "PCRLB-based multisensor array management for multitarget tracking," *IEEE Transactions on Aerospace and Electronic Systems*, vol. 43, no. 2, pp. 539–555, 2007.

[88] M. Hernandez, B. Ristic, A. Farina, T. Sathyan, and T. Kirubarajan, "Performance measure for Markovian switching systems using best-fitting Gaussian distributions," *IEEE Transactions on Aerospace and Electronic Systems*, vol. 44, no. 2, pp. 724–747, 2008.

[89] T. Sathyan, M. Hernandez, A. Sinha, and T. Kirubarajan, "Weiss-Weinstein lower bound for maneuvering target tracking," in *Signal and Data Processing of Small Targets 2006*, vol. 6236. International Society for Optics and Photonics, 2006, p. 62360G.

[90] A. Bessell, B. Ristic, A. Farina, X. Wang, and M. Arulampalam, "Error performance bounds for tracking a manoeuvring target," in *Proceedings of the 6th International Conference on Information Fusion*, 2003, pp. 903–910.

[91] A. A. Gorji, R. Tharmarasa, and T. Kirubarajan, "Performance measures for multiple target tracking problems," in *14th International Conference on Information Fusion*. IEEE, 2011, pp. 1–8.

[92] J. Gu, T. Su, Q. Wang, X. Du, and M. Guizani, "Multiple moving targets surveillance based on a cooperative network for multi-UAV," *IEEE Communications Magazine*, vol. 56, no. 4, pp. 82–89, 2018.

[93] C. Y. Chong, D. Garren, and T. P. Grayson, "Ground target tracking–A historical perspective," in *2000 IEEE Aerospace Conference. Proceedings*, vol. 3. IEEE, 2000, pp. 433–448.

[94] M. Treiber, A. Hennecke, and D. Helbing, "Congested traffic states in empirical observations and microscopic simulations," *Physical Review E*, vol. 62, no. 2, pp. 1805–1824, 2000.

[95] A. Kesting, M. Treiber, and D. Helbing, "General lane-changing model MOBIL for car-following models," *Transportation Research Record*, vol. 1999, no. 1, pp. 86–94, 2007.

[96] S. He, H.-S. Shin, and A. Tsourdos, "Trajectory optimization for multitarget tracking using joint probabilistic data association filter," *Journal of Guidance, Control, and Dynamics*, pp. 1–9, 2019.

[97] R. P. Mahler, "Multitarget Bayes filtering via first-order multitarget moments," *IEEE Transactions on Aerospace and Electronic systems*, vol. 39, no. 4, pp. 1152–1178, 2003.

[98] B.-N. Vo and W.-K. Ma, "The Gaussian mixture probability hypothesis density filter," *IEEE Transactions on signal processing*, vol. 54, no. 11, pp. 4091–4104, 2006.

[99] B. Chen and J. K. Tugnait, "Tracking of multiple maneuvering targets in clutter using IMM/JPDA filtering and fixed-lag smoothing," *Automatica*, vol. 37, no. 2, pp. 239–249, 2001.

[100] S. Puranik and J. K. Tugnait, "Tracking of multiple maneuvering targets using multiscan JPDA and IMM filtering," *IEEE Transactions on Aerospace and Electronic Systems*, vol. 43, no. 1, pp. 23–35, 2007.

[101] J. K. Tugnait, "Tracking of multiple maneuvering targets in clutter using multiple sensors, IMM, and JPDA coupled filtering," *IEEE Transactions on Aerospace and Electronic Systems*, vol. 40, no. 1, pp. 320–330, 2004.

[102] R. Danchick and G. E. Newnam, "A fast method for finding the exact N-best hypotheses for multitarget tracking," *IEEE Transactions on Aerospace and Electronic Systems*, vol. 29, no. 2, pp. 555–560, 1993.

[103] L. Bojilov, K. Alexiev, and P. Konstantinova, "An accelerated IMM-JPDA algorithm for tracking multiple maneuvering targets in clutter," *Information & Security: An International Journal*, vol. 9, 2002.

[104] H. L. Kennedy, "Controlling track coalescence with scaled joint probabilistic data association," in *2008 International Conference on Radar*. IEEE, 2008, pp. 440–445.

[105] H. A. Blom and E. A. Bloem, "Probabilistic data association avoiding track coalescence," *IEEE Transactions on Automatic Control*, vol. 45, no. 2, pp. 247–259, 2000.

[106] J. Raghu, P. Srihari, R. Tharmarasa, and T. Kirubarajan, "Comprehensive track segment association for improved track continuity," *IEEE Transactions on Aerospace and Electronic Systems*, vol. 54, no. 5, pp. 2463–2480, 2018.

[107] B. Pannetier and J. Dezert, "Track segment association with classification information," in *Proceedings of 2012 Workshop on Sensor Data Fusion: Trends, Solutions, Applications (SDF)*, 2012, pp. 60–65.

[108] S.-W. Yeom, T. Kirubarajan, and Y. Bar-Shalom, "Track segment association, fine-step IMM and initialization with Doppler for improved track performance," *IEEE Transactions on Aerospace and Electronic Systems*, vol. 40, no. 1, pp. 293–309, 2004.

[109] S. Zhang and Y. Bar-Shalom, "Track segment association for GMTI tracks of evasive move-stop-move maneuvering targets," *IEEE Transactions on Aerospace and Electronic Systems*, vol. 47, no. 3, pp. 1899–1914, 2011.

[110] T. Ge, R. Tharmarasa, M. Bradford, and T. Kirubarajan, "Sequence-aided data association for tracking multiple on-road targets with unknown interactions," *IEEE Transactions on Aerospace and Electronic Systems*, 2020, submitted to.

[111] N. Nadarajah, R. Tharmarasa, M. McDonald, and T. Kirubarajan, "IMM forward filtering and backward smoothing for maneuvering target tracking," *IEEE Transactions on Aerospace and Electronic Systems*, vol. 48, no. 3, pp. 2673–2678, 2012.